

Deposition of metallic copper
through UV light irradiation

Dissertation

zur Erlangung des Grades
des Doktors der Naturwissenschaften
der Naturwissenschaftlich-Technischen Fakultät
der Universität des Saarlandes



UNIVERSITÄT
DES
SAARLANDES

von

Juan Carlos Támara Florez, M. Sc.

Saarbrücken

2017

Tag des Kolloquiums: 20.10.2017

Dekan: Prof. Dr. Guido Kickelbick

Berichterstatter: Prof. Dr. Guido Kickelbick

Prof. Dr. Gregor Jung

Vorsitzender: Prof. Dr. Kaspar Hegetschweiler

Akad. Mitarbeiter: Dr. Ing. Mohammad Zamanzade

May this be a sign of peace, happiness and growth for all living beings
May this be a sign of peace, happiness and growth for all my brothers and sisters
May this be a path of peace, happiness and growth for myself
May all living beings be happy and free of pain

Preface

The present work was done at the INM Leibniz institute for new materials, in the research group of Optical Materials in collaboration and under the supervision of Prof. Dr. Guido Kickelbick from the inorganic solid state chemistry department of the University of Saarland.

The results of the present work have been submitted for patent application in the German patent and trade mark office, with the application number DE102016125667.6. The patent is due to be published by the office in June 2018 with the registry number DE102016125667A1.

Contributions statement

The idea of the project was proposed by the head of the group of optical materials of the INM Leibniz institute for new materials, Dr. Peter W. de Oliveira. At the initial stages of the project, discussion of the results and further steps of the project were regularly discussed with the head supervisor Prof. Dr. Guido Kickelbick, Dr. Peter W. de Oliveira and the designated internal supervisor in the group Dr. Karsten Moh. At intermediate and later stages of the project Dr. Peter Röglin was designated to continue with the internal supervision of the project and collaborated specifically in the planning of optical experiments and parts of the project related with physics and optical systems. Dr. Peter Röglin designed and constructed with assistance of the author a spectrometer for in-line follow up of photoreactions irradiated with UV-LED's.

Ab-initio simulations were performed by the author in the computational cluster of the physical and theoretical chemistry department directed by Prof. Dr. Michael Springborg.

Design of a photoreactor for larger scale experiments was done by the author with assistance of the institute workshop staff, Serwas Dietmar, Herbert Beermann and Uwe Magar.

TiO₂ layers over PET were provided by Jenny Kampka and TiO₂ particles for coatings were synthesized and provided by Christine Faller-Schneider and Dr. Peter König.

EDX measurements were acquired with the assistance of Dr. Oscar Torrents. ICP-OES and MS spectroscopic measurements were performed exclusively by the institute analytic group, Claudia Fink-Straube, Yuliya Silina and Thy Vinh Ha Rimbach-Nguyen.

The patent application product of this work was written by the institute project support and technology transfer department. The author and the other inventors provided the results, analysis, technical and scientific implications contained in the patent application document.

Authorship

The author performed the synthesis of the complexes, the irradiation experiments and spectroscopic measurements apart from the previously stated MS and ICP-OES measurements. The author processed and analyzed the raw data of the experiments and elicited the graphics, schemes and figures shown in this work unless stated elsewhere otherwise. The author conceived and wrote this dissertation entirely.

Acknowledgments

With great pleasure I thank all the persons that have directly and indirectly contributed, through all vicissitudes in my life and therefore too to this work as one of its outcomes. I profusely thank my parents, siblings for their unconditional love and understanding, for the precious values they have transmitted me through example and word that have let me grow freely and give. I thank my girlfriend Leidy for her unconditional love, understanding, encouragement and help.

In the times span of this work I would like to thank Prof. Dr. Guido Kickelbick for supporting my aspiration to become a doctor in chemistry, for his time in the supervision of my work, for the reading and revision of my thesis, for his energy in providing ideas and momentum to the project and for evaluating my work. Thank you Prof. Kickelbick for the permanent courtesy and patience, but most of all for backing my freedom and space to develop ideas, experiments and to work.

I would like to express my gratitude to Prof. Dr. Gregor Jung for his time, energy and for acceding to review and evaluate my thesis and dissertation.

I would like to express my appreciation and thanks to Prof. Dr. Eduard Arzt for giving me the opportunity to work in the INM. Likewise, I thank the head of the optical materials group, Dr. Peter de Oliveira, for the opportunity to work and pursue my Ph. D., for his time and energy in the regular discussion meetings and most of all for his flexible and comprehensive attitude.

I thank Dr. Karsten Moh for his time and energy supervising my work and the discussion about possible experimental strategies at early stages of the project; Dr. Peter Röglin for his joyful support and generous contribution of experimental ideas and the revision of my thesis; Dr. Thomas Müller for taking the time to answer my questions, for the interesting casual discussions in chemistry and for reviewing my thesis. I express my appreciation to Dr. Peter König for his affability and sincerity while discussing ideas and his time and energy in reviewing my thesis, thanks too for the refreshing conversations in the laboratory and the tips in chemistry. I thank Dr. Michael Opsolder for his time and energy in reviewing my thesis.

I wish to thank Jenny Kampka for her time, energy, attention, affability and helpfulness in providing me with information about instruments, materials and chemicals. I would like to thank also the team of chemical analytics for the ICP-OES and MS measurements, my thanks too to the workshop team of INM for their help in the design and construction of the photoreactor. Many thanks too to the team of project support and technology transfer department for their effort and commitment to prepare the patent application.

Prof. Dr. Michael Springborg share also my appreciation and thanks for allowing me to use the computational cluster of the physical and theoretical chemistry department and for the helpful discussions. I thank Stephan Kohaut and Nicolas Louis for the support and discussion regarding the simulation server and the simulations.

I would like to thank all friends inside and outside the INM who have foster my life through love, support, encouragement, refreshing moments and distractions. I thank all workers in INM, who have contributed to a friendly and respectful atmosphere and to establish a ground where it is possible to grow.

Contents

1	Theoretical background	16
1.1	Lambert-Beer law	19
1.2	Types of bands in the absorption spectra	19
1.3	Mechanistic principles of photochemical reactions	23
1.4	Bonding of copper complexes	24
1.5	Electronic properties and binding energies of solvated Cu(I) and Cu(II) ions.	25
1.6	Coordination in complexes with one ligand.	26
1.7	Coordination in complexes with more than one ligand	27
1.8	State of the art of copper complexes	29
1.9	Halide complexes	31
1.10	Diketonate complexes.	32
1.11	Pyridine complexes	34
1.12	Ring cleavage of copper complexes	37
2	Aims of the work	39
2.1	Aims and objectives.	39
2.2	Chemical strategy	39
2.3	Workflow.	40
2.4	Design of the complexes	41
3	Materials & Methods	42
3.1	Chemicals	42
3.2	Synthesis of complexes	42
3.3	Materials.	45
3.4	Methods	47
3.5	Computational methods	49
3.6	Procedures.	50
4	Characterization	51
4.1	Spectra and optical power of the light sources	51
4.2	Selection of solvents and sensitizers.	54
4.3	Selection of synthesized complexes for photoreduction.	58
4.4	Solubility	59
4.5	UV-Vis spectra, electronic configuration and electronic transitions.	60

4.6	Infrared spectra69
4.7	Mass Spectroscopy74
4.8	Charge decomposition analysis on complexes78
5	Kinetic of the reaction	81
5.1	Kinetic of copper complexes in alcohol solutions with alkyl and aryl sensitizers. .81	
5.2	Kinetic of reaction at different wavelengths89
6	Metallic depositions	94
6.1	EXD analysis of the deposited material on quartz and TiO ₂94
6.2	Depositions of systems irradiated with UV-LED's.96
6.3	Upscaling depositions of bigger areas98
6.4	Reduction mechanism	100
6.5	Reaction mechanism of the reduction of the CuPyr ₂ Cl ₂ complex	100
6.6	Reaction mechanism of the reduction of the CuPyr ₄ TBC complex	108
7	Conclusions	110
8	Outlook	112
	Annex A	115
	Annex B	116
	Annex C	117
	References	118

List of figures

Figure 1	Octahedral complex molecular orbital diagram of A. ligand with π and σ orbitals and B. ligand with only π orbitals.21
Figure 2	Electron transfer and energy transfer through electron exchange and dipole-dipole interaction between donor and acceptor molecules in excited states.24
Figure 3	Influence of oxygen in the photoreduction of Cu(II) to Cu(I) for $\text{Cu}^{2+}\text{Cl}^-$ in methanol-acetonitrile (10%v/v) irradiated at 313 nm and measured at A. 305 nm and B. 452 nm. $[\text{Cu}^{2+}]:[\text{Cl}^-]=1:8$, $[\text{Cu}^{2+}]=1 \times 10^{-3}$ M. -●- bubbled 15 min with Ar, -■- 60 min closed -◆- 90 min open to air.32
Figure 4	Schema describing the synthesis of heteroleptic copper complexes, synthesis is shown with 4TBC* as example of secondary ligand.43
Figure 5	Transmittance of used glass and fused quartz materials.46
Figure 6	Self constructed spectrometer. Incandescent bulb (G1), condenser lens (C), quartz aspheric lenses (As#), quartz beam splitter (B), UV-LED (L), quartz achromatic lens (Ac), monochromator (M), sensor/camera (S).48
Figure 7	Spectra of the <i>HBO 200W Hg Osram</i> lamp. A. reported spectrum from supplier ¹⁷⁸ , B. measured spectrum C. measured spectrum in the UV range.51
Figure 8	A. Measured spectra of the <i>Solar Simulator 1000W Hg LotOriël</i> lamp. B. measured spectra in the UV range.52
Figure 9	UV LED's spectra and their nominal optical output power reported by the supplier (mW).53
Figure 10	UV-Vis spectra of solvents tested for use with copper complexes.55
Figure 11	Molar absorption coefficient of alkyl and aryl ketones A. acetone and B. butanone C. benzophenone in 2-propanol.56
Figure 12	Molar absorption coefficient of A. Cu(II) acetylacetonate $\text{Cu}(\text{acac})_2$ and its ligand B. acetylacetonate (acac) in 2-propanol. Experimental (—), TDDFT B3LYP/6-31G(d,p) simulation (—).62
Figure 13	A. Molecular orbital diagram of $\text{Cu}(\text{acac})_2$. ■ = % Cu^{+2} , ■ = % $[\text{acac}]_2^{-2}$. B. Simulated UV-Vis spectra and molecular orbitals involved in the transitions with colors showing the phase.63
Figure 14	Molar absorption coefficient of A. Copper hexafluoroacetylacetonate $\text{Cu}(\text{hfacac})_2$ and its ligand B. Hexafluoroacetylacetonate (hfacac) in 2-propanol. Experimental (—), TD-DFT B3LYP/6-31G(d,p) simulation (—).64
Figure 15	A. Molecular orbital diagram of $\text{Cu}(\text{hfacac})_2$. ■ = % Cu^{+2} , ■ = % $[(\text{hfacac})_2]^{-2}$. B. Simulated UV-Vis spectra and molecular orbitals involved in the transitions with colors showing the phase.65
Figure 16	Molar absorption coefficient of A. Copper pyridine 4 tert-butyl catecholate $\text{CuPyr}4\text{TBC}$ B. Copper di-pyridine di-chloride ($\text{CuPyr}_2\text{Cl}_2$) and shifted simulated UV-Vis spectra. Experimental (—), TDDFT B3LYP/6-31G(d,p) simulation (—) C. Pyridine and D. 4 tert-butyl catechol (4TBC). All determinations were done in 2-propanol except $\text{CuPyr}_2\text{Cl}_2$ which was done in deionized-filtrated water.66

Figure 17	A. Molecular orbital diagram of $\text{CuPyr}_2\text{Cl}_2$. \blacksquare = % Cu^{+2} , \blacksquare = %[(Pyridine, Cl) $_2$] $^{-2}$. B. Simulated UV-Vis spectra and molecular orbitals involved in the transitions.68
Figure 18	Infrared spectra of A. acetylacetonate and B. $\text{Cu}(\text{acac})_2$. Experimental (—), literature (—) and simulation (—).70
Figure 19	Infrared spectra of A. hexafluoroacetylacetonate (hfacac) and B. copper hexafluoroacetylacetonate hydrate ($\text{Cu}(\text{hfacac})_2/\text{H}_2\text{O}$). Experimental (—), literature (—) and simulation (—).71
Figure 20	Infrared spectra of A. pyridine and B. $\text{CuPyr}_2\text{Cl}_2$. Experimental (—), literature (—) and simulation (—).72
Figure 21	Infrared spectra of A. 4 tert-butyl catechol (4TBC) and B. Copper pyridine 4 tert-butyl catechol (CuPyr4TBC). Experimental (—), literature (—) and simulation (—).73
Figure 22	MS spectra of copper(II) pyridine 4-tert butyl catechol CuPyr4TBC A. positive mode B. negative mode C. positive mode with 0.1% v/v formic acid D. negative mode with 0.1% v/v chloroform.74
Figure 23	Effluents of the equilibrium between $\text{CuPyr}_2\text{Cl}_2$ and $\text{Cu}(\text{4TSQ})_2$ complexes. Effluents detected in positive \oplus and negative \ominus mode in mass spectroscopy analysis.75
Figure 24	Possible products of the reaction detected with MS.77
Figure 25	Kinetic of the reaction of $\text{Cu}(\text{acac})_2$ with acetone in A. methanol B. ethanol and C. 2-propanol D. kinetic of deposition of copper followed with UV-Vis spectroscopy. The dashed line at 574 nm represents the plasmon resonance of metallic copper.82
Figure 26	Kinetic of the reaction of $\text{Cu}(\text{acac})_2$ with benzophenone in A. methanol B. ethanol and C. 2-propanol, D. kinetic of deposition of copper followed with UV-Vis spectroscopy. The dashed line at 574 nm represents the plasmon resonance of metallic copper.83
Figure 27	Kinetic of the reaction of CuPyr4TBC with acetone in A. methanol B. ethanol and C. 2-propanol D. kinetic of copper photodeposition followed with UV-Vis spectroscopy. The dashed line at 574 nm represents the peak of metallic copper.85
Figure 28	Kinetic of the reaction of $\text{CuPyr}_2\text{Cl}_2$ with acetone in A. methanol and B. ethanol, D. kinetic of copper photodeposition followed with UV-Vis spectroscopy. The dashed line represents the peak of metallic copper.87
Figure 29	Kinetic of the reaction of CuPyr4TBC with acetone in A. acetonitrile, B. chloroform and C. n-hexane followed with UV-Vis spectroscopy. The dashed line represents the peak of metallic copper.88
Figure 30	Kinetic of the reaction of CuPyr4TBC in ethanol with a TiO_2 layer over PET as sensitizer.89
Figure 31	Kinetic of copper complexes irradiated with different wavelengths in methanol sensitized with benzophenone A. CuPyr4TBC B. $\text{Cu}(\text{hfacac})_2$ C. $\text{Cu}(\text{acac})_2$90
Figure 32	Reaction kinetics at 574 nm irradiated with 275 nm UV-LED with different CuPyr4TBC/benzophenone (C/S) ratios A. concentration of complex 4.4×10^{-4} M and B. 3.6×10^{-4} M C. reaction kinetics of CuPyr4TBC/benzophenone (C/S) ratio below optimal D. reaction kinetics of CuPyr4TBC/benzophenone (C/S) ratio near optimal value.91

Figure 33	Ketone sensitized metallic deposition on A. irradiated window of a quartz cuvette B. removable quartz glass slide C. removable PET piece with TiO ₂ layer D. irradiated window next to the PET piece.94
Figure 34	Experimental setup for deposition of metal over a substrate piece inside the cuvette.	94
Figure 35	EDX analysis of deposited particles on TiO ₂ layer over a piece of PET. CuPyr4TBC complex in methanol sensitized with benzophenone A. sample spot on a copper particle B. sample spot on the substrate..95
Figure 36	Deposition of metallic copper at different wavelengths at equivalent concentration of complex and sensitizer. Total irradiation time 120 min.96
Figure 37	Microscopic images in A. bright field B. back light and C. dark field of deposited copper spots with different content of oxide.98
Figure 38	Irradiation of Cu(acac) ₂ and CuCl with 1000 W Hg lamp sensitized with benzophenone.	99
Figure 39	Absorption spectra and phosphorescent spectra of A. acetone and B. benzophenone taken from literature.. . . .	102
Figure 40	Schemes of techniques that can be implemented with different light sources A. direct laser writing B. photolithography.	114

List of tables

Table 1	Properties of copper related with bond formation.26
Table 2	Energies of the peaks emitted by the used Hg lamps.52
Table 3	Optical power of the used UV-LED's at different focusing spot diameters.53
Table 4	Oxidation and reduction potentials of acetone and benzophenone in the ground and triplet excited states.57
Table 5	Screening of the photoreducing activity of copper complexes sensitized with ketones by irradiation with the 200W Hg lamp.58
Table 6	Solubility of Cu(acac) ₂ , Cu(hfacac) ₂ and CuPyr4TBC in different solvents measured with UV-Vis.59
Table 7	Solubility of CuPyr ₂ Cl ₂ and CuPyr4TBC in methanol measured with ICP-OES..59
Table 8	Extended charge decomposition analysis of copper complexes Cu(acac) ₂ , Cu(hfacac) ₂ and CuPyr ₂ Cl ₂79
Table 9	Data of hydrogen abstraction reaction by benzophenone and potentials of the produced alkoxy radical.	108

Abbreviations and Symbols

T	Transmittance
E_i	Incoming light intensity
E_e	Outgoing light intensity
A	Absorbance
ε	Molar extinction coefficient
c	Concentration [mol/L]
l	Light path length [m]
h	Planck constant [$\text{m}^2 \text{Kg/s}$]
ν	Frequency [s^{-1}]
Δ	Crystal field band splitting energy [kJ]
H	Molar enthalpy [kJ/mol]
E_0	Standard potential [V]
ν	Stretching vibration [cm^{-1}]
δ	In-plane deformation vibration [cm^{-1}]
γ	Out-of-plane deformation vibration [cm^{-1}]
τ	Twisting vibration [cm^{-1}]
ω	Wagging vibration [cm^{-1}]
ρ	Rocking vibration [cm^{-1}]
σ	Standard deviation
R^2	Coefficient of determination
α	Statistical significance
UV	Ultraviolet
UV-Vis	Ultraviolet-Visible
IR	Infrared
EDX	Energy dispersive X-ray spectroscopy
MS	Mass spectroscopy
MO	Molecular orbital
LLCT	Ligand to ligand charge transfer
LMCT	Ligand to metal charge transfer
MLCT	Metal to ligand charge transfer
CTTS	Charge transfer to solvent
CID	Collision induced dissociation
ZEKE	Zero electron kinetic energy
CVD	Chemical vapor deposition
ALD	Atomic layer deposition
4TBC	4-tert-butyl catechol
PCA	Protocatechuic acid
PET	Polyethylene therephthalate

Abstract

The use of photolithography for metal interconnects below 0.2 μm continues to be unrivalled in resolution and precision as a fabrication technique in the microelectronic industry. Current photolithographic deposition of fine metal structures relies on the use of a photoresist.

A photolithographic technique that deposits metallic copper after UV irradiation from a solution containing a copper complex has been envisioned as a suitable technique to avoid the use of a photoresist and to attain a more profitable process. In this study commercial complexes containing acetylacetonate and hexafluoroacetylacetonate and synthesized copper complexes containing pyridine and catechol derivatives were tested and compared to improve the deposition efficiency of metallic copper by irradiation with UV light. Ab initio DFT was used to simulate the compounds structure, UV-Vis, IR spectrum and distribution of charge.

Metallic copper has been successfully deposited and the irradiation time has been decreased, complete coverage of copper was achieved after 15 min of irradiation with UV-LED's, using at least 50 times less concentration of copper complex than with commercial complexes. Copper complexes containing chloride and pyridine, and 4-tert-butyl catechol and pyridine showed the best deposition rates and higher quality of deposited material than β -diketonate complexes reported in literature.

Zusammenfassung

Photolithographie bleibt in Auflösung und Genauigkeit konkurrenzlos bei der Herstellung von schmalen Leiterbahnen ($< 0,2 \mu\text{m}$) in der Mikroelektronik. Die aktuelle photolithographische Abscheidung feiner metallischer Strukturen erfordert den Einsatz von Photolacken.

Im Rahmen der vorliegenden Arbeit wurde eine photolithographische Technik zur Abscheidung von metallischem Kupfer aus Lösungen eines Kupferkomplexes vorgeschlagen, um die Verwendung von Photolacken zu vermeiden und ein günstigeres Verfahren zu schaffen. Die Kupferphotoabscheidungseffizienz von kommerziellen Kupferkomplexen, die Azetylazeton und Hexafluoroazetylazeton Liganden enthalten, und synthetisierten Kupferkomplexen, die Pyridine und Benzocatechin Derivate enthalten, wurden verglichen. Ein Ab-Initio Dichtefunktionaltheorie-Verfahren wurde angewendet, um die Stoffstruktur, UV-Vis- und IR-Spektrum sowie die Ladungsverteilung zu simulieren.

Das metallische Kupfer wurde erfolgreich abgeschieden, bei der die Bestrahlungszeit reduziert wurde. Hierbei wurde Kupfer nach ca. 15 Minuten UV-LED Bestrahlung abgeschieden, bei der die Kupferkonzentration mindestens fünfzigmal weniger ist, als die kommerziellen Komplexe. Die Kupferkomplexe mit Pyridine und Chloride sowie die mit Pyridine und 4-tert-Butylbrenzocatechin zeigten die beste Abscheidungsrate und eine höhere Qualität des abgeschiedenen Materials als die in der Literatur untersuchten β -Diketonate Komplexe.

1 Theoretical background

Although several techniques exist to deposit metallic conductive material, like plating, CVD and PVD, the development of the microelectronic industry had led to the miniaturization of conductive metallic structures. Photolithography is currently the leading technology for the production of metallic structures below $0.2\ \mu\text{m}$ and is expected to remain the standard technique in the near horizon ¹. Current photolithographic techniques rely in the use of a photoresist for selective deposition, however the use of the photoresist introduces extra manufacturing steps which make the process inefficient; selective CVD depositions without photoresist is only possible on pre-patterned substrates ².

Aluminium, silver and copper are currently used as metal interconnects. Silver is quite expensive due to its low availability of 0.055 ppm on earth's crust compared with 27 ppm for copper and 84149 ppm for aluminum, therefore silver is expected to be replaced by copper, which is more cost-effective. Copper has 94% of the conductivity of silver but only at a fraction of its price. Copper has a lower resistivity than aluminium, $1.68\ \mu\Omega/\text{cm}$ compared with $2.82\ \mu\Omega/\text{cm}$ and is two orders of magnitude more resistant to electromigration, both characteristics are desirable in the semiconductor industry. Diffusion into silicon wafer is the major disadvantage of using copper as interconnect, this problem has been circumvented with the use of TiN barrier layers ¹. The use of an efficient photochemical reaction that selectively deposits metallic copper would be of great advantage for the fabrication of microelectronic devices, such a technique would be realizable with current fabrication methods with the advantage of not using a photoresist and using copper as cost-effective material.

First realization of a photochemical reaction producing deposition of metallic material was carried out in the field of photography, silver halides were used to deposit grains of metallic silver to develop an image. The large tendency of silver to reduce to its metallic form has been long used in analytic chemistry with the *Tollen's reagent* ³. Copper belongs to the same group of the periodic table than silver, but simple copper salts do not show the same photochemical reactivity as those of silver ⁴, moreover, the reduction potential of copper is much lower than silver which makes it more prone to oxidation.

First reports of photosensitive copper compounds consider copper halide ^{5,6,7} and copper oxide ⁴, nevertheless no direct metallic deposition was obtained from actinic irradiation of these compounds and the deposition efficiency of black precipitate, composed of copper oxides, was poor ^{8,4}. Early efforts were rather focused on the photo-precipitation of particles for image formation, and therefore the result of the irradiation of complexes in this early research stages gave black precipitates that must be later developed in a reducing bath ^{9,10,11,12}. A formulation

containing copper beyond simple inorganic copper compounds must be then used, such as copper coordination complexes.

Aimed research at metallic copper photodeposition from coordination complexes is first described with experiments performed with $\text{Cu}(\text{acac})_2$ complex^{13 14 15}. *Buono-core et al.* reports that with an unsensitized solution of $\text{Cu}(\text{acac})_2$ deposition of copper only happens after several hours of irradiation (>24 hours) with a Hg 140 W lamp and in very low yields (<0.04); while the sensitized photoreaction under inert atmosphere gave a black precipitate after 3 h and on continued irradiation (18 h) a copper mirror or copper particles. The unsensitized reduction was reported to happen through activation of a ligand-to-metal charge transfer band located around 230-250 nm¹³. The acetylacetonate ligand was proposed to detach from the complex in the form of a radical, which could be later scavenged as long as there was a specie with good hydrogen donating ability to form the acetylacetone¹⁴ hindering the re-complexation reaction. *Chow et al.* reported that the photoreduction of $\text{Cu}(\text{acac})_2$ could also be performed in benzene under hydrogen, showing that the singlet state of benzene which is not capable of hydrogen abstraction could participate in the reaction as an energy source and molecular hydrogen acted as the hydrogen source to produce acetylacetone from the ligand, therefore configuring an energy transfer mechanism between the excited molecule and the complex quencher¹⁶. Similar results as the $\text{Cu}(\text{acac})_2$ complex were obtained with Cu(II) polypyrazolylborate complex in alcohol solutions and THF sensitized with benzophenone, prolonged irradiation (>1h) was necessary to deposit copper particles in suspension¹⁷.

It was shown later that the photodeposition of copper could also be achieved by using 4-acylpyrazolone as ligand and that the deposition reaction could be extended to other metals like nickel, cobalt, palladium, platinum and uranium^{18 19}. *Hill* and colleagues also showed that copper could be deposited by lithography via a lamp and mask setup, and that the bulk copper resistivity could be achieved after annealing under H_2 atmosphere a deposit of copper from $\text{Cu}_2(\text{OH})_2(\text{O}_2\text{CC}_2\text{H}_4\text{OC}_2\text{H}_5)_4$, nevertheless no information was offered about the time needed for the photodeposition¹⁹. *Chu et al.* showed that the photodeposition technique could be used to deposit a film composed of various metals^{20 21}, showing that the strategies used to deposit one metal could be extrapolated to metal mixtures.

Other several diketonate complexes combining chain and bulkier ligands have been tried to increase the deposition of copper, however the product of deposition has a significant organic contamination, or is either CuO ²² or Cu_2O ²³; besides the irradiation times are considerably high (1.5 - 3.5 h). Similar results were observed with complexes studied by *Hill et al.*, where the reduction time for deposition of a copper film needed many hours of irradiation, the film was contaminated by the organic ligand and H_2 gas was used during the photoreduction process²⁴. *Hill et al.* enlightened a possible path for deposition of metal from a complex by photochemistry,

the strategy they used was focused on the activation of the reduction reaction only by the absorption of light by the copper complex, even though in some experiments H_2 was used while the photoreaction was taking place. Although the presence of H_2 could itself trigger the reduction reaction of the complex the reaction was treated as purely photochemical.

Much of the complexes used in the reported literature comprise the use of ligands in which the binding atom is oxygen, such as carboxylates²⁵, acetates²⁶, formates, oxalates²⁷ and diketonates²⁸. The focus on carboxylates might be because the ligand itself was conceived to work as a medium for sensitization but also as an electron donor for the reduction of copper, therefore it was necessary to have ligands which contained the carboxyl group which strongly absorbs in the UV region of the spectrum and can serve as electron donor because of the electron pair located in oxygen. As reported by *Foster* and colleagues, no definite trend of reduction can be observed in the carboxylic acids²⁷ and the same might extend to the other whole spectrum of organic ligands. What are the best ligands for copper photoreduction, remains to be a fundamental question that can only be explored by experimentation.

The exploration of photochemical systems to reduce copper have not only been limited to homogene catalyst or sensitizers of the reaction but also to heterogeneous systems, as investigated by *Foster* by irradiating several copper complexes in the presence of TiO_2 particles²⁷ and others²⁹. But it must be said from the beginning that the presence of a heterogeneous catalyst in solution and not as a substrate would be useless for the envisioned photolithographic process, because the metal is reduced as particle in solution.

Despite all efforts done to deposit metallic material from copper complexes which have been mentioned above, the complexes reported need long irradiation times to deposit metallic copper, which means that the energy input is considerably high and the reaction efficiency is low. There is room for exploring copper complexes that deposit metallic copper in few minutes of irradiation and with higher efficiency.

A brief introduction to physical and chemical concepts will be introduced in the following sections which are considered to be the background of the work developed during this study.

1.1 Lambert-Beer law

The absorption spectra is quantified as optical density and it is related with the amount of light transmitted through matter. The amount of light transmitted through a medium is called transmittance T and the amount of light absorbed is called absorbance A , these quantities correlate with the intensity of the incoming light E_i and the intensity of the transmitted light E_e , as shown in Eq. (1). The light transmitted through a medium is attenuated by the concentration of the light absorbing specie i , c_i , and the length of the light path ℓ in the medium; the attenuation of light by any material is quantified as the molar extinction coefficient ε_i , Eq. (2).

$$T = \frac{E_e}{E_i} = 10^{-A} \quad \text{Eq. (1)}$$

$$A = \sum_{i=1}^N A_i = \sum_{i=1}^N \varepsilon_i c_i \ell \quad \text{Eq. (2)}$$

1.2 Types of bands in the absorption spectra

The term band or absorption band refers to the observation of a peak or group of peaks in the UV-Vis spectra, a term often used in spectroscopy, and it is associated with the physical process of excitation or transition of an electron to a higher energetic level. Taking into account only the ligands and the metal in a complex, four types of bands can be found: metal centered bands, metal to ligand, ligand to metal and ligand centered bands. There are also bands related to the complex and the solvent. Due to the fact that the metal and the ligand coordination can be thought as an acid-basis reaction, the term charge transfer is more used when explaining the chemical redox behavior linked to the complex transitions, such transitions quite often lead to a change in the oxidation state of two species. Such change in the oxidation states can be cyclic, like in *Fenton* type reactions³⁰, or may lead to destabilization of the complex where no back reaction is possible, thus rendering them unidirectional.

A charge transfer transitions can be then defined as those which involve adding and removing one electron from the shell of two different moieties in the complex with a subsequent change in their oxidation state ± 1 . The assignment of absorption bands to charge-transfer bands is based on the assumption that the central atom and the ligand interact weakly thus they are quasi-independent moieties. If all of the ligands of the organometallic complex are the same, this is an homoleptic complex. In case of a ligand to metal charge transfer, the electron in this kind of complexes is assumed to come from any ligand, moreover the electron transfer is assumed to come

from a delocalized molecular orbital (MO) centered in the ligands ³¹. In contrast, in heteroleptic complex one may discern between the ligand that is participating in the electron transfer and the others.

1.2.1 Metal to Metal transfer bands

Also called ligand field bands, are bands originated in the transition between electrons of the *d* shell in metals, the name is given because of the influence of the ligands in the splitting of the metal bands. The transition is possible due to the splitting caused by the ligand field in the *d* shell, which also introduces a change in the degeneracy of the divided shell and is dependent on the coordination number and symmetry of the organometallic compound. Ligand field bands can be explained by the ligand field theory (LFT) and the crystal field theory (CFT) on a basic level. The underlying assumption of the theories is that the ligands are treated as point charges and that the repulsion between the electrons of the ligand and the central atom is maximum when opposing in the same axis. The distortion of the ligand in the complex *d* bands is called the band splitting (Δ).

The electronic transition between pure *d* bands is forbidden by symmetry selection rule hence such transitions are weak. For the d^{10} configuration, metal centered transitions are not possible and the splitting of the *d* band is thought to be independent of the ligands ³², thus indicating a difference between the expected spectra from Cu(I) or Cu(II) complexes.

Experimental studies show that the splitting of the *d* orbitals is also dependent on the nature of the ligand. The capacity of *d* orbital splitting can be arranged in a *spectrochemical series*. The series is only valid when the central metal ion of the complex has a normal oxidation state ³¹.

$CN > NO_2^- > Phen > Bpy > SO_3^{2-} \approx En > NH_3 \approx Py > NCS^- > H_2O \approx Ox^{2-} > ONO^- \approx OH^- > OC(NH_2)_2 > F^- > SCN^- > Cl^- > Br^- > I^-$

The octahedral configuration can be chosen as an example for understanding the molecular orbital mixing and its effect in the splitting. The molecular orbital theory assumes that the difference in splitting of the *d* orbitals in transition metal complexes with changing ligands is due to the differences in the σ and π character of the ligands. The effect of the σ character is not significant when compared with the influence of the π character. Figure 1 shows that the molecular orbitals of the complex are lowered in energy when ligand that have π bonding orbitals are introduced, a transition within the band arising from such splitting is only possible with Cu(II), that is when the *d* metal orbital is not completely filled, although such transition is in principle symmetry forbidden. Nevertheless, the mixing of the metal orbitals and the ligand can lead to a symmetry change in the upper *d* orbital and the transition can become partially allowed.

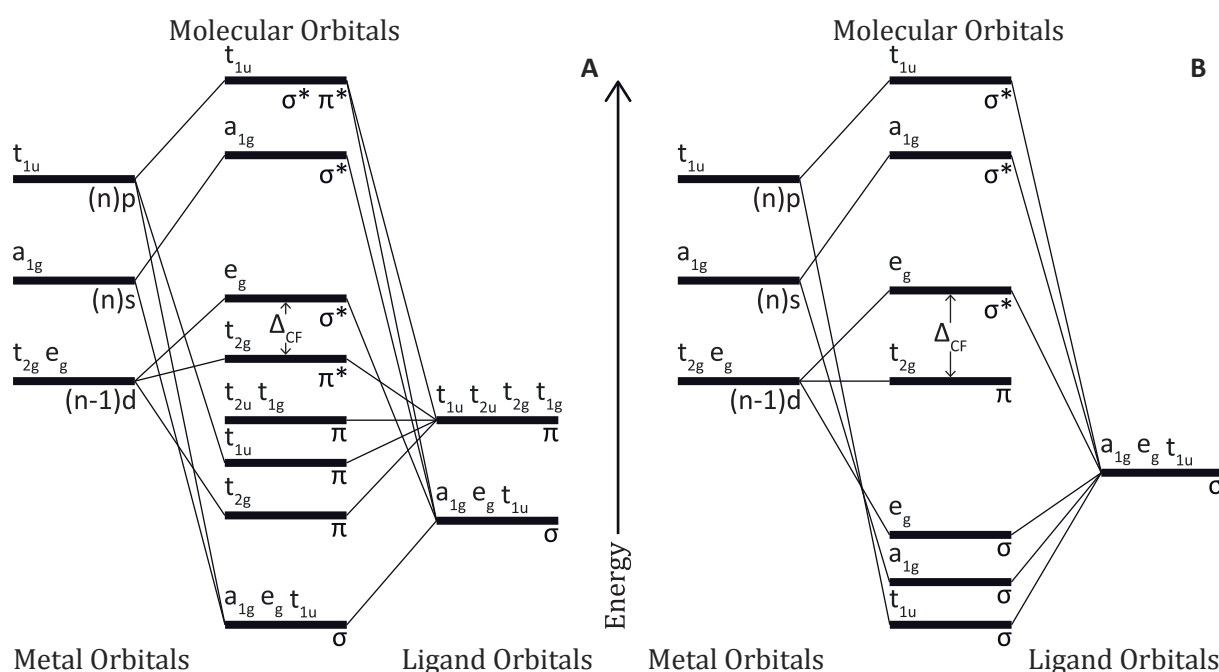


Figure 1: Octahedral complex molecular orbital diagram of **A.** ligand with π and σ orbitals and **B.** ligand with only π orbitals.

To understand the molecular orbital diagram in Figure 1 proposed by *Montalti et al.*³¹ it is key to know that Δ_{CF} orbitals are more localized on the metal and some are more localized in the ligand. The e_g and t_{2g} orbitals are mainly localized on the metal and are stabilized by the ligand. On the other side, the σ bonding molecular orbitals have more ligand character, this is the electron density is concentrated on the ligand. For σ antibonding molecular orbitals the opposite is true³¹. Also, if the ligand possess π orbitals, the stability or shift to higher or lower energies of the t_{2g} MO depends on the difference between the ligand π level and the t_{2g} level of the metal. The t_{2g} molecular orbital will have a higher stable energy the higher the π orbital of the ligand, and thus the Δ will be greater when compared with ligands without π orbitals. The opposite will happen in the case the π orbital of the ligand is lower in energy than the t_{2g} orbital of the metal. Obviously, in the case the ligand has high and low energy π orbitals (e.g. CN^- , CO , Cl^-) an equilibrium between these two aforementioned tendencies will be found. In case there are no π orbitals in the ligand (e.g. NH_3), the t_{2g} remains unshifted as a pure metal orbital³¹.

1.2.2 Ligand to Ligand bands (LLCT)

Also called ligand centered transitions, are transition between two ligand molecular orbitals, the molecular orbitals belong either of the same ligand or another ligand type³³. The inter-ligand transitions, do not change the charge distribution or bonding between the metal and the ligand directly³¹ and the metal causes a relatively small (less than 1000 cm^{-1}) perturbation of the transition energy³². Such transitions can be thought to lead to a charge redistribution between

the ligands in homoleptic copper complexes, or to oxidation and reduction of the different ligands in heteroleptic complexes. The transition would change the dipole moment, acidity, reduction or oxidation potential and the equilibrium geometry of the ligand, thereby having an influence on the metal-ligand dissociation constant. When heteroleptic ligand charge transfer is desired, the central atom can be used to induce and bridge the charge transfer, and it would be better called an inter-ligand rather than an intra-ligand charge transfer. Such bridged charge transfer between ligands has been observed when Zn(II) and Cd(II) are coordinated to an N-heterocyclic bidentate ligand such as phenanthroline and either a bidentate aromatic dithiolate and two monodentate benzenethiolate ligands³².

1.2.3 Ligand to metal charge transfer (LMCT)

Are electron transfers initiated in a molecular orbital mainly located in the ligand and finished in a molecular orbital mainly located in the metal. Such bands are observable preferentially when the complex has reducing ligands, those located at the right end of the spectrochemical series mentioned above, such as I⁻, Br⁻ and O_x²⁻. Such transitions are expected when oxidable ligands are bound with reducible metals. In the halide group, ligand to metal charge transfer will increase in energy following the sequence I⁻ < Br⁻ < Cl⁻ < F⁻ when the ionization potential or the ease of oxidation is considered³⁴. For a d⁹ configuration, the transfer occurs to the partially filled *d* sub-shell or to higher *s* or *p* orbitals. Filling of the *d* orbital shell due to an electron transfer or electron relaxation from an excited state due to a previous electron transfer would lead to destabilization of the complex.

1.2.4 Metal to ligand charge transfer (MLCT)

Are generally weak transfers that initiate in a metal and finish in a ligand orbital. Ligands with low lying empty orbitals of appropriate symmetry bound to metals, which are easily oxidized, will give rise to these type of transitions although less common than in the case of LMCT. Within the ligands that are unsaturated and show this kind of transitions are the acetylacetonates, and particularly aromatic ligands such as pyridine or oxidizing ligands as pyridine oxides through π anti-bonding levels³⁴.

1.2.5 Charge Transfer to Solvent

Are bands originated where the charge is transferred from either the metal or the ligand in the organometallic complex in the first coordination sphere to the solvent which is commonly located in the outer sphere of coordination. Intense absorptions in the spectra of Cu(I) complexes present the character of charge transfer to solvent transitions, CTTS. Such absorptions are observed in the ultraviolet spectra of complexes with halide and pseudo halide ligands. The energy of the charge transfer to solvent transitions is predicted by several models and derivations from the *Mulliken* charge transfer theory³⁵.

1.3 Mechanistic principles of photochemical reactions

There are two laws that govern the energetics of chemical reactions that react to light³⁶. The *Grotthuss-Daper* law, first formulated by the chemist Johann Dietrich *Theodor von Grotthuss* in 1817 and, later formulated independently by scientist and philosopher *John William Draper* on 1842, states that absorption of light by a compound is necessary for a photochemical reaction to take place. Absorption of light leads to an excited state of a molecule. The law could be restated as: an excited state caused by light absorption has to precede before any photochemical reaction can proceed.

The second law of photochemistry, called the Stark-Einstein law, first proposed by *Johannes Stark* in 1908 and later derived by *Albert Einstein* during his elaboration of the quantum light theory in 1913, states that for every photon that is absorbed by a compound one primary chemical or physical reaction is triggered. The law is restricted to light sources with moderate intensities, because lasers and flash light sources are known to cause biphotonic processes.

Figure 2 shows some of the possible interactions between an excited donor or acceptor in the excited state when they come in close contact. The possibility of an electron transfer between two molecules is favored in the excited state compared with the ground stated. The electron transfer lead to an oxidized and a reduced specie , while a dipole-dipole interaction and an electron exchange lead to and energy transfer between excited states between molecules.

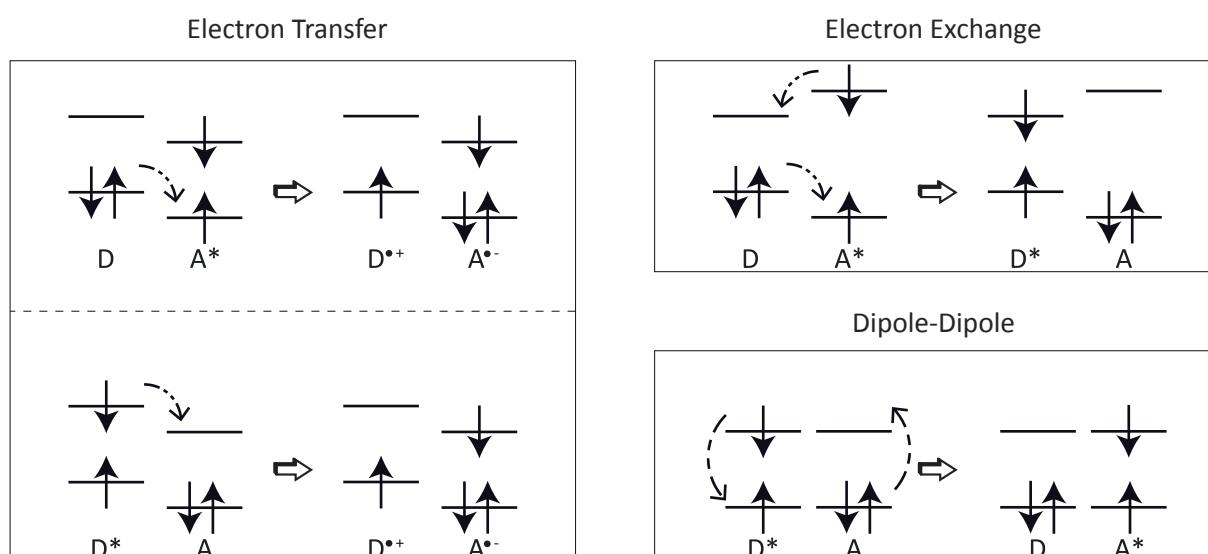


Figure 2: Electron transfer and energy transfer through electron exchange and dipole-dipole interaction between donor and acceptor molecules in excited states.

Photochemical reactions can be also grouped into outer sphere mechanism and inner sphere mechanism, photo-redox intra-molecular rearrangements and photo-redox elimination and addition reactions³⁶, these groups are concurrent. The outer sphere mechanisms specifically for organometallic complexes are those involving a reaction with a compound out of the coordination sphere, these types of reaction regularly involve the change of the oxidation state of one of the entities of the complex, mostly the central atom due to its cationic nature.

A photochemical reaction through the inner sphere mechanism involves the entities contained in a coordination sphere. Generally only the first coordination sphere is considered. In organometallic chemistry the inner sphere mechanism is related with a charge transfer or redistribution of charge between the central metallic atom and the organic ligand, inter-ligand charge transfers can be also regarded as an inner sphere mechanism.

A reaction may be considered a photo-redox intra-molecular rearrangement when the absorption of light leads to a conformational isomer of the molecule, the configuration change is caused by an increase or decrease in the oxidation state of the entities of the complex and in some cases may lead to a change in the coordination number but without detachment or elimination of the ligand.

Photo-redox elimination and addition reactions involve the change in the oxidation state of the central atom and change in the coordination number. There is no unequivocal relation between the oxidation and coordination number, although there is a tendency that the higher the oxidation the higher the coordination number³⁶.

1.4 Bonding of copper complexes

Experimental information has shown that the interaction of the copper cations with the organic ligand is not only electrostatic but it also has a covalent character³⁷. The covalent character of the bond is based on the dative interaction of the ligand with the 4s orbital of copper and the back bonding interaction of the *d* energy level of the metal with orbitals in the ligand with similar symmetry³⁸.

Other marked tendency of copper cations is their tendency to oxidize organic ligands they are bound to, thus reducing copper to a lower oxidation state and changing its electronic structure. Such behavior has been observed in Cu(II) and Cu(III) complexes^{38,39}. The ligands are left electron depleted and therefore prone to deprotonation, being the deprotonation of the bases the first step of the mechanism of proton transfer between bases bound to copper and explaining why in gas phase analysis and experiments deprotonated single charged complexes $[\text{CuL} - \text{H}]^+$ are more common than the double charged species $[\text{CuL}]^{2+}$ ³⁸.

1.5 Electronic properties and binding energies of solvated Cu(I) and Cu(II) ions

The electronic state of copper determines much of the behavior that is observed in complexes, regarding the configuration of the complex and possible excitation transitions or the oxidation reduction reactions with the ligands; but the behavior is modulated by the organic ligand. In terms of electronic transition and using the ligand field theory as approximation, no electronic transitions are expected for Cu(I) complexes as a ligand band, while transitions are expected for the Cu(II) because it has an unfilled *d* shell.

Other property of the final complex arising from the electronic configuration of the central atom is the multiplicity of the complex. The majority of organic molecules have a singlet electronic configuration, which means that the total net spin of the molecule is 0 and the multiplicity is 1, being molecular oxygen an exception worth mentioning, for which the ground state is a triplet. Cu(II) has an odd number of electrons, the net spin of the molecule is $\frac{1}{2}$ and the multiplicity is two, hence it is a doublet. The unpaired electron in Cu(II) conditions that the complexes found with organic ligands containing hydrogen, carbon, nitrogen and oxygen will have an odd configuration of electrons, or in theoretical chemistry argot, will be an open shell complexes. Equivalent Cu(I) complexes would have an even configuration of electrons and Cu^0 complexes would be open shell complexes, but coordination complexes with Cu^0 are very unusual⁴⁰.

Table 1: Properties of copper related with bond formation.

Copper oxidation	Electronic state	Ground term	Ionization energy (eV)
Cu ⁰	[Ar]3d ¹⁰ 4s ¹	¹ S _{1/2}	7.73
Cu(I)	[Ar]3d ¹⁰	¹ S ₀	20.29
Cu(II)	[Ar]3d ⁹	² D _{5/2}	36.84

Table 1 shows that Cu(II) has a high second ionization potential, this observation is important because it is directly related with observation in mass spectroscopy analysis, where transition metals with high ionization potentials lead to detection of the deprotonated complex with the metal (ML-H)⁽¹⁺⁾ rather than a double charged complex ML⁽²⁺⁾ ⁴¹. The high ionization potential can be thought as a preface of the high electronegativity showed when the copper cation is bonded, the ionization potential is related with the binding energy of the complex, for example in the cases of thiouracil complexes the binding energies were found to vary with the second ionization potential of the central atom and the first ionization potential of the ligand ⁴².

The ease of reduction of copper is related with the reduction potential. The reported reduction potentials, enthalpies of reaction and second temperature coefficients (dE₀/dT) ^{43 44 45} of copper in its most common oxidation states are:



It is known that the disproportionation constant of $k_{\text{dis}} = C_{\text{Cu(II)}}/C_{\text{Cu(I)}}^2$ is 10⁶ L/mol, and point the large tendency of Cu(I) to disproportionate in acidic and neutral aqueous solutions contrary to Cu(II) which cannot disproportionate to Cu(III) and Cu(I) in same conditions ⁴⁴. The reduction reactions show there is a positive reduction potential to reduce the copper ions towards metallic copper, the *Gibbs energy* of the reaction will be negative meaning that all reduction processes are spontaneous.

As indicated by the redox potential, the main difference between the copper cations is their electrophilicity, as reported by ³⁸ Cu(II) tends to bind with more lone pairs than Cu(I), reported experiments with thiouracil derivatives and copper ions ⁴², show the tendency of Cu(I) to coordinate with the lone pairs located either in oxygen or sulfur while Cu(II) coordinates preferentially with the two electron pairs from two oxygens, the preference towards oxygen rather than sulfur can be explained by the fact that in the coordination oxygen and Cu(II) act as a hard

base-acid.

Rappaport et al. points out other aspects regarding the different reactivity of the cations, and that it is the ability of Cu(I) to react with hydrogen and play the role of a carrier or intermediate between a molecule donating an hydrogen and a molecule accepting it ³⁸. Studies with 2-propanol-Cu⁺, ethylenediamine-Cu⁺ and alkene-Cu⁺, explained the systematic loss of H₂ by introducing Cu(I) as a carrier in the reaction mechanism, thus suggesting that the Cu(I) is not only an intermediate of the reactions but also participates actively in further steps of the reaction with molecules that can donate hydrogen, which can be expected for alcohols.

1.6 Coordination in complexes with one ligand

When coordinating with one ligand the copper ions will try to adopt a coordination geometry in which the coordination environment reduces the *Pauli repulsion*. For Cu(I) this is done when the coordination is linear and is associated with a *sd* hybridization ^{46 47}. An angular arrangement must involve the 4p and 3d_{xz} orbitals, and it is discouraged because the higher energy of the 4p orbital hybridization is less effective and a the decrease in repulsion is smaller ^{48 38}. Glycine coordination with copper can illustrate the preferences of coordination and interaction depending on the oxidation state of copper. The preference of Cu(I) for bisligated structures is evident in the theoretical experiments performed with glycine, diglycine and tryglycine ^{49 50} where the coordination number never exceeded n=2, although multiple coordination sites with oxygen and nitrogen and different bite angles are available for coordination. When Cu(I) coordinates with glycine the twofold coordination is formed through the amino group and the carbonyl ⁵¹, this behavior has been confirmed and also observed in other amino acid complexes ^{52 53}.

Differently from Cu(I), when Cu(II) interacts with glycine it interacts rather with its zwitterionic form through the oxygens ⁵¹, the same was observed in alanine where Cu(I) interacts with nitrogen and oxygen while Cu(II) interacts only with oxygen atoms ⁵⁴. When urea and thiourea are coordinated with Cu(II) the change was rather in the angle and the length of the bonds with oxygen and nitrogen ⁵⁵. As a side effect of the coordination of Cu(II) with the carboxylic group in amino acids, the proton transfer to the amino group is favored; the proton transfer toward the amino effect has been proven by the destabilization of the zwitterionic structure though substitution of H for Cl in the amino group ⁵⁶.

The association of Cu(II) with oxygen is systematically favored because oxygen acts as a point of accumulation of negative charge, behaving as a hard base which is more reactive towards a hard acid as Cu(II) ⁴². The large second ionization potential of copper, causes Cu(II) the behave with most organic bases rather in the form Cu(I)-Ligand⁺• than in the form Cu(II)-Ligand, which means that it tends to displace the charge towards itself leaving the ligand electron deficient

³⁸. The charge transfer from the base towards the metal ion seems to be strongly favored in monodentate complexes, whereas for bidentate structures the spin density is more delocalized ³⁸.

1.7 Coordination in complexes with more than one ligand

When dealing with the coordination of copper ions with several ligands it is observed that Cu(I) prefers a bis-ligated linear arrangement while Cu(II) prefers a tetra-coordinated tetrahedral or planar configuration. The bond length of the complexes is dependent on the Pauli repulsion between the electron of the central atom and the ligand, in the case of pyridine the bond length of the neutral complex $\text{Cu}(\text{Pyr})_2$ has a longer Cu-N length due to the electron repulsion between the nitrogen lone pair and the 4s electron when compared with the charged complex $\text{Cu}(\text{Pyr})_2^+$. The six coordinated configuration is discouraged in Cu(II) complexes by a Jahn-Teller distortion, which is found for example in pyridine complexes where four of the Cu-N bonds are 195 pm in length, and the remaining two are 375 pm ³⁸. Similar results of Jahn-Teller distortion have been observed in aqueous copper ^{57 58 59} and acetone ⁶⁰ complexes. The preferred formation of tetrahedral over octahedral complexes is exemplified by the $[\text{Cu}(\text{acetone})_n]^{2+}$ complex where maximum abundance in the gas phase is found when $n=4$ ⁶¹. The coordination of Cu(II) has been investigated with alcohols, methanol, ethanol, 1-propanol, 2-propanol, also with ketones, acetone, butanone, 2-pentanone, 2,4-pentanedione and other organic bases such as pyridine, pyrazine, tetrahydrofuran, dioxane, benzene, benzonitrile and ethylenediamine ⁶⁰.

Wright and colleagues found that the most stable coordination for many of the complexes of Cu(II) was found with a tetrahedral arrangement. More interestingly they found that a charge transfer would be more probable in small coordination environments where the coordination number was lower than 4, and that the possibility of a charge transfer declined very fast beyond a coordination number of six. The charge transfers for a coordination number of four was found with the loss of one ligand and the charge transfer was an LMCT. In the case of the triplet excited copper pyridine complex, the LMCT was found to be the dominant decay mechanism. One general outcome of the study is the suggestion that the probability of finding a charge transfer is related with the coordination environment.

For Cu(I) the intensity distributions recorded for the interactions with acetone, pyridine, tetrahydrofuran and acetonitrile are clearly dominated by an intense $[\text{CuL}_2]^+$ unit, followed by a rapid decline in the intensity measured for complexes of larger size ³⁸. Additional evidence of the linear coordination of Cu(I) can be found with $\text{Cu}(\text{dimethyl ether})^+$, $\text{Cu}(\text{glycine})^+$, CO , H_2O and NH_3 , $\text{Cu}(\text{imidazole})^+$.

For Cu(II) the preferred tetra coordination is evidenced in Cu(glycine)²⁺⁶², Cu(diaquaguanine)²⁺⁶³. Interestingly both of the complexes have a tendency to coordinate with a water molecule in the equatorial position, but the coordination bond of the water molecule is affected by a positive Jahn-Teller distortion. Interestingly, the capability of tetrahedral coordination by copper with phenanthroline based ligands has been used to synthesize novel catenanes for the design of molecular machinery; this research has been subjected to the latest nobel prize⁶⁴.

Alcohols were found to build also a coordination sphere around copper. For 1- and 2-propanol the maximum coordination intensity is reached when 4 molecules are coordinated. For ethanol and methanol, up to 8 ligands can be coordinated in the first and the second coordination sphere of copper, the formation of hydrogen bridges favors the formation of the second coordination sphere. Ammonia^{65 66 67} and water⁶⁵ were also found to coordinate with copper central atom with coordination number n=6, but also were capable of forming a second coordination sphere via hydrogen bonds⁶⁰.

The reduction from Cu(II) to Cu(I) has also been found to change the coordination number and geometry. In copper methionine complexes it was found that the preferred coordination of Cu(II) with the methionine ligand was a tetra coordinate complex while the Cu(I) ion preferred a tri coordinated complex, where the complex is hydrated and bent⁶⁸, the triple coordination is possible in most of the studied structures due to the high flexibility of the ligand which can coordinate Cu(I) though S, N and O atoms and behave therefore more as a chelate. Studies with histidine complexes (3-(1H-imidazol-5-yl)-N-[2-(1H-imidazol-5-yl)ethyl] propanamide with Cu(II) and Cu(I), showed that while Cu(II) forms a tetra-coordinated deformed square planar complex, for Cu(I) the most energy favorable complex is found when the coordination number is decreased to two^{69 70}.

1.8 State of the art of copper complexes

When taking into account the oxidation state of the central atom without considerations of the detachment of the ligand or the reaction of the organic substrate or ligand, the reactions of copper complexes can be grouped in: a) photoreduction of Cu(II) to Cu(I), or Cu(I) to Cu⁰ or disproportionation from Cu(I) to Cu(II) and Cu⁰, b) photo-oxidation Cu(II) to Cu(III) and c) oxidation reduction Cu(II)-Cu(I)-Cu(II) with reversible photoreduction to Cu(I)⁷¹ or *Fenton* type reaction^{30 72} where the complex acts as a redox catalyst. The reaction products of copper complexes involve in many cases the formation of radicals of copper complexes or ligand radicals which participate in further stages of the reaction³⁵, generation of CO₂ and generation of Cu(I) or Cu(II), mostly observed in small copper complexes. In terms of the physical mechanism of reaction, the complex can photo-sensitize or photo-assist the reactions⁷¹.

The change in the oxidation state of copper in organometallic complexes triggers isomerization, oxidations, substitutions and double bond migration reactions in a variety of organic moieties ⁷¹. Focusing on oxidation reactions, the copper complex can participate directly as reducing partner or act as a catalyst in the oxidation of the organic moieties. Oxidation of alcohols to aldehyde has been observed with $\text{Cu}(\text{acac})_2$, aryl ketones and as chain reaction in the photoreduction of $\text{CoCl}(\text{NH}_3)_5]^{2+}$, $\text{Co}(\text{edta})^-$, $\text{Co}(\text{acac})_3$ ⁷³ and photoreduction of paraquat ⁷⁴ with $[\text{CuL}(\text{PPh}_3)_2]^+$ for $\text{L}=\{2,9\text{-dimethyl-1,10-phenanthroline}\}$, alkyl alcohol oxidation by copper halogen complexes, oxidation and oxygenation of phenols in the presence of CuL complexes $\text{L}=\{\text{Cl}, \text{Br}, \text{I}, \text{NO}_3, \text{bpy}, \text{phen}\}$ ⁷¹, Cu -morpholine ⁷⁵, copper-ammonia ⁷⁶, CuCl_2 ⁷⁷, CuCl in pyridine ⁷⁸, $\text{Cu}(\text{NO}_3)_2$ ⁷⁷, $[\text{Cu}(\text{NCO})(\text{Pyr})_2]_2\text{H}_2\text{O}$ ⁷⁹ and CuSO_4 ⁸⁰, decarboxylation of 2-hydroxy acids to α -keto acid (lactic acid) with CO_2 elimination in the presence of CuSO_4 through a *Fenton* reaction mechanism ⁸¹, ligand oxidation with production of CO_2 through a *Fenton* reaction mechanism for $\text{Cu}(\text{L})\text{L}=\{\text{malonato}, \text{acetato}, \text{oxalato}\}$ ^{82 83 71}.



A primarily photo-sensitization scheme is represented by Ch. (5)-Ch. (8) as a general example of photo-reaction of copper complexes. The scheme considers the open shell molecules as analogue to their radicals. Initially the open shell complex absorbs the light and leads it to an excited state complex Ch. (5), the excited complex can undergo radical decomposition ⁸⁴ leaving the complex in a closed shell reduced form and creating a ligand radical Ch. (6), because of the change in the electronic configuration that leads copper to a closed shell configuration in its +1 oxidation state, the complex is unstable, leading to further decomposition into metallic copper and the ligand Ch. (7). The reduction to metallic copper can undergo also by direct disproportionation reaction from the intermediate copper complex Ch. (8).

A wide literature search was made on reviews of copper complexes that could be helpful to achieve the photoreduction of copper ^{35 85 71 36 86}. Copper halide, pyridine and β -diketonate complexes were found to be the most promising because a direct reduction to metallic copper could be observed in the reaction mechanism. Carboxylate complexes were disregarded because the photoprocess mainly involves the formation of copper ions and decarboxylation, as in the copper acetate complex photoreaction ⁸⁷. Another example is the copper malonate, photochemistry, which involves a decarboxylation of the ligand and reduction to $\text{Cu}(\text{I})$ but without further detachment

and reduction to metallic copper^{82 83}. The use of homoleptic copper carboxylates was disregarded also by the fact that, as explained in previous sections, oxygen has the tendency to stabilize Cu(II), in fact Cu(I) carboxylates are stabilized when a tertiary ligand as phosphine or amine is introduced^{88 89 90}. Just recently a study found that a Cu(I) heteroleptic carboxylate complex could be reduced to metallic copper upon prolonged irradiation times of several hours⁹¹.

No tendency towards reduction to metallic copper has been observed neither in copper phenanthroline nor in copper ethylenediamine complexes³⁵. In copper phenanthroline, the transition of the electron to the low ligand levels of the phenanthroline ligand oxidizes Cu(I) to Cu(II)⁹². Transitions observed in the spectra of phenanthroline complexes has been assigned to long lived metal-ligand charge transfer or mixed MLCT states according to DFT calculations^{93 94} and not LMCT. Phenanthroline complexes show a cyclic redox reaction involving the central atom +1 and +2 oxidation states and the ligands with a subsequent change in the symmetry of the molecule from tetrahedral to planar. In the cycling reactions the detachment of the copper central atom from the coordination cage has not been reported, the high stability is explained due to the cage effect of the organic moiety. In the case of ethylenediamine, the ultraviolet irradiation of Cu(en)₂²⁺ produces CO₂ and NH₃. These products probably originate in secondary redox reactions of a primary Cu (I) ligand-radical.

1.9 Halide complexes



The copper chloride system can be used to exemplify commonly observed reactions in copper halide systems. In the set of equations Ch. (9) - Ch. (12)^{71 35} the copper complex is not reduced to metallic copper, the halogen stays bound to the copper forming a product of lower oxidation state. Common products or intermediates of the irradiation of copper halides are Cu(II)⁸⁷, Cu(I), polyhalo copper complexes with and without production of H₂^{95 96 97 98 85 99}, aldehydes or ketones as products of alcohol oxidations⁸⁷ and solvated electrons^{96 97 98 85}. Cu(II) halide complexes are usually reduced reversibly to cuprous halides Ch. (9), the reversibility might be explained by the presence of an oxidizer in solution such as oxygen. The complexes react further with other organic moieties in the system configuring a Fenton type mechanism involving the oxidized and

reduced forms of the complex. Halogen radicals are formed in the process and have been detected experimentally ⁷¹. Further transformations in the system have been also attributed to reactions of the organic substrate with halogen radicals, chlorine or bromine ¹⁰⁰. Primary alcohols, methanol and ethanol are oxidized to aldehydes, t-butyl alcohol, n-butyronitrile and tetrahydrofuran are transformed to haloderivatives, both routes expressed in Ch. (11) as oxidation or chlorination of the scavenger. The molar absorbances of the halide ions increase with the following tendency $\text{Cl}^- > \text{Br}^- > \text{I}^-$ that can be attributed, mostly to the change in the polarizabilities of the ions ⁸⁵.

The chlororadical anion $[\bullet\text{Cl}_2]^-$ has been detected in transient absorption experiments of Cu(II)chloride ⁷¹. It is formed by the reaction of the chloride radical with free chlorine in solution Ch. (10) and is a powerful oxidizer $E_0=2.3 \text{ eV}$ ¹⁰¹. The scavenger participating in the reaction with the $[\bullet\text{Cl}_2]^-$ radical might be Cu(I) with a quenching constant $k_1=2.7 \times 10^8 \text{ dm}^3/\text{mol s}$ or Cu(II) $k_2=1.7 \times 10^8 \text{ L/mol s}$ and is definitely not quenched by Li^+ , Cl^- , O_2 or the solvent. The oxidation of the copper chlorine complex depends on the ability of Cu(II) to be reduced, more interestingly, the results show that the driving force for oxidation as well as the quantum yield of Cu(I) production decrease when the number of chlorine ligands is increased, and that the efficiency of the reaction is highly influenced by the concentration of oxygen in the media, as shown in Figure 3 where the absorbance of the Cu(I) ion is decreased because of different degrees of exposure of the solution to oxygen ⁷¹. The reduction of the complex to metallic copper is possible by disproportionation reaction of the ions or the halides with and without irradiation ¹⁰².

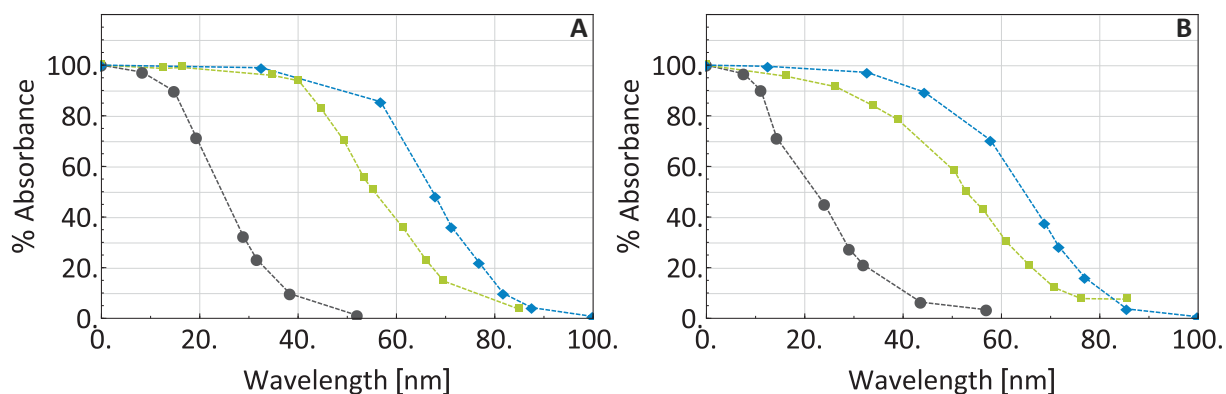
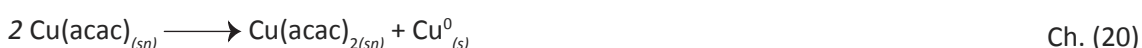
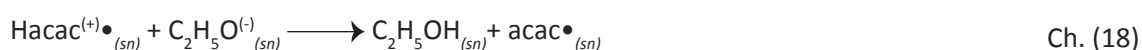
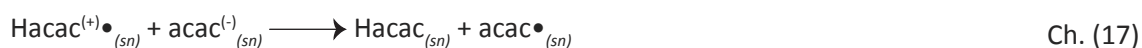
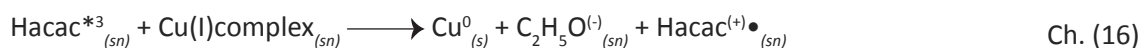
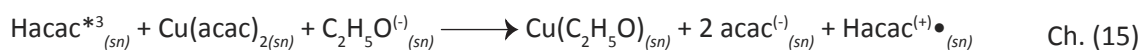
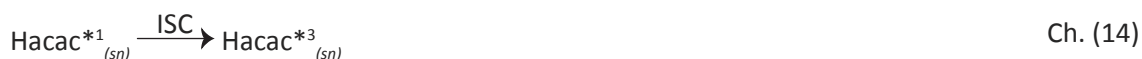


Figure 3: Influence of oxygen in the photoreduction of Cu(II) to Cu(I) for $\text{Cu}^{2+}\text{Cl}^-$ in methanol-acetonitrile (10%v/v) irradiated at 313 nm and measured at **A.** 305 nm and **B.** 452 nm. $[\text{Cu}^{2+}:\text{Cl}^-]=1:8$, $[\text{Cu}^{2+}]=1 \times 10^{-3} \text{ M}$. –●– bubbled 15 min with Ar, –■– 60 min closed –◆– 90 min open to air.

The photo-redox behavior in terms of light absorption, reported in Figure 3 for chlorocupric complexes ⁷¹, is in agreement with assignments of the high intensity bands to LMCT transitions. Irradiation of copper chlorine complexes in butanol showed an isosbestic point at 240 nm which is due to the concentration decrease of Cu(II) and the increase of Cu(I) ⁷¹. For Cu(I) Cl complex the yield of Cu^0 is rather small and the kinetic of reaction slow and the reduction to metallic copper was found to be competitive with the formation of H_2 when it was observed ^{85 99 103 104}.

1.10 Diketonate complexes

Among the β -diketonates, acetylacetone has been widely studied because it can form a complex with almost all transition metals^{105 106 107 108 109 110}. Copper acetylacetonate, $\text{Cu}(\text{acac})_2$, is one of the most intensely studied copper diketonate complexes along with its fluorinated derivative copper hexafluoroacetylacetonate, $\text{Cu}(\text{hfacac})_2$,^{111 112 113}, and has been successfully used to deposit metallic copper. The complexation of acac and Cu is spontaneous, such behavior has been attributed to the acid-complex ability of the chelate and it is explained by its keto-enol equilibrium^{28 114 115}. First studies with $\text{Cu}(\text{acac})_2$ showed that it can be reduced to Cu^0 ¹¹⁶ and suggested that the reaction can be accelerated in the presence of a sensitizer; later studies confirmed the reduction acceleration in the presence of an aromatic ketone in hydrogen donating solvents^{15 112}. Studies performed by *Marciniak* and colleagues, informed that $\text{Cu}(\text{acac})_2$ did not form a ground state complex in alcohols, therefore suggesting that the complex had photochemical activity on its own and that it was fully coordinated¹¹².



Intense investigations of these kind of complexes have been done to elucidate the mechanism of the reactions^{28 15 117 118}, nevertheless the mechanism of reaction and sensitization is not yet completely clear. The studies have gradually enlightened the steps that must be involved in the reaction mechanism based on experimental observations, a proposed mechanism by¹¹⁸ is shown in set of equations Ch. (13) - Ch. (20). Reaction Ch. (13) and Ch. (14) represent the light absorption by the hydrogenated acetylacetone (Hacac) and its inter system crossing triplet state formation. The reaction mechanism proposed in literature are sensitized either by the ligand itself¹¹⁸ or by an added substance¹⁵, in both cases the sensitizer is a ketone. The studies also agreed that the sensitized photoreaction lead to higher reaction rates.³⁵ based on previous studies by¹¹⁷. *Lintvedt et al.* focused on the role of the sensitizer and illustrated a possible interaction between

the excited state sensitizer and the copper complex¹¹⁷, which is represented in the reaction Ch. (15) and points to the key interaction of a triplet state excited ketone with the complex to yield a Cu(I) complex, in this case represented by a Cu(I)ethoxy complex. In the review by *Ferraudi* and college the solvent reaction was kept obscured and played implicitly the role of serving as a dielectric medium where the exciplex and ion couple formation was possible³⁵. Prolonged irradiation, longer than 2 hours in most cases, of Cu(acac)₂ complex yielded an unstable black precipitate^{116,28}, which reacted with triphenyl phosphine to give acetylacetonato bis(triphenylphosphine)Cu(I), the black precipitate was observed previous to the reduction to copper metal and the lag phase observed between the first appearance of the black precipitate and the metal, was suggested as indicative that the reduction to copper metal proceeded through a disproportionation reaction, represented in equation Ch. (20). The disproportionation reaction can involve any Cu(I) complex, the use of Cu(acac) in the equation instead of the Cu(I) complex formed with the deprotonated solvent in Ch. (15) is a reminder that the solvent can be exchanged by any free ligand in solution¹¹⁹. Along with the appearance of Cu⁰, the protonated ligand Hacac was also observed in solution¹¹⁶ thus proving that a hydrogen abstraction reaction was participating in the reaction mechanism. β-Diketonate copper complexes sensitized with benzophenone were then studied in protic solvents¹¹², and showed the active role played by the solvent by serving as hydrogen donor to regenerate the sensitizer and by possibly forming an intermediate complex with copper. The charge neutralization of the radical cation product of copper reduction reaction is done either by a deprotonated solvent or ligand in Ch. (17) and Ch. (18). The regeneration of the radical sensitizer is finally done by the solvent in Ch. (19) by hydrogen abstraction. The yield of the reaction was observed to increase with the hydrogen donating ability of the solvent and was always higher for Cu(hfacac)₂ than for Cu(acac)₂¹¹². Copper β-diketonates complexes Cu(acac)₂ and Cu(hfacac)₂ have been identified and measured as quenchers of the triplet state of benzophenone, the quantum yields were determined in methanol, ethanol and 2-propanol³¹, no sensitization was observed when the sensitizers were aromatic hydrocarbons or fluorene³⁵.

The reduction potential of several β-diketonate complexes, among them Cu(acac)₂ and Cu(hfacac)₂ were measured by *Denison* and *Lintvedt et al.*^{120,117}. Reported polarography measurements shows a higher reduction potential for Cu(hfacac)₂ (+0.038) than for Cu(acac)₂ in 75% aqueous dioxane and showed that the reduction potential of the complex is linearly dependent with the yield of the reactions. Recent measurements reported by *Denison et al.* found that the reduction potential for Cu(acac)₂ to Cu⁰ has a greater range of variability than in the case of Cu(hfacac)₂, the reduction potential of Cu(hfacac)₂ was found to be higher than that of Cu(acac)₂ when the concentration of the complex was 0.2M and in the pH range of 3.5 – 5.5 approximately, their report suggests that if the before mentioned conditions are not met for Cu(hfacac)₂ then copper oxide will be the product of the reaction and not metallic copper. Because of the intermediate formation of the oxide, the hfacac ligand was labeled as a poor electron donor for

copper and the reason was attributed to the presence of electron withdrawing fluorine. However, no relation has been found between the energy of the electron transition, associated with a charge transfer, and the ligand reduction potential³⁵. Moreover, in a photochemical reaction, the true reduction potential of the excited specie is rather different to that of its ground state; the zero spectroscopically energy and the excitation energy that increase its reducing or oxidizing ability must be taken into account.

1.11 Pyridine complexes

Copper pyridine complexes have been explored to detect the presence of copper ions by colorimetry¹²¹ and more interestingly due to their catalytic oxidative activity in various organic substrates^{78 122 123 124}.

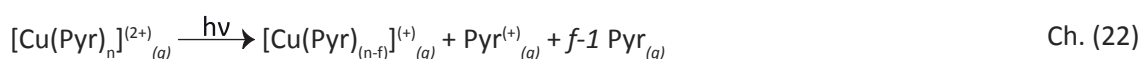
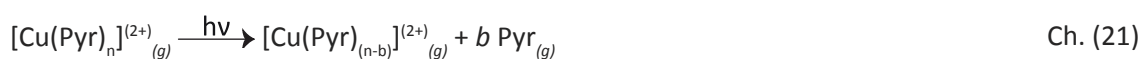
During the oxidative polymerization of 2,6-xylenol with copper nitrogen complexes as catalysts,¹²² observed that the amine copper complex was active when oxygen was present in solution while the copper pyridine complex was active even in the absence of oxygen, the activity of copper pyridine was attributed to the possibility of pyridine of accepting a π -electron, oxygen was said to function as a final electron acceptor configuring the constellation of a *Fenton* reaction. Most importantly, the source of the electrons to trigger the reduction was pointed to be a 2,6-xylenol radical, showing the possibility of electron transfer of copper pyridine complex with phenol radicals.

The photo reducing properties of copper pyridine complexes have been subjected to investigation without an oxidation partner. Recently photo dissociation experiments were performed in $[\text{Cu}(\text{Pyr})_n]^+$ ($n=1-5$) complexes, and the fragmentation of the monomer $\text{Cu}(\text{Pyr})^+$ was studied by irradiation with UV light in the range 220-284 nm¹²⁵. During irradiation, pyridine⁺ was detected as a product and very defined peak in the mass spectrogram, when the expected product was Cu(I) because the ionization of Cu (7.72 eV) is lower than that of pyridine (9.25 eV). The presence of Pyr^+ is a strong evidence that there is a ligand to metal charge transfer configuring a photo induced dissociative intra-molecular charge transfer. Collision induced dissociation (CID) experiments, where an Xe ion beam triggered the dissociation reaction in $\text{Cu}(\text{Pyr})^+$ ¹²⁶, resulted in the endothermic loss of a neutral pyridine molecule. Zero electron kinetic energy (ZEKE) measurements performed in neutral CuPyr complexes¹²⁷ delivered an ionization energy of 5.418 eV, 2.308 eV lower than the ionization potential of Cu^0 , which indicates a considerable stabilization of the complex upon ionization with respect to Cu^0 . Comparatively, studies performed in ammonia copper complexes, no ligand to metal charge transfer was observed in the photo dissociation¹²⁸ nor in the CID experiments¹²⁹, just the dissociation of NH_3 . Comparison of the binding energy and the ionization energy of neutral CuL and charged CuL^+ copper ammonia (56.6 kcal/mol 5.761 eV)

and Cu-pyridine (65.5 kcal/mol, 5.418 eV), shows that the Cu-NH₃ bond is stronger than the CuPyr bond and that upon ionization of CuPyr is more stable than that of CuNH₃.

In irradiation experiments at 280 nm with [Cu(Pyr)_n]²⁺ (n=4-7) complexes, carried out to investigate if either the dissociation of the complex or inter-ligand band transitions was the preferred process, it was observed that the preferred process was the loss of neutral pyridine without evidence of dissociative charge transfer^{130 131}. Similar results were obtained when the complex was irradiated with higher wavelengths 450-1000 nm¹³². The most stable coordination number was found to be n=4. But when a smaller complex [Cu(Pyr)₃]²⁺ was irradiated with UV light, a small signal of Pyr⁺ was observed along with stable [Cu(Pyr)₂]⁺ complex showing evidence of ligand to metal charge transfer. The investigation performed in CuPyr_n⁺ and CuPyr_n²⁺ complexes where done in the gas phase nevertheless, the joined results and calculations of Cu⁶¹, Ag¹³⁴ and Au¹³⁵ complexes in the gas phase follow the same trend as in the condensed phase, showing that copper complexes are resistant to hydrolyzation and have higher reduction potentials than Ag and Au complexes^{136 130}. Wu *et al.* 2006 performed infrared multiphoton dissociation experiments (IRMPD) experiments on [Cu(Pyr)₄]²⁺ complexes and found that the most stable configuration was D_{4h}, moreover DFT calculations predict that the D_{4h} symmetry is at least 0.35 eV lower in energy than the D_{2h} and D_{2d} symmetries¹³⁷. They also found that the complex releases a neutral pyridine ligand upon sequential absorption of IR photons leaving [Cu(Pyr)₃]²⁺ as a product that could not be further dissociated with the CO₂ (910 – 1090 cm⁻¹) at 560 mW.

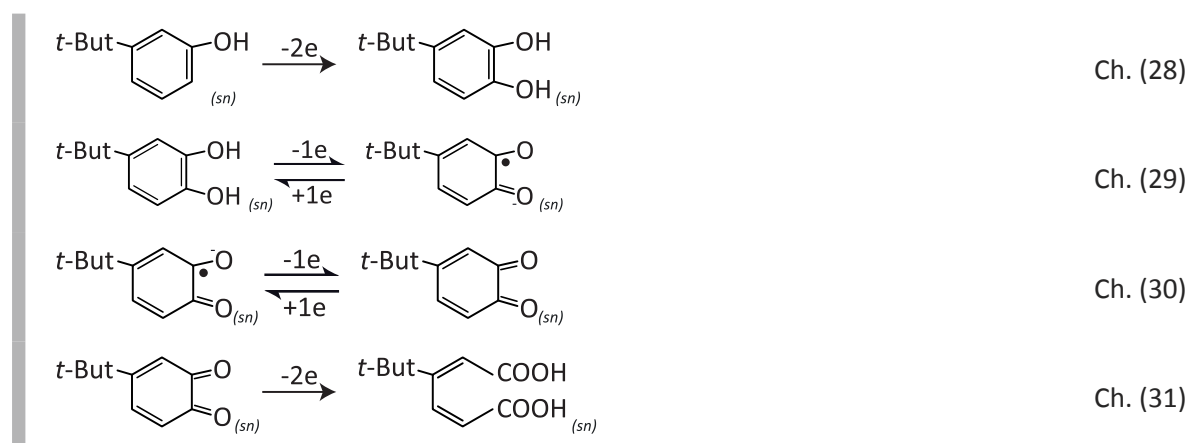
The similar charge transfer phenomena was observed with CuPyr₂Cl⁺ complexes¹³⁸ where the loss of a Cl• leaves the same reduced complex Cu(Pyr)₂⁺. Similar results were observed when to the pyridine ring a methyl was added in *para* position to give 4-picoline; where [Cu(picoline)₃]²⁺ photo dissociated into (4-picoline)⁺ and [Cu(picoline)₃]⁺³⁸. Polarographic studies performed in various CuPyr₂Cl₂ complexes¹³⁹, showed that electron withdrawing substituents lower the stability of the Cu-N bond thus increasing the reduction potential of the complex and that reduction potentials were higher in alcohol solutions than in aqueous solutions.



The presented set of equations Ch. (21) - Ch. (27) constitute the results obtained by ¹³⁰ ¹²⁵ ¹³⁸ respectively, summarizing the behavior of copper pyridine complexes. Photodissociation of copper pyridine complexes where the number of coordinated pyridine is $n \geq 4$ lead to loss of neutral pyridine molecules Ch. (21), if $n=3$ a slightly charge transfer from pyridine to the remaining copper pyridine complex is observed Ch. (22), if the coordination with pyridine is reduced to $n=1$ with Cu(I) as observed by ¹²⁵, the photodissociation produces a Pyr^+ thus leaving copper reduced Ch. (23). The set Ch. (24)-Ch. (27) proposed by ¹³⁸, shows that collisional activation of CuPyr_2^+ , where Cu has oxidation state +1, results in the loss of neutral pyridine Ch. (24). If copper pyridine is coordinated with Cl in form of $\text{Pyr}_2\text{CuCl}^+$, the reaction triggers the lost of Cl^\bullet with reduction of the complex to Pyr_2Cu^+ , as shown in Ch. (26), in the same complex the lost of a pyridine instead of Cl does not lead to reduction of the complex Ch. (27). Ch. (25) shows the possible hydrolyzation reaction of CuPyr^+ under their experimental conditions.

1.12 Ring cleavage of copper complexes

Multiple copper catechol complexes have been studied to understand the mechanism of reaction of copper containing enzymes, such as tyrosinase and catechol oxidase, responsible of the oxidation of catechols to benzoquinones ¹⁴⁰ ¹⁴¹ ¹⁴² ¹⁴³ ¹⁴⁴.

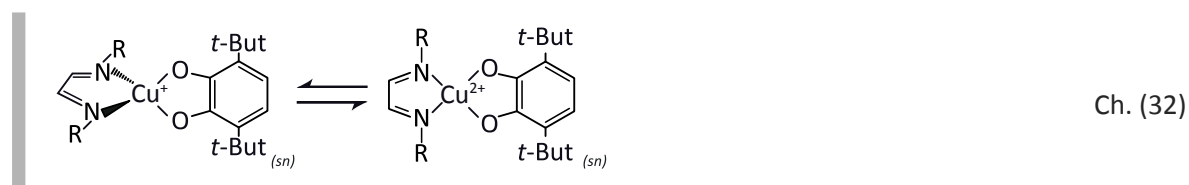


The oxidation of phenol in the equation set Ch. (28) - Ch. (31), transitioning benzendiol, semiquinone, quinone and finally alkyl dicarboxylic acid, shows the electrons that must be transferred during the process, and that could be potentially used for reduction of other substances. Because of its reduction capabilities benzendiols, such as hydroquinone and benzoquinone are common additives in the preparation of developer solutions in the photographic industry ¹⁴⁵.

The ring cleavage reaction of catechol to muconic acid has been observed with other transition metals, but copper is a prominent case ³⁸. *Tsuji et al.* observed the oxidation of catechol by CuCl in pyridine solutions, to produce traces of cis,cis muconic acid, the reaction conversion

yield could be improved by the addition of methanol to produce only muconate methyl ester with no muconic acid ¹⁴⁶, the reaction proceeded with oxygen intake. *Tsuji et al.* investigated the reaction with labeled oxygen, showing that oxygen was incorporated in the acid carbonyl rather than in the ester carbonyl ¹⁴⁷. The oxidation of phenols to produce muconic acid, proceeded through catechol formation Ch. (28), with higher yields obtained using CuCl instead of CuBr ¹⁴⁶. *Rogic et al.* showed that the oxidation and cleavage reaction could be performed under anaerobic conditions, also that the reaction could be done with catechol or quinones and most importantly that the role of oxygen in the reaction was to oxidize the copper complex to its Cu(II) form ¹⁴⁸.

Brown et al. performed experiments on the oxidation of catechol and the cleavage of aromatic rings with heteroleptic copper complexes containing oxygen and nitrogen atoms, their results show the presence of a Cu-catechol species during the oxidation process, pointing that the N-containing counter ligand largely influences the reaction rate and that the reaction rate of the ring cleavage is rather low ¹⁴⁹.



The tautomerism between catechol and quinone Ch. (29) - Ch. (30) is translated to the complex equilibrium as a change of oxidation of the copper central atom ^{150 151} in Ch. (32). The similarity between the energy levels of the quinone ligand and copper is particularly strong and the change in the oxidation state of the central atom, configures an intra-molecular electron transfer ¹⁵². Any copper catechol complex has to be viewed as an equilibrium of benzoquinone, catecholate and semiquinone triggered by delocalization of charge, each with a distinctive structural feature.

2 Aims of the work

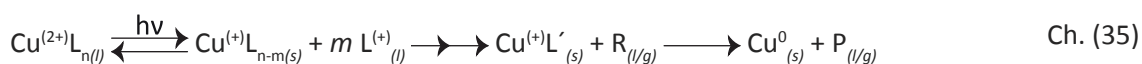
2.1 Aims and objectives

The project is intended to improve the deposition of metallic copper by photolithography, given the few and inefficient complexes available for that end. During fabrication of chips and electronic components, the creation of metallic interconnects for power distribution and signal transmission comprises a bottleneck. Most of the commercial formulation for deposition copper structures comprises the use of pastes, which limit the resolution of the deposited structures to micrometers, the available studies and patents for deposition of metallic copper by photochemistry need of prolonged irradiation times and low reproducibility.

The aim of the project is to efficiently achieve a film of metallic copper on a desired substrate, glass or polymer by photoreduction. To achieve the aim it is necessary to prepare a coordination copper compound which is sensitive to photoreduction by UV light. The copper compound must be easy and safe to handle, if possible easy to prepare, to react specifically in the UV region (100-400 nm) and not to react in the visible region of electromagnetic spectra, if possible. The copper complex should have a high quantum yield for deposition of metallic copper and should deposit copper faster than available copper complexes. The deposited material should have a conductivity as near as possible to the bulk conduction of copper.

2.2 Chemical strategy

Different strategies can be used to achieve the reduction of copper from a copper complex. The reduction process can be triggered by the absorption of energy from light by a copper complex, the photoreaction can be mediated by another substance than the copper complex, or the reduction reaction can be aided by light irradiation. The mentioned strategies, which will be individually explained, can be stated in chemical equations as follows



Ch. (33) represents the most complex strategy, a pure inner sphere mechanism in which the following processes must happen in order to achieve reduction. The first process is direct absorption of light by the ligand, followed by a ligand to metal charge transfer (LMCT), the charge transfer leading to destabilization of the complex by reduction of the central atom and change in the coordination sphere of copper. In case the complex has Cu(II), two LMCT transitions must be available to accomplish the reduction to Cu⁰. The ligand should have a decreasing affinity with reduced forms of copper, to hinder the complexation counter reaction.

The second strategy Ch. (34) comprises the use of a sensitizer (R), with this strategy either the sensitizer or the complex ligand can be excited after UV irradiation. The sensitizer or the ligand are expected to reach an excited state or to serve as an electron source or channel; with this strategy the steps of excitation and electron transfer are expected to be caused by different molecules. The ligand might serve as an electron source while the second substance might act as a sensitizer. The complex must act as the final electron acceptor, and within the complex the electron is expected to be held in an orbital with more metal character, thus reducing copper.

Finally the last strategy Ch. (35) comprises the use of a photoreaction and a redox reaction. In the first step of the reaction deposition of a Cu(I) complex is expected to happen after irradiation with UV light, for this to happen the chemical potential of the Cu(II) and Cu(I) complexes have to be very different. After deposition of the reduced copper complex a redox reaction will take place by addition of a reducing agent. This strategy covers up the deposition of copper oxides with further reduction in a reducing atmosphere.

2.3 Workflow

In detail the following studies should be carried out in the search of a suitable complex for photoreduction:

- Synthesis of various copper complexes for photoreduction reactions
- Screening of the complexes with irradiation experiments to test them for photoreducing activity
- Characterizing the properties of complexes and sensitizers relevant for measuring the efficiency of copper deposition. Characterizing the cupreous deposited material
- Systematic studying photoreduction reactions using different solvents, sensitizers and light sources, to gain insight about the optimal reaction conditions
- Simulating the copper complexes using *ab initio* methods to study the electronic transitions and charge transfer from the ligands

- Optimizing the deposition process by manipulating the conditions of reaction
- Upscaling the system for bigger area depositions. Which means using larger volumes of solutions, larger areas of irradiation and light sources with higher energy output

2.4 Design of the complexes

The main idea behind the design of the complexes was first to increase the availability of electrons around the central atom and to find a ligand in which a ligand-to-metal charge transfer (LMCT) could be facilitated. The electron density around the central atom was increased by complexing atoms with electron pairs and aromatic molecules, considering them as a possible sources of electrons or as electron bridges ^{117 153 154}. Nitrogen was preferred over oxygen as coordinating atom because the lower stability constants of nitrogen complexes compared with oxygen complexes, a tendency that is also observed in chelates ^{155 156}. The use of nitrogen ligand was encouraged by reports ¹⁵ where reduction to Cu(I) was also detected when some nitrogen ligands were used, for example in copper complexes with 1,10-phenanthroline and 2,2'-dipyridine, where the presence of Cu(I) was confirmed by reaction with triphenylphosphine, suggesting that the mobilization of charge due to bonding could reduce the central metal atom, thus making a lower oxidation state complex and therefore simplifying the reduction till metallic copper. The use of monodentate nitrogen ligands was preferred because of their lower stability compared with polydentate ligands due to the chelate effect and also in order to decrease the production of organometallic derivatives ⁷⁹. Cage complexes were avoided based on the experimental results of *Blades et al.* ¹⁵⁷ which states that multidentate cage nitrogen ligands lead to stabilization of multiple charge complexes. *Blades* also found that pyridine ligand specifically could promote the reduction of the central atom in an organometallic complex ¹⁵⁷.

The use of catechol molecules as one of the ligands was decided based on the fact that it is an electron rich molecule as an aromatic molecule and also because literature has shown that some copper nitrogen complexes could cleave the aromatic ring and oxidize the compound ¹⁴⁸, therefore rendering the electron contained in the aromatic ring available for copper to reduce. The idea was to make the complex reduction auto-catalytic; a ligand could detach from the complex and further participate in the reduction of copper as a reagent and source of electrons. The synthesis of an heteroleptic copper complex can be supported on report suggesting that oxidation reaction of organic moieties has been improved by the presence of N and O atoms ¹⁵⁸.

Copper acetylacetonate $\text{Cu}(\text{acac})_2$ and copper hexafluoroacetylacetonate $\text{Cu}(\text{hfacac})_2$ were used in this work as first attempts to achieve fast and efficient metallic copper photo-deposition and later as comparison with synthesized complexes. $\text{Cu}(\text{acac})_2$ and $\text{Cu}(\text{hfacac})_2$ are usually used as precursors in CVD and ALD processes to achieve copper films ¹⁵⁹.

3 Materials & Methods

3.1 Chemicals

Chemicals used for synthesis were bought from commercial suppliers Fluka, Roth, Merck, Acros Organics, Fisher chemicals and Sigma Aldrich. 2-Propanol, and methanol were supplied by the Central chemical storage from Saarland University. THF \geq 99.9% Riedel de H en. Protocatechuic acid \geq 97%, ethanol \geq 98.9%, acetone $>$ 99.8% were obtained from Roth. Diethyl ether $>$ 99.5%, pyridine \leq 100% were obtained from Merck. Benzophenone \geq 99%, 3(3,4) dihydroxyphenyl Alanine \approx 98%, 3 hydroxytyramine hypochloride \geq 98.5% and 4-tert-butylcatechol \geq 98% from Fluka. Acetylacetone \geq 99.3%, hexafluoroacetylacetone \leq 100%, copper hexafluoroacetylacetone hydrate (\leq 1% hydration), copper acetylacetonate 97%, copper powder 99%, copper(I) chloride \geq 99% and copper(II) chloride 97% were obtained from Sigma Aldrich.

Copper(I) chloride was purified by washing with cold acetic acid and ethanol absolute in an Ar inert atmosphere. Solvents were not dried and were degassed with the freeze thaw pump procedure. TiO₂ particles for TiO₂ layers over PET were synthesized in the institute by a lyothermal method using titanium(IV) propoxide, and were provided prepared.

3.2 Synthesis of complexes

The route used for the synthesis of the precursor complex CuPyr₂Cl₂ was followed as reported in the literature ^{160 161}. It was performed in an inert atmosphere. The reaction of Cu(I) or Cu(II) chloride with pyridine in Ar atmosphere always gave a blue precipitate and excess of pyridine. No changes in coloration of the liquid excess of pyridine were observed.

The synthesis of the complexes was carried out adding first the ligands with a lower formation constant and saturating the coordination sphere of the central atom to obtain a homoleptic precursor complex as exemplified in synthesis of similar heteroleptic copper complexes ¹⁶². The primary ligand used for the catechol complexes was pyridine. Later the secondary ligand was added to the solution in the desired stoichiometry to displace the monodentate ligand and form a heteroleptic complex. The synthesis of the complex takes into advantage that the equilibrium constants of the ligands in terms of the bonding atom are different, the bonding equilibrium constant with oxygen tends to be higher than that of nitrogen. Due to the chelate effect the

catechol type ligands will have a higher preference and displace the monodentate nitrogen ligands. Copper complexes, in solution are labile toward ligand substitution, and the formation of new species is driven thermodynamically rather than kinetically⁸⁶. Mixed ligand copper complexes containing N and O donor atoms are more stable than homoleptic complexes containing oxygen as donor atoms^{163 164 165} which favors the formation of an heteroleptic complex as product.

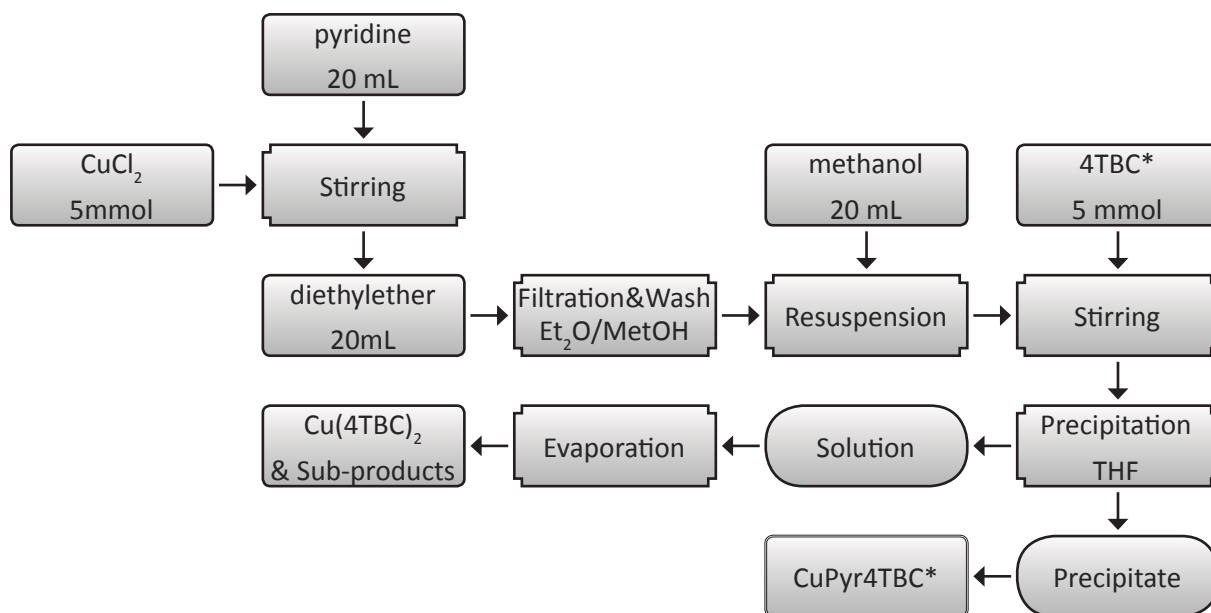
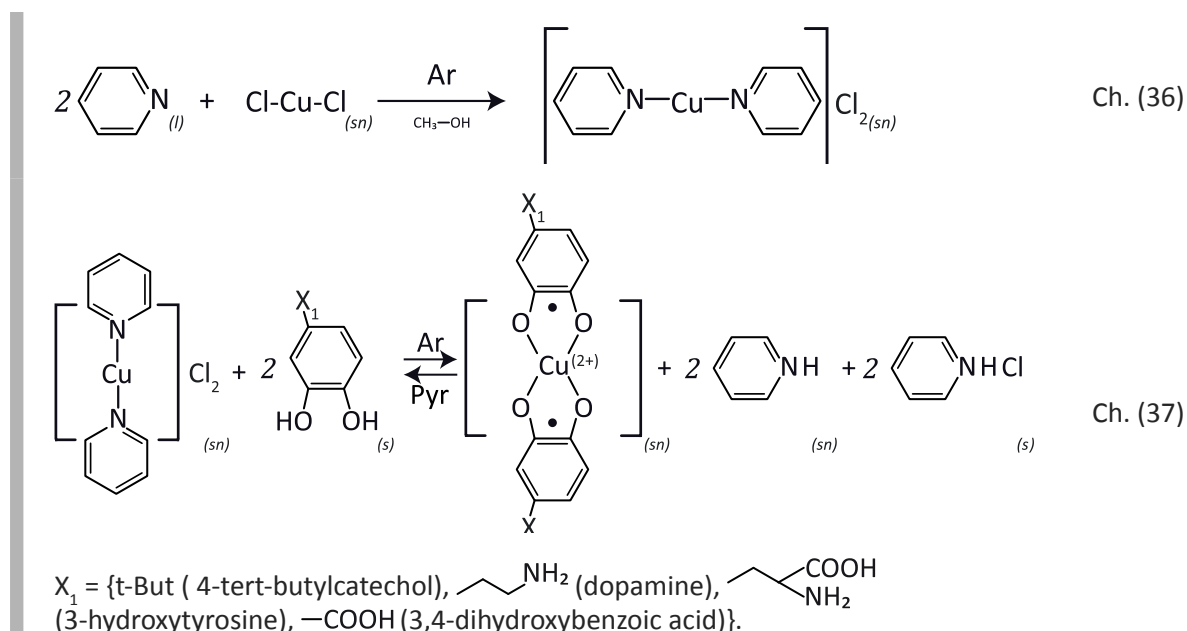


Figure 4: Schema describing the synthesis of heteroleptic copper complexes, synthesis is shown with 4TBC* as example of secondary ligand.



Equations Ch. (36) shows the synthesis of the precursor complex $\text{CuPyr}_2\text{Cl}_2$ which has a characteristic blue color. Tertiary complexes were prepared from precursor complex following the schema in Figure 4 with 4TBC, dopamine, 3-hydroxytyrosine and protocatechuic acid Ch. (37).

3.2.1 Synthesis of CuPyr₂Cl₂

The synthesis was carried out according to a literature procedure¹⁶¹. 502 mg (3.7mmol) of CuCl₂ were solved in 20 mL of degassed pyridine under Ar atmosphere and stirred for 20 min. 15 mL of diethyl ether were added slowly and a blue solid precipitated. The solution was filtrated and washed with degassed diethyl ether and ethanol. Yield 99% blue powder.

IR (ATR)[cm⁻¹] = (h, 1601, νPy), (h, 1489, νPy), (h, 1448, νPy), (m, 1152, δCH), (h, 1081, δCH), (m, 1040, δCH), (h, 760, δPy), (h, 642, δPy).

3.2.2 Synthesis of CuPyr4TBC

The synthesis was done taking as reference literature procedures^{166 167}. Under Ar atmosphere 685 mg (2.3 mmol) of CuPyr₂Cl₂ were suspended in approximately 15 mL of degassed methanol and stirred for 20 min after which 446 mg (2.6 mmol) of 4TBC were added. A dark green solution and a blue precipitate was observed in the reaction flask. The reaction was left to react for 45 min, after which THF was added, a pale blue solid and a dark solution were obtained. The excess of solvent from the dark solution was rotoevaporated at 60 rpm, 40°C, 261-110 mbar. The pale green-blue solid was washed with degassed THF and kept in a flask filled with Ar. ATR infrared spectra is shown in characterization section. Yield 64%.

IR (ATR)[cm⁻¹] = (h, 1601, νPh/Py), (h, 1489, νPh/Py), (h, 1438, νPh/Py), (s, 1366, νPh), (m 1218, νCO Ph), (s, 1153, δCH), (h, 1081, δCH), (h, 1043, δCH), (h, 759, δPy), (h, 644, δPy).

3.2.3 Synthesis of CuPyrPCA

The synthesis was done following a protocol adapted from literature^{166 167}. Under Ar atmosphere 510 mg (3.8 mmol) of CuCl₂ were added to excess of pyridine and agitated for 30 min. Degassed diethyl ether was added and the formed blue precipitate was washed with more diethyl ether. The recovered solid was suspended in 20 mL of degassed ethanol after which 1543 mg (10 mmol) of PCA were slowly added. The solution was stirred for 20 min after which a yellow solution and a blue precipitate were formed. The yellow solution was filtrated and the solids were washed with degassed THF and stored in a Ar filled flask. Yield 40%.

IR (ATR)[cm⁻¹] = (m, 1365, δOH), (h, 759, δPyr), (h, 686, γOH), (m, 644, δPyr). No C=O vibrations.

3.2.4 Synthesis of CuPyr(DOPA)

The synthesis was done taking as reference literature procedures^{166 167}. 500 mg (3.7 mmol) of CuCl were suspended in 17 mL of pyridine, the excess of solvent was evaporated. The remaining green substance was dissolved with 30 mL of methanol and stirred for 20 min. 1919 mg

(10 mmol) of 3-hydroxytyramine hypochloride. The reaction was left overnight. A brown solution was obtained, which was rotoevaporated 36 rpm, 55°C, 80 mbar, yielding a brown sticky substance. Yield 57%.

IR (ATR)[cm⁻¹] = (s, 3365, ν NH₂), (s, 1604, δ NH₂), (h, 1472, ν Ph), (m, 1261, ν CO), (s, 1190, τ NH₂), (h, 1174, ν CO), (m, 813, γ Ph), (h, 760, δ Pyr), (m, 644, δ Pyr).

3.2.5 Synthesis of CuPyr(DL-DOPA)

The synthesis was performed using literature procedures as reference ^{166 167}. 500 mg (5 mmol) of CuCl were added to an excess of pyridine under Ar atmosphere, the solution was stirred for 20 min. The excess of solvent was distilled and the remaining green substance was dissolved with 30 mL of degassed methanol. 1994 mg (9.4 mmol) of DL-Alanine were loaded in the flask. The green solution turned to a dark purple solution. The solution was rotoevaporated and a dark purple powder was recovered. Yield 39%.

IR (ATR)[cm⁻¹] = (s, 1350, δ OH), (s, 1200, ρ/τ NH₂), (h, 1604, δ NH₂), (h, 687, γ OH), (m, 759, δ Pyr), (s, 643, δ Pyr), (h, 1247, τ CH₂), (h, 1448, δ CH₂). No C=O vibrations.

3.3 Materials

3.3.1 Inert gas equipment

For the inert gas operations and synthesis of complexes, a glass vacuum inert gas manifold equipped with a dual stage rotary vane pump model *DS 302 1 Ph* from the company *Varian* was used. Ar 5.0 from the company *AirLiquide*), or N₂ from a liquid nitrogen storage tank were used as inert gas, most of the experiments were carried out using Ar 5.0. *Baysilone*[®] medium viscosity was used as joint lubricant. Silicone septa and silicone tubing bought from the company *Carl Roth* and *Gastight*[®] syringes from the company *Hamilton* were used for material transfer operations.

3.3.2 Glass materials and quartz cuvettes

For UV photodeposition experiments in small scale 3.5 mL two windows and four windows fused silica cuvettes with 10 mm optical path from the company *Hellma Analytics* were used for small volume experiments. The cuvettes are specified for anaerobic applications and come with a Silicone Septa and *14 GL* cap. The transmittance of the cuvettes was measured when received with the *Cary 5000* UV-Vis spectrometer, the measured transmittances comply with the specifications of the company. Transmittance was always measured prior to experimentation and after the cleaning procedure to check the cleanliness and the suitability of the cleaning.

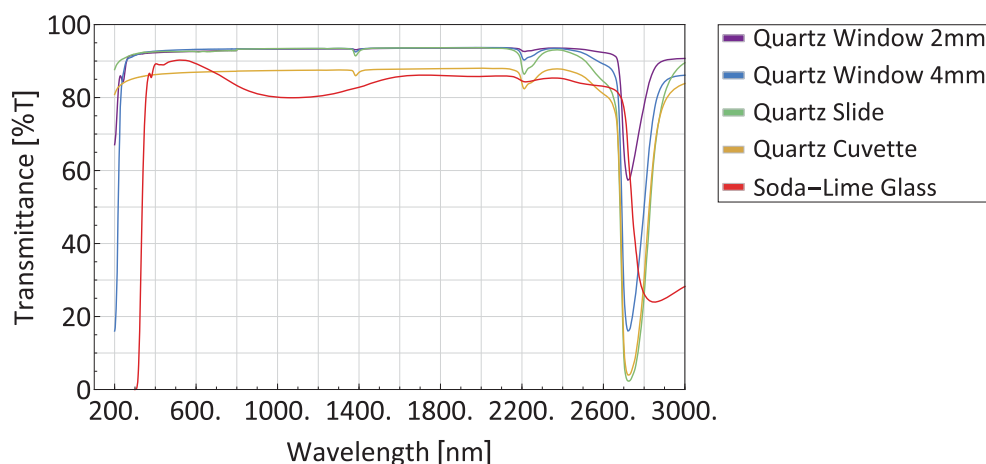


Figure 5: Transmittance of used glass and fused quartz materials.

3.3.3 Photoreactor

For photodeposition experiments in large scale, in terms of larger volumes and areas, a 1000 Watt Hg lamp and a self-designed photoreactor were used. The photoreactor was constructed in the workshop of the Leibniz Institute for New Materials. One window of the photoreactor is made of quartz and the other window of Soda-lime glass, the interior of the photoreactor is made of polytetrafluoroethylene (PTFE), the sealing elements are perfluoroelastomer FFKM 60° shore O-Rings from the company *Alfred Strauch* and the sealing caps are *Duran® 14 GL* from the company *Duran Group*. The Photoreactor has an inner volume of 66 cm³ and one irradiation window has an area of 55 cm². The transmittances of the window materials are shown in Figure 5. A technical drawing of the photoreactor design can be found in the „Annex A“.

3.3.4 UV-LED's

UV-LED's, brought from the company *Thor Labs*, with different emission wavelength in the UV range were used for irradiation of complexes solutions. The emission spectra of the UV-LED's is reported in Figure 9 in the characterization chapter. The line at 367nm in Figure 9 corresponds to a UV-LED *Nichia NCSU033A(T)* from the *Nichia Corporation*. The optical power of the LED's was measured with a tunable UV Radiometer *Fieldmaster (Detector: LM-2 UV)* from the company *Coherent* at different focal lengths behind a 25mm concave quartz condenser lens. The results of the optical power depending on different spot diameters are summarized in Table 3 in the characterization chapter.

3.3.5 Mercury lamps

An *HBO200* 200 Watt Hg lamp from the company *Osram* was used for irradiations in the quartz cuvettes. Up scaled experiments were carried out in a photoreactor with a *Solar Simulator* 1000 Watt Hg lamp from the company *LotOriél*.

Measurements of the lamp spectra and relative optical power were measured with a spectrophotometer *Spectro 100* (sensor: 589-549, optical fiber: OFG-424) from the company *Instrument Systems*. The relative optical power of the lamps was corrected to absolute optical power by integrating their spectra, having as reference the peak of the lamps at 365 nm with a calibrated radiometer *Model IL1400-A* (Detector *XRL140-B*), with measure range 320-400 nm, from the company *International Light Technologies*.

For the calculation of the peak energies, the spectra was measured with the calibrated radiometer, the area of each peak was integrated and an integration constant was calculated for each lamp, the integration constants were 0.465 and 0.241 mW/cm² for the LotOriél and the Osram Hg lamps respectively. The spectra of the lamps and their optical power is found in the characterization chapter Figure 7, Figure 8 and Table 2.

3.4 Methods

3.4.1 Optical microscopy

Optical microscopy images were taken in bright field and dark field, back and front light, with an Optical Microscope *Nikon H600L*. The comparison of the bright and the dark field delivers information about the presence of oxide in the deposited material. The comparison between back and front light offers information about the optical density of the film. The verification of the metal deposition was made mainly with this optical microscope.

3.4.2 EDX

EDX measurements were carried out with an instrument from the company *EDAX* equipped with an *Octane Super SSD* (Silicon Drift Detector). EDX was used to assess if the deposition was metallic copper and to measure the purity of the deposited material.

3.4.3 Infrared spectroscopy

A *Bruker Tensor 25 MIR* from the company *Bruker* was used to investigate the structure of the copper complexes. The instrument is equipped with a *Silicon Carbide detector DLa TGS* with a 400 - 5500 cm⁻¹ measure range, 16 scans, 20 KHz scanner velocity and 4cm⁻¹ resolution. The ATR

technique was used to measure the spectra. The software OPUS, Origin and Wolfram Mathematica were used for analyzing the IR spectra.

3.4.4 Mass and atomic spectroscopy

Mass spectroscopy was measured on an *Agilent 1260 Infinity* from the company *Agilent Technologies*. The injection volume was 25 μL and methanol-water 50% vol. was used as mobile phase at 0.5 ml/min and pressure of 30 bar. The detection was made in positive mode (200-1500 Da/ TIC Mode) and negative mode (135 - 2500 Da/ TIC Mode) operating at the following gas conditions, temperature 350°C, Gas nebulizer 60 psig and 9 L/min gas flow. The capillary voltage was 3000 V and fragmentation was done at 70 eV.

Atomic spectroscopy was used to measure with higher accuracy the solubility of some complexes. Atomic spectroscopy was done with an *ICP-OES Ultima 2* from the company *Horiba Jobin Yvon* equipped with a conical nebulizer and performed at 2.02 bar pressure and 0.73 L/min Argon flow. Experimental lower detection limit (LOD): 1.60 $\mu\text{g/l}$, limit of quantification (LOQ): 4.8 $\mu\text{g/l}$. The detection signal of copper was set at 324.754 nm.

3.4.5 UV-Vis spectroscopy

Two spectrometers were used for measuring and following the irradiation experiments on copper complexes. A commercial spectrometer *Cary 5000* from the Company *Varian* was used to measure the reactions in 10 mm optical path quartz cuvettes every 15 minutes for maximum 120 minutes.

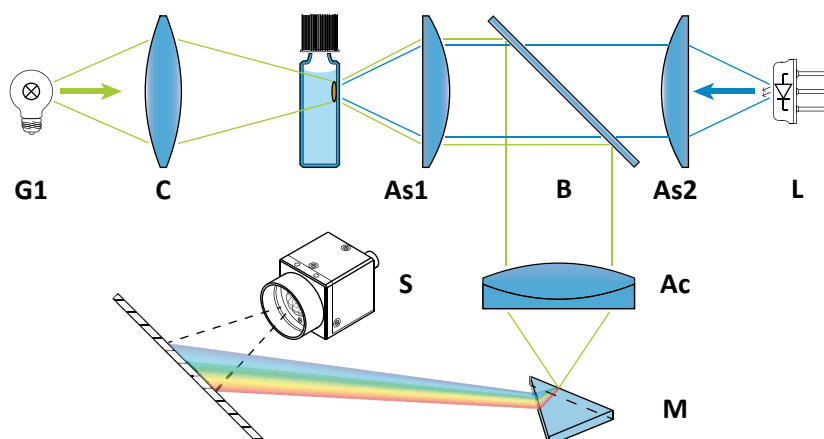


Figure 6: Self constructed spectrometer. Incandescent bulb (**G1**), condenser lens (**C**), quartz aspheric lenses (**As#**), quartz beam splitter (**B**), UV-LED (**L**), quartz achromatic lens (**Ac**), monochromator (**M**), sensor/camera (**S**).

The reaction kinetics were also followed with a self-made spectroscope constructed with quartz lenses and optical instruments bought from *Thor Labs*. The camera used to record the spectra is a *BlackFly2*[®] from the company *Point Grey*. For the reaction kinetic follow up, UV-LED's

(Figure 9) were used as a light source to trigger the reaction and common white light to examine the spectra of the deposited material with the configuration shown in Figure 6. Reactions were measured every 2-5 minutes for maximum 120 minutes.

Molar absorption coefficients were determined from solutions of known concentration well below the saturation limit and also in the linear regions of the *Lambert-Beer* law, as suggested in the literature¹⁶⁸. At least four concentrations were measured to determine the molar absorption coefficient of substances. The linearity of the *Lambert-Beer* law was confirmed by fitting a linear function. The intervals of confidence and statistical significance of the measurements were determined using $\alpha = 0.05$.

UV-Vis spectra were also used to determine the solubility of the complexes. The saturation concentration was calculated from quadruplicated UV-Vis spectra measurements in sets of eight dilutions made from saturated solutions of the complexes. Dilution of the saturated solutions was necessary to assure that the absorbance was lower than 1.0 and the measurement was in the linear region of the *Lambert-Beer* law¹⁶⁸. The solubility of the complexes was determined in methanol (99.9%), ethanol (>99.8%), 2-propanol (99.9%) and methanol 98% for $\text{Cu}(\text{acac})_2$ and $\text{Cu}(\text{hfacac})_2$ and for CuPyr4TBC complex solubility was determined also in DMSO (>98%) and acetonitrile reagent grade.

3.5 Computational methods

Ab initio simulations were performed to obtain the electronic structure of complexes and spectroscopic properties. The input coordinates of the complexes were extracted from the crystallographic files (.cif) of the Cambridge Crystal Database (CSD)¹⁶⁹ using the software Mercury¹⁷⁰. The geometry search of the complexes was performed in the *ab initio* simulation packages GAMESS-US and Gaussian09^{171 172 173}. *Ab initio* simulations were performed at the B3LYP/6-31G(d,p) level of theory with density functional theory (DFT) for geometry optimization and frequency analysis. For the generation of excitation energies the TD-DFT approach was used at the B3LYP/6-31G(d,p) level of theory. Calculations were also performed at the B3LYP/cc-TVZ level of theory with DFT to check for the basis set dependency of the calculations¹⁷⁴ and BHHLYP functional was also used to check the sensitivity of the result with the correlation factor. Charge decomposition analysis (CDA), extended charge decomposition analysis (ECDA), molecular orbital diagrams of the results were obtained using the software package Multiwfn¹⁷⁵. *Mulliken* molecular orbital contribution analysis and simulated UV-Vis spectra graphics were done using Chemission software. Chemcraft, Avogadro and wxMacMolPlt were used as visualization packages and input file generators^{176 177}. The Wolfram Mathematica language included in the Wolfram Mathematica software was used for the detailed analysis of raw data.

3.6 Procedures

3.6.1 Cleaning procedure of quartz and glass material

Consistent cleaning procedure was done on quartz cuvettes. *Mucaso!*[®] from the company *Merz* was used in a concentration of 2% vol. using deionized water in at least five washing cycles. Rinsing was made with deionized water and final cleaning and drying was done with ethanol or acetone and compressed air. The cleaning procedure was tested regularly measuring the transmission of the cuvettes after cleaning and comparing it with the transmission spectra of the cuvettes when bought. The cleaning procedure was consistent during all experimentation.

3.6.2 Degassing procedure

Solvents used for synthesis or preparation of solutions for irradiations were degassed, not dried, with the Freeze-Pump-Thaw technique, where a solvent is placed in a *Schlenk* flask with sufficient glass wall thickness and subjected to cycles of freezing with liquid nitrogen, thawing the frozen solvent in 25°C water baths and removing all gas inside with a vacuum pump.

4 Characterization

This chapter is dedicated towards the characterization of the materials, reagents and products of reaction. The characterization of the materials used for experimentation is crucial for the interpretation of results, and therefore early conclusions from the measurements will be discussed in order to construct the arguments that support the mechanism of reaction in later chapters. The chapter begins with the characterization of the light sources used and the results of calculating their optical power followed by characterization of materials for irradiation such as solvents and sensitizer. Followed by characterization of the reagents by spectroscopy methods, UV-Vis, IR and MS.

4.1 Spectra and optical power of the light sources

4.1.1 Spectra and optical power of Hg light sources

For small scale irradiations in quartz cuvettes an *HBO 200 W Hg OSRAM* lamp was used, the spectra of the lamp is shown in Figure 7. Comparing the spectrum given by the supplier in Figure 7 A and the measured spectra in Figure 7 B and C it is evident that the lamp has aged, the peak in the UV-C region at about 254 nm reported in the spectrum of the vendor is totally absent in the measured spectra. The absence of the peak is attributed to the aging of the lamp. Instability of the lamp was also recorded on the emission spectra and was evident experimentally as the light was constantly flickering.

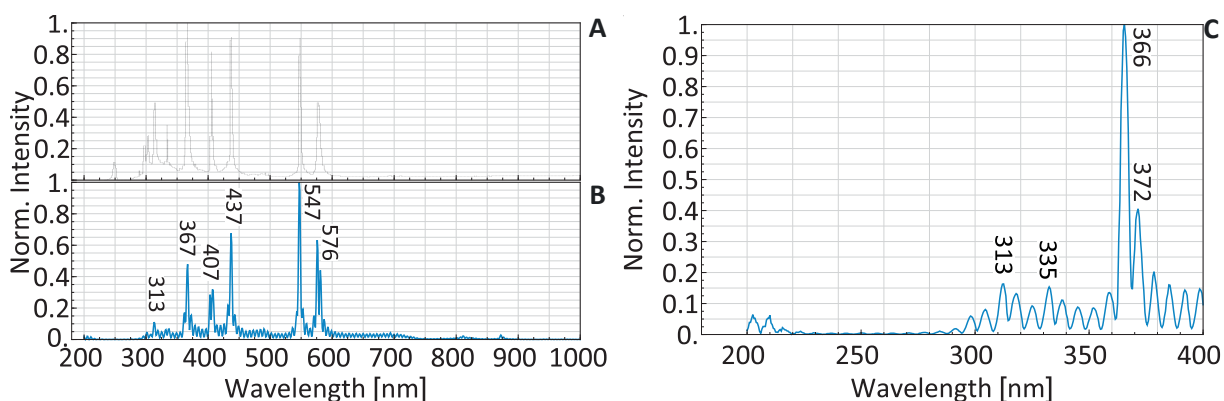


Figure 7: Spectra of the *HBO 200W Hg Osram* lamp. **A.** reported spectrum from supplier¹⁷⁸, **B.** measured spectrum **C.** measured spectrum in the UV range.

For large scale irradiations in the self-made photoreactor a *Solar simulator 1000W Hg LotOriél* lamp was used, the spectra of the lamp is presented in Figure 8. The lamp has high emission in the UV-B region, with high intensity peaks at 365, 313 and 334 nm, and low emission in the UV-C region, seen as low intensity peaks at 266 and 250 nm. The experimentation with this lamp was always done with large volume solutions in a self constructed photoreactor, experimentation with cuvettes was avoided because of the damage induced in the cuvettes due to its small wall thickness and generated pressure due to the heat produced during irradiation.

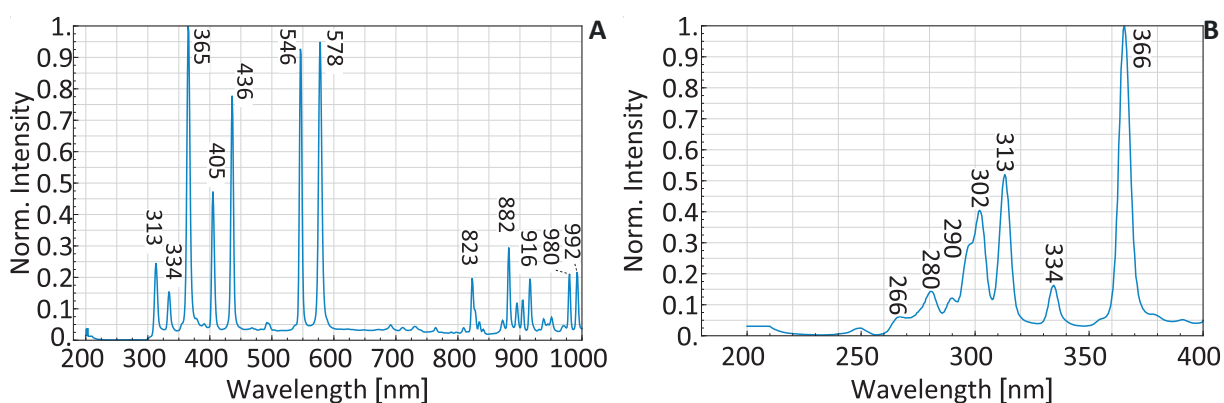


Figure 8: **A.** Measured spectra of the *Solar Simulator 1000W Hg LotOriél* lamp. **B.** measured spectra in the UV range.

The energies of the peaks observed in the UV region were calculated as explained previously in the materials chapter „Mercury lamps“ of this work and are presented in Table 2. From this calculation it is evident that the available *200 W HBO Osram* lamp can be regarded as a low power irradiation source in the UV region, given the low optical power in that region. It is also clear that the higher energy outputs of both mercury lamps, *Osram* and *LotOriél*, lie in the UV-A region.

Table 2: Energies of the peaks emitted by the used Hg lamps.

Peak No.	Peak [nm]	Base Max[nm]	Base Min [nm]	Energy [mW/cm ²]
<i>Solar Simulator 1000W Hg LotOriél</i>				
1	365.40	375.70	357.00	3.20
2	334.40	340.80	328.60	0.51
3	313.00	320.00	307.60	1.55
4	301.90	307.60	292.40	1.85
5	290.00	292.40	285.50	0.33
6	280.70	285.50	274.50	0.55
7	266.70	270.50	263.10	0.19
<i>HBO 200W Hg Osram</i>				
1	372.00	379.20	372.70	0.20
2	366.00	372.70	366.00	0.66
3	335.50	339.30	332.50	0.15
4	313.00	316.30	312.50	0.08

4.1.2 Spectra and optical power of UV-LEDs

UV-LEDs were used for small scale experiments with quartz cuvettes. The spectra of UV-LEDs are shown in Figure 9. Their spectra and optical energies were measured after focusing to address the energy that could be delivered for the photoreaction. The results of the optical energies with different focusing lengths, represented as the diameter of the light spot, are presented in Table 3. The narrow band emission of the UV-LEDs, in average 11 nm wide at 50% emission, offered the opportunity to check the kinetics of the reaction depending on the irradiation wavelength, and correlate them with the absorption spectra of the sensitizer and the complex used during experimentation.

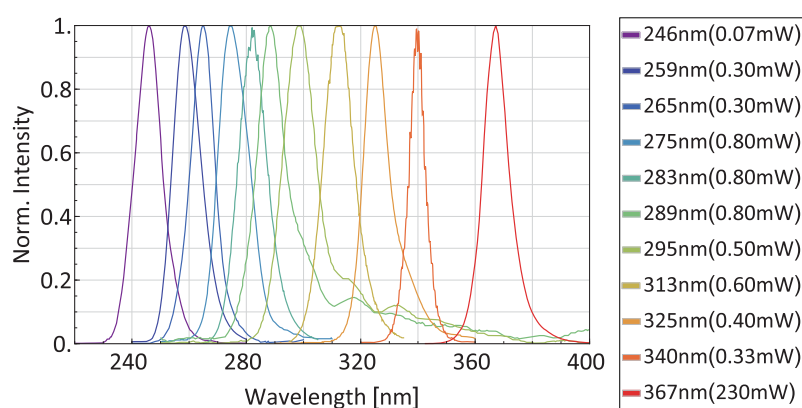


Figure 9: UV LED's spectra and their nominal optical output power reported by the supplier (mW).

Table 3: Optical power of the used UV-LED's at different focusing spot diameters.

Wavelength[nm]	325	315	300	285	275	260	245 ^a
Spot diameter [mm]	Optical Power [$\mu\text{W}/\text{cm}^2$]						
4	66.9	177	153	105	159	98.6	64.1
3	75.7	216	183	175	281	169	120
2	85.5	234	210	253	305	189	122
1	94.7	262	293	267	330	202	45.6

^a Measurement was done with minimum detection wavelength set in the instrument of 250 nm.

The power reported by the vendor and the measured power differ substantially, most probable because of the energy lost due to scattering and absorption by the focusing materials; the measured power of irradiation of the LED's renders them as low energy light emitting sources.

Summarizing the results of the light sources characterization and their relevance in this work. Regarding the Hg lamps used, they can be deemed as low output energy sources. Nevertheless, they can be used to explore and compare the photochemical response of complexes with an appropriate irradiation time. The irradiation time was set to 120 min for all experiments based on the fact that there is already literature that reports the deposition of metallic copper after two hours of irradiation²⁸. The lower the optical power of the lamp at a given wavelength the slower the photochemical reaction, this is a direct consequence of the *Grotthuss-Dapper* law, the

higher the influx of photons in the system the higher the excitation probability and the processes that depend on it. For an industrial application the time needed for deposition should be as short as possible, nevertheless, considering that the lamps have a low energy output in the UV region, the photoreaction with these light sources is expected to proceed slowly. It is also important to notice that the Hg lamps are medium and high pressure lamps, which means that the emission at 253 nm is self-absorbed; for experimentation in the UV a low pressure lamp would be more suitable.

Regarding the UV-LEDs, the major advantage of using these light sources is the wavelength selectivity, which permits to determine the range of wavelength where the reaction is taking place. The narrow wavelength emission of the UV LEDs avoids additional energy input in the reaction that can be converted into heat, this is particularly evident when compared with the Hg lamps which have considerable emission in the IR region. Although the UV-LEDs are low output energy sources for this application, the reaction might be well accelerated with respect to the Hg lamps because of the focusing of the light which sets a much lower volume of reaction and area of deposition.

4.2 Selection of solvents and sensitizers

4.2.1 Absorption spectra of solvents

The properties of the solvents, like solvent polarizability and dielectric constant influence the complex equilibrium, the aggregation of excited pairs and quenching processes, and can also deter the charge transfer after excitation by not favoring exciplex formation. The reciprocal dielectric constant of the solvent can be regarded as a “screening” term. Polar conditions where the ion pair is slightly retained to escape from the solvent cage are desirable. In the polar environment, the radical ions become well separated and this blocks the electron return. Escape from the solvent cage is a key feature of photoinduced transfer in solution ¹⁷⁹.

Analyzing in a more mechanistic manner; within an exciplex, the probability of electron transfer is distance and orientation dependent ¹⁸⁰. If an electron transfer within the inner sphere is assumed, the reagents are in closer contact with one another and therefore the effect of the solvent would be deemed as less relevant. On the other hand if an outer sphere mechanism is assumed the properties of the solvent become crucial for the electron transfer to happen.

Focusing on the experimental design and based on the aforementioned low energies of the light sources, a solvent with no absorption in the wavelength of reaction has to be selected. In Figure 10 the absorption spectra of common solvents are presented. Solvents containing the C=O group, or resonant double bond structures could not be used because of their high absorption in

a broad range of UV region, as seen for example in acetone, acetylacetone and pyridine.

The solvents that were considered suitable for the reaction were those with cut off wavelengths lower than 250 nm to avoid a filtering effect. Among them we find chloroform, n-hexane, diglyme, 2-propanol, ethanol, methanol, water and acetic acid. Initial laboratory test showed that among these solvent candidates, the complexes $\text{CuPyr}_2\text{Cl}_2$ and the ones containing derivatives of catechol as ligands were almost insoluble in n-hexane and water. Diglyme was dismissed because of its toxicity and its ability to act as a ligand, however it is worth noting that it has been used successfully as a sensitizer in the photoreaction of $\text{Cu}(\text{acac})_2$ by ²⁸, but their result could not be reproduced in this work. Acetic acid was dismissed because its chelating properties by forming copper acetate. 2-Propanol, ethanol and methanol were chosen based on the low absorption in most of the UV region, availability and to circumscribe the experiments to alcohol solvents for comparison with literature ^{28 15}. The relative dielectric constant (ϵ) for methanol, ethanol and 2-propanol are 32.7, 24.5 and 17.9 respectively ¹⁸¹.

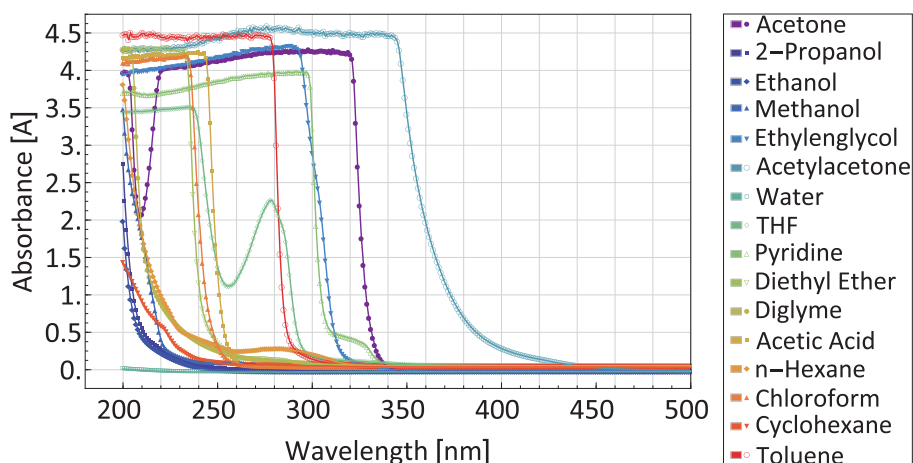


Figure 10: UV-Vis spectra of solvents tested for use with copper complexes.

4.2.2 Absorption spectra of sensitizers

Ideally, the absorbance peaks of the sensitizers should overlap with the emission spectra of light sources, to maximize the probability of excitation. The aromaticity of the ketone influences the intersystem crossing behavior and available triplet states. Therefore, the reaction was explored with alkyl and aromatic ketones. Acetone and benzophenone were the sensitizers mostly used for experimentation. Figure 11 shows the calculated molar absorption coefficients of alkyl and aryl ketone sensitizers.

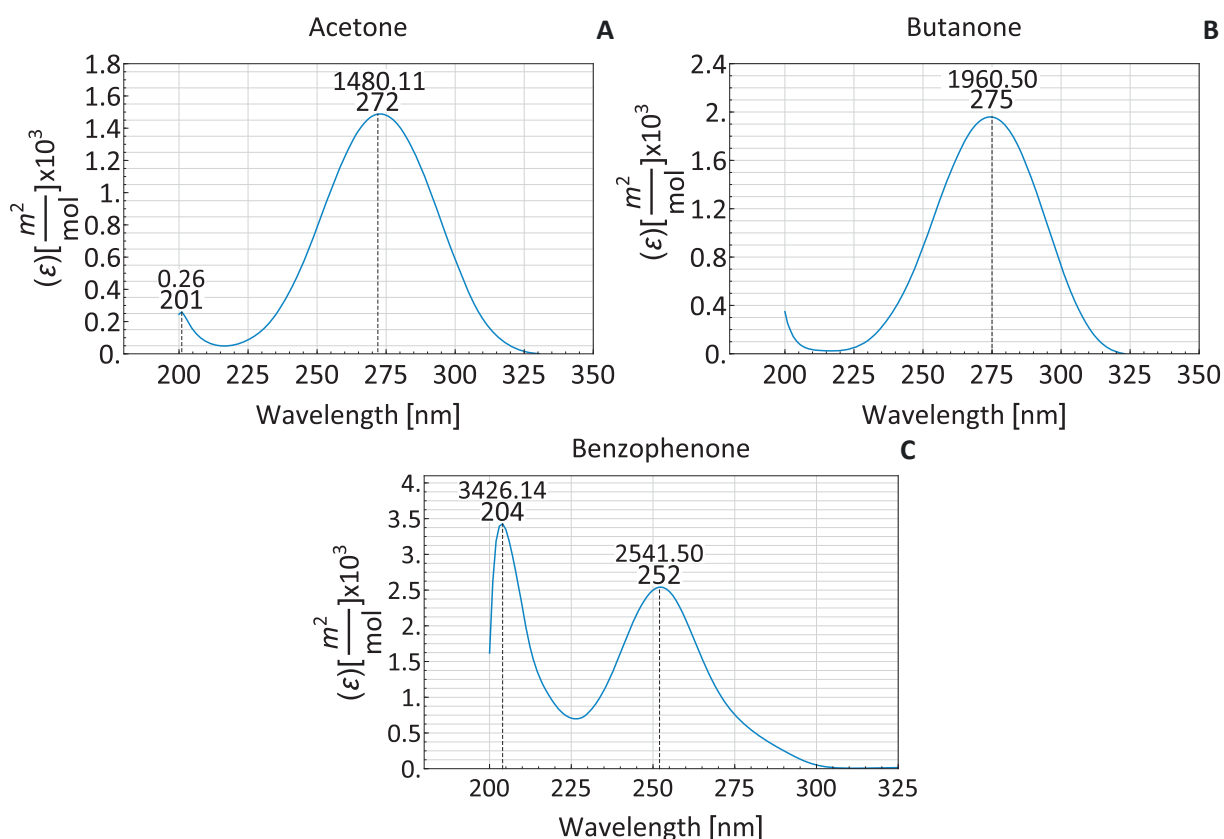


Figure 11: Molar absorption coefficient of alkyl and aryl ketones **A.** acetone and **B.** butanone **C.** benzophenone in 2-propanol.

Comparison between the triplet states of acetone and the benzophenone shows that although both molecules possess lowest n,π^* singlet and triplet states, the $S_1 \rightarrow T_1$ crossing in benzophenone is of the ${}^1(n,\pi^*) \rightarrow {}^3(\pi,\pi^*) \rightarrow {}^3(n,\pi^*)$ type whereas acetone is of ${}^1(n,\pi^*) \rightarrow {}^3(n,\pi^*)$ type. The former is always much faster than the later. All ketones in principle have mixed n,π^* and π,π^* states. Alkanones tend to possess relative “pure” n,π^* , S_1 and T_1 states. Benzophenone possesses near equally “mixed” n,π^* and π,π^* states, but the state is better represented as a π,π^* state. Naphthyl ketones may possess mixed $n,\pi^* \leftrightarrow \pi,\pi^*$ singlet states but tend to possess pure π,π^* triplet states¹⁸².

Aryl ketones such as acetophenone, undergo rapid intersystem crossing of the $n \rightarrow \pi^*$ singlet excited state to an energetically close $\pi \rightarrow \pi^*$ triplet state. The latter then quickly decays to the lower energy $n \rightarrow \pi^*$ triplet. This pathway is not available to most aliphatic ketones, so their intersystem crossing rates from $n \rightarrow \pi^*$ singlets to triplets are slow. Conjugation with the π -electrons of a double bond or a benzene ring shifts $n \rightarrow \pi^*$ absorptions to longer wavelength and increases the strength of absorption when compared with acetone.

The intersystem crossing (ISC) probability of the ketones is very high, for acetone the intersystem crossing yields and triplet energies are $\phi_{np} = 0.9$ and $\phi_p = 1.0$ (332 kJ/mol) and for

benzophenone they are $\phi_{np} = 1.0$ (289 kJ/mol) and $\phi_p = 1.0$ (287 kJ/mol) in non-polar and polar solvents respectively³¹. Excitation of acetone and benzophenone will lead to a triplet state given its very high ISC. The primary process of light excitation does not involve the formation of radicals, since the methyl and the phenyl radical are not stable. It has been experimentally observed in this work that the presence of the sensitizer is key for the photoreaction to proceed at higher rates, none of the complexes alone is able to produce a significant metallic deposition without the use of a sensitizer under the standard experimentation conditions of irradiation times lower than 120 min.

The reduction potential of the sensitizer in the excited state in its donor (D) or acceptor (A) state, $E^0(D^+/D^*)/E^0(A^*/A^-)$, can be calculated using the reduction potential in the ground state ($E^0(D^+/D)/E^0(A/A^-)$) and the spectroscopic energy of the transition (E_{00}) as shown in the following equations¹⁷⁹.

$$E^0(D^+/D^*) = E^0(D^+/D) - E_{00} \quad \text{Ch. (38)}$$

$$E^0(A^*/A^-) = E^0(A/A^-) + E_{00} \quad \text{Ch. (39)}$$

Yet the absolute value of the energy is not deterministic in the feasibility of the electron transfer, the relative ordering of the energies of unoccupied and occupied orbitals of the excited molecule and the quencher. It can be surely stated that for the electron transfer to proceed, the driving force of the transfer has to be positive, which means that the energy level from which the electron is transferred has to be higher than the energy of the orbital accepting the electron. The potentials for acetone and benzophenone to act as an oxidation¹⁸³ or reduction¹⁸¹ partner in the ground and excited state are shown in Table 4.

Table 4: Oxidation and reduction potentials of acetone and benzophenone in the ground and triplet excited states.

Sensitizer	${}^3E_{00}$ [V]	$E_0(D^+/D)$ [V]	$E_0(D^+/D^*)$ [V]	$E_0(A/A^-)$ [V]	$E_0(A^*/A^-)$ [V]
Acetone	3.44	-0.129	-3.57	2.84	6.28
Benzophenone	2.98	-0.129	-3.11	1.80	4.78

Summarizing the section of the selection of solvent and sensitizers. Alcohol solvents were selected for experimentation because they do not absorb in the UV region, the result can be compared with literature reports. The main solvent selected for experimentation methanol, ethanol and 2-propanol are polar and protic. Regarding the sensitizers, they are ketones with high absorption in the UV region between 240 and 280 nm, have high triplet states which make them reactive towards hydrogen abstraction reactions. The excited sensitizers, acetone and benzophenone, are more prone to accepting an electron than donating one.

4.3 Selection of synthesized complexes for photoreduction

All synthesized complexes and copper salts used for the synthesis were screened for deposition of metallic copper under same conditions. The standard procedure was the preparation of saturated alcohol solutions of complexes, sensitized with 1:3 v/v ratio of acetone to solvent and irradiated with a 200W Hg lamp for 120 min after at least 30 minutes of warming-up and stabilizing the lamp. Those complexes which showed most promising results in terms of deposition of films with metallic appearance or deposition particles, that could be presumably copper particles, were selected for characterization and further irradiation experiments. The copper films or particles are the result of the photoreduction process triggered by the incoming light in the reaction vessel, particles of copper can coalesce on the interface between the wall of the cuvette which acts as a substrate and the irradiated liquid. All synthesized complexes were assumed to be heteroleptic and contain pyridine and catechol derivatives as ligands. Only the coordination of the precursor complex $\text{CuPyr}_2\text{Cl}_2$ is known to this point as it has been reported in the literature and the synthesis reaction has been shown to yield only this complex with no further pyridine attached to it¹⁶¹. The results are summarized in the Table 5.

Table 5: Screening of the photoreducing activity of copper complexes sensitized with ketones by irradiation with the 200W Hg lamp.

Complex	Color	Solvent	Photodeposition results
CuPyr4TBC	 Blue-Green	2-propOH	Spot with metallic appearance and copper color
CuPyr ₂ Cl ₂	 Blue	2-propOH	Spot with metallic appearance and copper color
CuCl	 White	2-propOH	Film with red brick color
CuPyrPCA	 Pale blue	2-propOH	Particles with red brick color
CuPyrDOPA	 Deep brown	2-propOH	Particles with red brick color
CuCl ₂	 Green	2-propOH	Film with gray color
CuPyr(DL-DOPA)	 Deep violet	2-propOH	Film with gray color

Pyr= pyridine, 4TBC = 4-tert-butylcatechol, PCA = (protocatechoic acid / 3,4-dihydroxybenzoic acid), DOPA = (dopamine / 3-hydroxytyramine), DL-DOPA = 3-hydroxytyrosine.

The most promising results were shown by the complexes copper(II) di-pyridine di-chloride ($\text{CuPyr}_2\text{Cl}_2$) and copper pyridine catecholate (CuPyr4TBC), which yield an homogeneous deposition of a lustrous film with copper color. The aforementioned complexes and the commercial complexes

copper di-acetylacetonate, $\text{Cu}(\text{acac})_2$, and copper di-hexafluoroacetylacetonate $\text{Cu}(\text{hfacac})_2$ were selected for further experimentation and optimization of the photoreduction process.

4.4 Solubility

The solubility of the complexes was determined experimentally by UV-Vis spectroscopy and atomic spectroscopy (ICP-OES). Experiments where the concentration of complex is not explicitly shown were done in saturation conditions, the complex characterized are the ones that showed photodeposition of spots with metallic copper appearance at irradiation times shorter than 120min.

Table 6: Solubility of $\text{Cu}(\text{acac})_2$, $\text{Cu}(\text{hfacac})_2$ and CuPyr4TBC in different solvents measured with UV-Vis.

Solvent	Solubility [M]	Statistics		
		σ [M]	R ²	α
$\text{Cu}(\text{hfacac})_2$ ^a				
2-propanol (absolute)	6.25	3.89×10^{-1}	0.999	0.05
methanol (absolute)	1.15	1.06×10^{-2}	0.999	0.05
methanol (>98%)	1.15	9.98×10^{-2}	0.999	0.05
$\text{Cu}(\text{acac})_2$ ^b				
2-propanol (absolute)	3.36×10^{-3}	1.24×10^{-4}	0.999	0.05
methanol (absolute)	3.63×10^{-2}	3.31×10^{-3}	0.999	0.05
methanol (>98%)	9.20×10^{-3}	3.23×10^{-4}	0.999	0.05
CuPyr4TBC ^c				
2-propanol (absolute)	2.21×10^{-4}	5.60×10^{-5}	0.982	0.05
methanol (absolute)	2.65×10^{-3}	1.82×10^{-4}	0.982	0.05
methanol (>98%)	1.08×10^{-3}	8.72×10^{-5}	0.982	0.05
acetonitrile	7.33×10^{-4}	6.18×10^{-5}	0.982	0.05
DMSO	7.32×10^{-2}	1.37×10^{-3}	0.982	0.05

^a: calculated at 326 nm, ^b: calculated at 244 nm, ^c: calculated at 263 nm, σ : standard deviation, R²: coefficient of determination, α : statistical significance.

Table 7: Solubility of $\text{CuPyr}_2\text{Cl}_2$ and CuPyr4TBC in methanol measured with ICP-OES.

Solvent	Dilution	Measurement [mg/L]	Concentration [M]
CuPyr4TBC			
methanol (>98%)	1:100	1.661 ± 0.021	2.61×10^{-3}
methanol (>98%)	1:50	3.317 ± 0.020	2.61×10^{-3}
$\text{CuPyr}_2\text{Cl}_2$			
methanol (>98%)	1:50	0.636 ± 0.002	5.00×10^{-4}

The solubility values in Table 6 and Table 7 show a marked solubility difference between the studied complexes. The commercial complexes have higher solubility than the synthesized complexes in alcohol solvents, although the solubility of commercial complexes was not measured,

such tendency can be extended also to the acetonitrile and DMSO solvents based on experimental observations. The average solubility in methanol, ethanol and 2-propanol of $\text{Cu}(\text{hfacac})_2$ is four orders of magnitude higher than the solubility of synthesized CuPyr_4TBC . The solubility of $\text{Cu}(\text{acac})_2$ is one order of magnitude higher than the solubility of CuPyr_4TBC . The same tendency regarding the solubility is found when making the comparison between the β -diketonate complexes and the precursor complex $\text{CuPyr}_2\text{Cl}_2$ in methanol.

The rate of deposition is expected to increase as the concentration of the complex in solution increases. As most of the experiment were carried out in saturated conditions, the comparison between rates of reaction between complexes will indicate if the rate is higher because of the higher complex concentration or because the efficiency of the reaction is higher or both.

4.5 UV-Vis spectra, electronic configuration and electronic transitions

The simulations are performed as a mean to confirm the observations of the electronic transition in the UV-Vis spectra and to give some insight about the type of electronic transition in the complex, whether LMCT, MLCT or LLCT. By analyzing the charge density of the complex and the ligands donor and acceptor ability compared with the central atom, the simulations constitute also a form to quantitatively inform which ligand increases the electron density towards the metal center. For simulating the UV-Vis spectra of metallic complexes first a structure with minimum energy must be found, the minimum energy is confirmed by simulating the IR spectra and verify that there are no imaginary frequencies; the obtained simulated IR spectra can also be compared with experimental results and indicate the validity of the results.

Electronic configuration of the molecules were simulated *ab-initio* using the Software General Atomic and Molecular Electronic Structure System (GAMESS)^{171 172} and Gaussian09¹⁷³. Experimental crystallographic data extracted from Cambridge Crystallographic Database (CCDC) served as input for the calculations. Crystallographic information was found for commercial complexes $\text{Cu}(\text{acac})_2$ ^{184 185} and $\text{Cu}(\text{hfacac})_2$ ¹⁸⁶. The geometries of the complexes were optimized at a B3LYP/6-31G(d,p) level of theory with DFT. The complexes that were simulated were $\text{Cu}(\text{acac})_2$, $\text{Cu}(\text{hfacac})_2$ and $\text{CuPyr}_2\text{Cl}_2$. The optimized geometries of the complexes are reported in „Annex B“.

Mulliken decomposition analysis was performed to determine if a given molecular orbital had more metal or ligand character. The molecular orbitals are generated by combination of the atomic orbitals of the atoms involved, the contribution of any atomic orbital to a molecular orbital is given by a function involving the overlap integral and the coefficients used to construct the atomic orbital from the basis function. If the metal orbital contributes more to the molecular

orbital the orbital is metal centered, meaning there is more electron density from the metal in that orbital.

For analyzing the result of the TD-DFT simulations, only the major contribution of the transition will be considered, the percentage of the major contribution will be shown in parenthesis. From this major contribution the orbital transitions with the highest intensities will be considered. The complexes are set always in two fragments, the ligands and the metal central atom. An orbital will be assumed to be a ligand centered orbital if the percentage of coefficient contribution of the ligand fragment is higher than the percentage contribution of the central atom fragment. The major percentage coefficient of contribution of the given fragment will be annotated in parenthesis next to the number of the orbital. The spatial distribution of the orbitals involved in the more intense transitions will be shown and used to signalize and confirm if the orbital is ligand or metal centered.

4.5.1 UV-Vis absorption spectra of copper complexes

4.5.1.1 Absorption spectra of $\text{Cu}(\text{acac})_2$

Absorption spectra of acetylacetonone are characterized by a peak at 273 nm ($\epsilon = 2032.12$). For $\text{Cu}(\text{acac})_2$ complex, three peaks at 201 nm ($\epsilon = 303.50$), 244 nm ($\epsilon = 424.36$), 294 nm ($\epsilon = 670.89$) and a shoulder at 306 nm ($\epsilon = 504.20 \text{ m}^2/\text{mol}$) can be detected,.

The 273 nm peak of acetylacetonone corresponds to a $\sigma \rightarrow \pi^*$ transition in the enol form of the molecule; in a more polar protic solvent the $\pi \rightarrow \pi^*$ transition of the ketone form would become observable with less intensity at approximately 294 nm¹⁸⁷.

In the spectrum of $\text{Cu}(\text{acac})_2$ the first absorption band at 280-310 nm has been assigned to a $\pi \rightarrow \pi^*$ transition. The second band 230-255 nm has been assigned to a charge-transfer transition from ligand to metal, such assignment has been supported in several publications with experimental observations^{116 28 15}. The three maxima are the product of the strong tetrahedral distortion from octahedral symmetry and it has been suggested that the shoulders of absorption, located at 306 nm is due to vibrational fine structure. Copper acetylacetonate $\pi \rightarrow \pi^*$ band splits into two bands the $b_{1u} \rightarrow b_{3g}$ transition and $b_{3g} \rightarrow a_u$ transition¹⁸⁸.

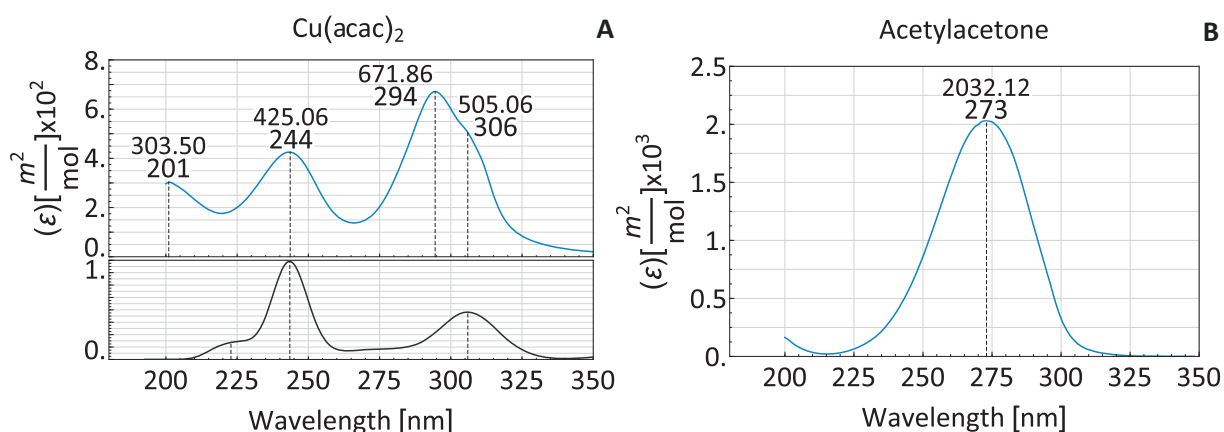


Figure 12: Molar absorption coefficient of **A.** Cu(II) acetylacetonate $\text{Cu}(\text{acac})_2$ and its ligand **B.** acetylacetonate (acac) in 2-propanol. Experimental (—), TDDFT B3LYP/6-31G(d,p) simulation (—).

The simulated spectrum shown in Figure 12 A is shifted to lower wavelengths to match the experimental spectra. Comparison between the experimental and the simulated spectrum reveals that two peaks are reproduced, although shifted. It is not clear if the higher wavelength peak in the simulation corresponds to the peak at 294 nm or to the shoulder observed at 306 nm. There is striking correspondence between the wavelength spacing between the simulated peaks and the peaks located at 244 and 306 nm in the measured spectra and therefore it will be assumed that the simulation reproduces the aforementioned peaks.

4.5.1.2 Energy transitions in $\text{Cu}(\text{acac})_2$ simulated spectra

The complex has a square planar geometry in crystal form^{184 185}, the structure obtained in the simulations differs from the structure in the crystal form, the main difference was a tilt in the plane of each ligand with respect to one another. The tilt in the structure was accepted in order to eliminate imaginary frequencies from the calculations and to obtain a local or global minimum. The difference in the structures might be due to the fact that the simulation considers a gas molecule while the reported structure^{184 185} is in the crystal state.

Three energy transitions are observed in the simulations and are located at 210, 231 and 293 nm. The experimental values are located at 244, 294 and 306 nm. The difference between the two biggest transitions in the simulated (293-231) and the experimental spectrum (306-244) give the same result 62 nm; it is assumed that those transitions have been correctly reproduced by the simulated spectrum although the transitions in the simulation are shifted 13 nm to lower wavelengths. The peak located at 294 nm in the experimental measurement is not reproduced by the simulations as observed in Figure 13 B. The small shoulder observed in the simulated spectra at 210 nm has no parallel in the experimental spectra.

The simulated transition predicted at 231 nm seems to be a charge transfer transition involving a ligand and a metal centered orbital. The strongest amplitude of this transition (32%) is observed from orbital 60, which is mainly a ligand orbital (77% acac), to orbital 68, which is a metal orbital (61% Cu). It can be also seen in Figure 13 that the wavefunction representing the orbital 68 is centered in the copper atom but involves also the oxygen ligand atoms, the wavefunction in orbital 60 is more homogeneously distributed in the complex, thus suggesting that indeed some charge was delocalized from the ligands and has been centered around the metal.

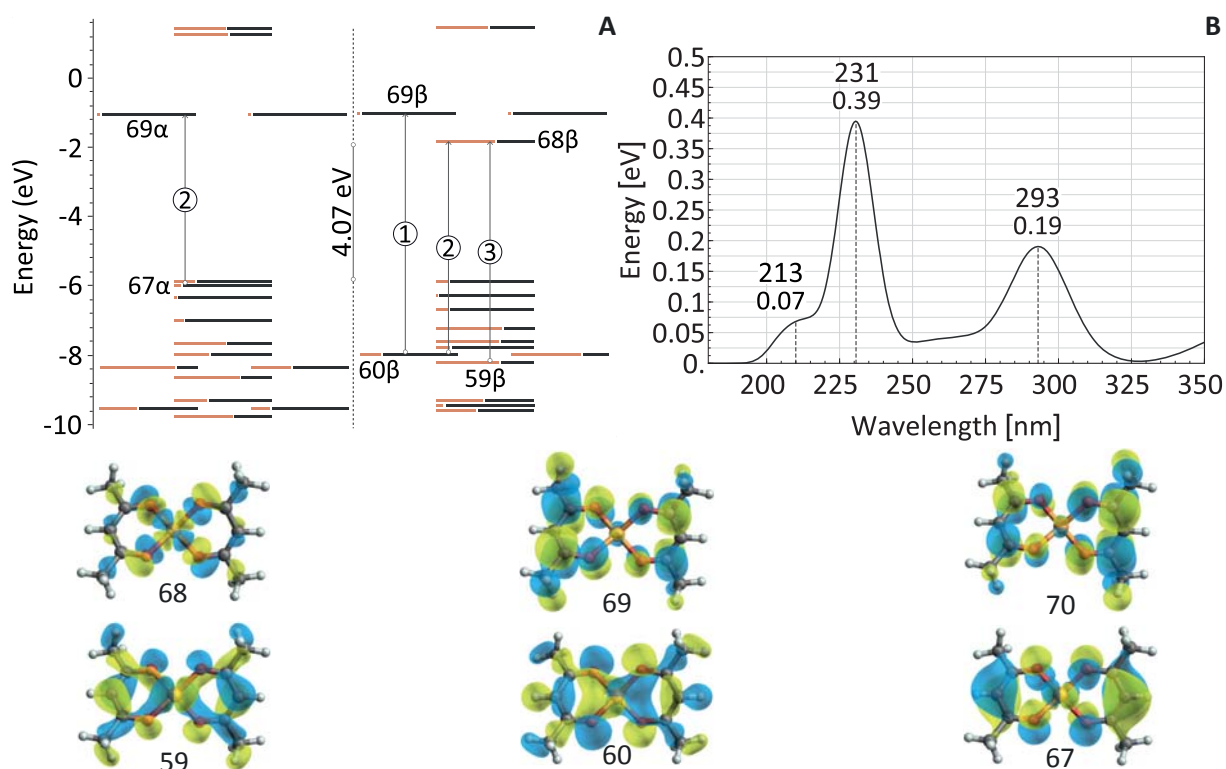


Figure 13: A. Molecular orbital diagram of $\text{Cu}(\text{acac})_2$. $\color{red}\blacksquare$ = % Cu^{+2} , \blacksquare = % $[\text{acac}_2]^{-2}$. B. Simulated UV-Vis spectra and molecular orbitals involved in the transitions with colors showing the phase.

The strongest amplitude of the transition observed at 293 nm (70%) involves a metal centered orbital 59 (66% Cu) and another metal centered orbital 68 (61% Cu), suggesting it is a ligand field transition, in the orbital picture in Figure 13 the charge is only concentrated around the metal in the final orbital (68), while in the former orbital (59) the electron density was more delocalized. Ligand field transitions are rather expected at longer wavelengths.

The strongest amplitude of the transition at 213 nm (47%) involves the ligand centered orbital 60 (77% acac) and the ligand orbital 69 (99% acac), the final ligand orbital is doubly degenerated, the transition could be also done to the orbital 70 (99% acac); both orbitals 69 and 70 have a clear concentration of charge around one of the ligands, which means that this transitions leads to a charge polarization in one of the ligands and is a interligand charge transfer.

4.5.1.3 Absorption spectra of $\text{Cu}(\text{hfacac})_2$

The absorption spectrum of hexafluoroacetylacetonate is characterized by peaks at 202 nm ($\epsilon = 70.59$), 270 nm ($\epsilon = 141.55$), 303 nm ($\epsilon = 52.68$) and 316 nm ($\epsilon = 36.71$). The absorption spectrum of $\text{Cu}(\text{hfacac})_2$ is characterized by peaks at 227 nm ($\epsilon = 810.95$), 308 nm ($\epsilon = 1387.73$), and 326 nm ($\epsilon = 787.376 \text{ m}^2/\text{mol}$).

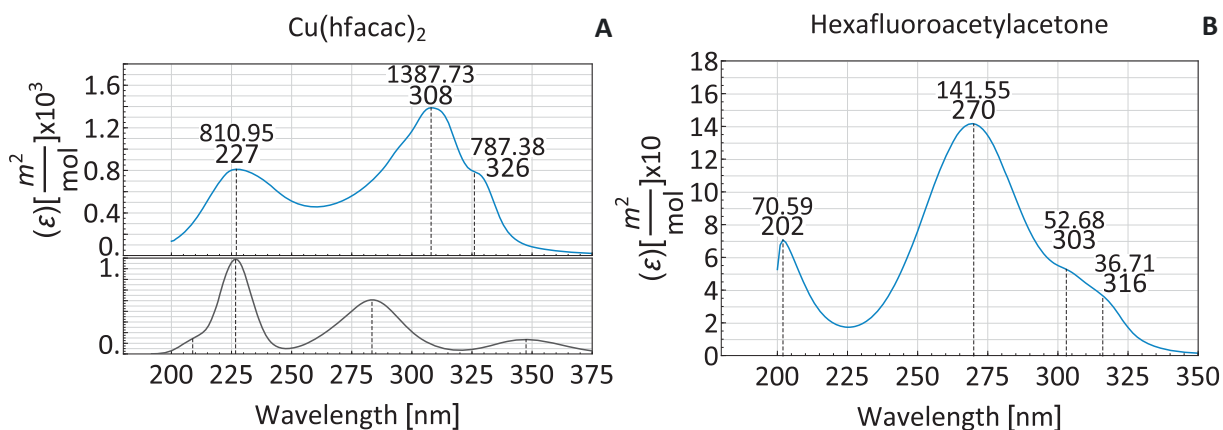


Figure 14: Molar absorption coefficient of **A.** Copper hexafluoroacetylacetonate $\text{Cu}(\text{hfacac})_2$ and its ligand **B.** Hexafluoroacetylacetonate (hfacac) in 2-propanol. Experimental (—), TD-DFT B3LYP/6-31G(d,p) simulation (—).

The 270 nm peak of hexafluoroacetylacetonate corresponds to a $\pi \rightarrow \pi^*$ transition¹⁸⁷, the peak observed at 202 nm and shoulder at 303 nm are attributed to the hydration after exposure to the atmosphere.

For $\text{Cu}(\text{hfacac})_2$ the first band at 230 nm has been assigned to a $\pi_3 \rightarrow \pi_5^*$ transition. The bands at 310 nm has been assigned to $b_{2g} \rightarrow a_u$ component of a $\pi_3 \rightarrow \pi_4^*$ transition and the shoulder at 326 nm to the $b_{1a} \rightarrow b_{3g}$ component¹⁸⁹. There seems to be a disruption of the smoothness of the 308 band at 293 nm, which is detectable using a second derivative. But the resolution is not enough to affirm the presence of a peak at 293 nm, the presence of these two short successive peaks would suggest tight upper levels in which the electronic transition can occur.

4.5.1.4 Energy transitions in $\text{Cu}(\text{hfacac})_2$ simulated spectra

$\text{Cu}(\text{hfacac})_2$ has a square planar geometry in the crystal state, which is typical of β -diketonate complexes, upon crystallization a bipyramidal coordination is obtained by coordination with two fluorine atoms of adjacent molecules¹⁸⁶⁻¹⁹⁰. The compound readily forms a dihydrate upon exposition to atmospheric conditions.

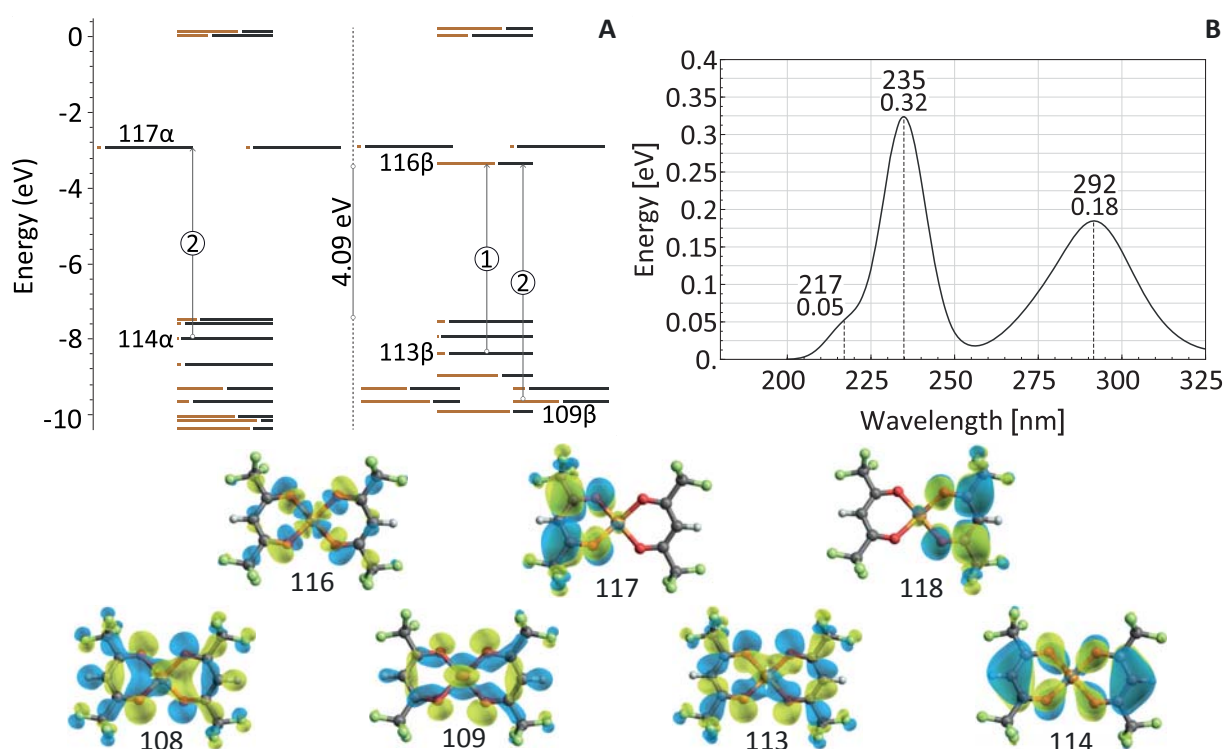


Figure 15: **A.** Molecular orbital diagram of $\text{Cu}(\text{hfacac})_2$. $\color{red}\blacksquare$ = % Cu^{+2} , \blacksquare = % $[(\text{hfacac})_2]^{-2}$. **B.** Simulated UV-Vis spectra and molecular orbitals involved in the transitions with colors showing the phase.

The structure optimizations of the compound at the B3LYP/6-31(d,p) level of theory gave also a twisted structure, in which one of the ligands is twisted with respect to the plane of the other structure, although energy minima structures were found which resembles the crystal planar structure, explored planar geometries had always imaginary frequencies which means that the planar configurations were no local or global minima but saddle points. The issue was resolved as well as for previously mentioned with $\text{Cu}(\text{acac})_2$ by accepting the twist in the optimized geometry.

The transitions observed in the simulated spectrum in Figure 15 are located at 217, 235 and 292 nm. The experimental values as indicated previously are located at 227, 308 and 326 nm. The shoulder calculated at 217 nm is not observable in the experimental spectrum, the simulated spectrum shows also transitions that are closer to the visible region and are too shifted for direct comparison with the experimental peaks in the UV region.

The simulated peak observed at the 292 nm has an unique maximum amplitude (94%) which is associated with a hole in the ligand centered orbital 113 (90% hfacac) and a particle located at a metal centered orbital 116 (61% Cu). The source molecular orbital 113 has a wider electron distribution than the final molecular orbital 116 which is centered in the central atom of copper, suggesting that the transition could be associated with a LMCT.

The 235 nm transitions has a maximum amplitude (45%) when the source is the molecular orbital 109 (51% hfacac) to the clearly metal centered orbital 116 (61% Cu). The electron density of the source orbital seems to be again spread thought the whole molecule while the end orbital has a clear density concentrated around the central atom, as suggested by the pictures of the wavefunction. This transition can also be assigned to a LMCT.

4.5.1.5 Absorption spectra of $\text{CuPyr}_2\text{Cl}_2$ and CuPyr4TBC

The absorption spectrum of the sensitized complex will be analyzed based on the absorption spectra of the precursors and ligands. Copper di-pyridine di-chloride complex and the 4-tert-butyl catechol are the precursors of the CuPyr4TBC complex.

The copper pyridine precursor complex contains the pyridine ligand and a stabilization ion, Cl. The absorption spectrum of pure pyridine was recorded also in the same solvents as the precursor complex and the final complex. The pyridine absorption spectrum, Figure 16 C, has characteristic peaks located at 203 nm ($\epsilon = 8228.0$), 240 nm ($\epsilon = 5094.7$), 245 nm ($\epsilon = 7224.5$), 251 nm ($\epsilon = 9588.5$), 257 nm ($\epsilon = 10195.3$), 263 nm ($\epsilon = 6971.6 \text{ m}^2/\text{mol}$).

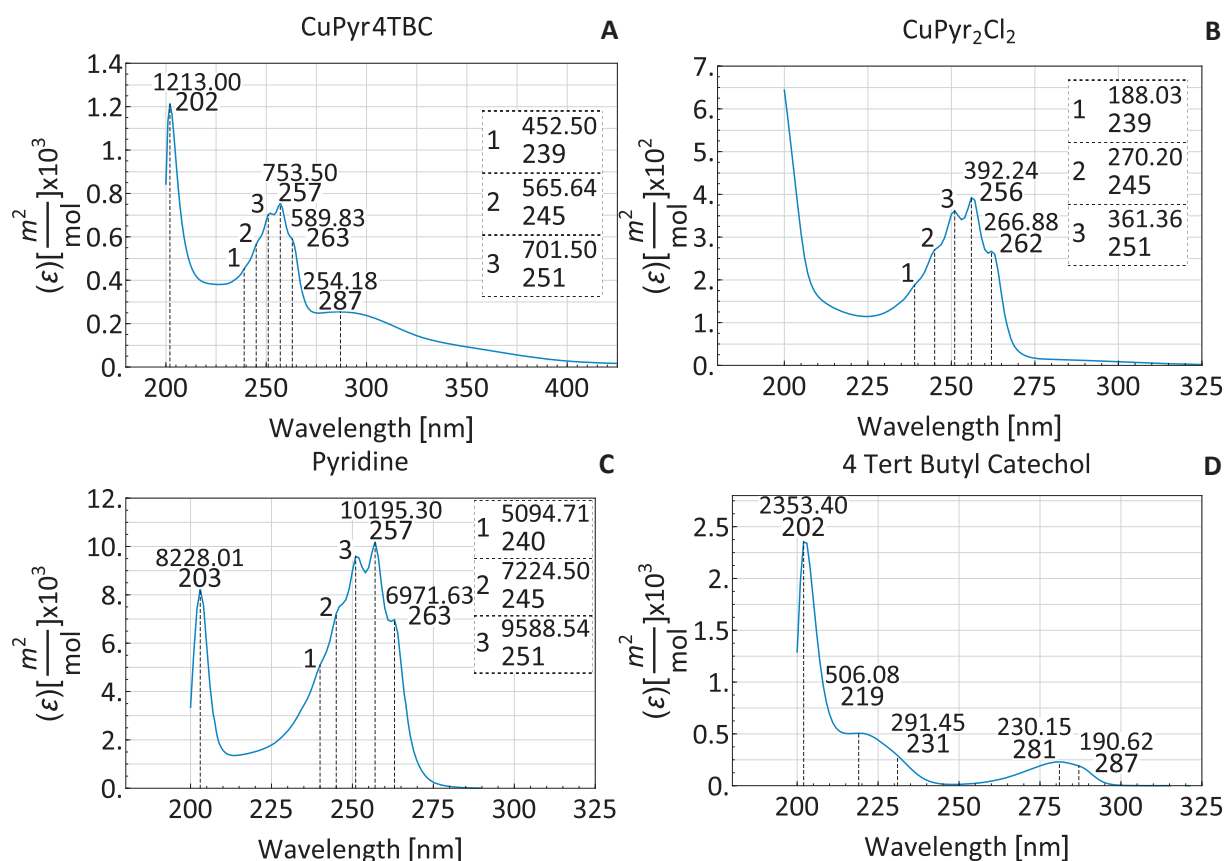


Figure 16: Molar absorption coefficient of **A.** Copper pyridine 4 tert-butyl catecholate CuPyr4TBC **B.** Copper di-pyridine di-chloride ($\text{CuPyr}_2\text{Cl}_2$) and shifted simulated UV-Vis spectra. Experimental (—), TDDFT B3LYP/6-31G(d,p) simulation (---) **C.** Pyridine and **D.** 4 tert-butyl catechol (4TBC). All determinations were done in 2-propanol except $\text{CuPyr}_2\text{Cl}_2$ which was done in deionized-filtrated water.

The peaks at 251, 257 and 263 nm have been assigned to a $\pi \rightarrow \pi^*$ transition^{191,192}. The low intensity bands at higher and lower wavelengths at 239, 245 nm and the shoulder 270 – 290 nm have been assigned to a $n \rightarrow \pi^*$ transitions. The assignment of the $n \rightarrow \pi^*$ transition is supported on the evidence that those transition vanish in the spectra of the pyridinium ion (Pyr-H⁺) when the covalent bond is formed¹⁹². Pyridine has a triplet state from an intersystem crossing mechanism, its triplet state is very short lived and decays through a radiationless mechanism¹⁹³ and it has a large tendency to be quenched by oxygen¹⁹⁴. Pyridine has a low symmetry group C_{2v} compared with its parental molecule Benzene which is D_{6h} . Studies have demonstrated that the binding of pyridine to copper is mainly done through the σ lone pair instead of the π back-bonding^{195,196}.

The precursor complex $CuPyr_2Cl_2$ (Figure 16 B) contains the same peaks as pyridine but the molar absorption coefficient is much lower 239 nm ($\epsilon = 188.0$), 245 nm ($\epsilon = 270.2$), 251 nm ($\epsilon = 361.4$), 256 nm ($\epsilon = 392.2$), 262 nm ($\epsilon = 266.9$ m²/mol).

The band observed between 225 and 270 nm for $CuPyr_2Cl_2$ resembles that of the uncoordinated ligand, but the small shifts in the band energies suggest coordination as in similar copper pyridine complexes¹⁹⁷. The band also seems structured, as a collection of transitions lying very near in energy with one another, such resemblance of the structured band of the complex with the free ligand has also been observed in polypyridine complexes³². Low lying excited states have been found for simulated pyridine copper cluster complexes, many of the which have been identified as charge transfer excited states¹⁹⁸. Although the pyridine is bound to copper and in this should cause the disappearance of the $n \rightarrow \pi^*$ transition as in the pyridinium ion, that does not happen in this coordination compounds or equivalent metal dipyrindine dichloride compounds¹⁹⁹. In the $CuPyr_2Cl_2$ complex the shoulder attributed to the $n \rightarrow \pi^*$ in pyridine is wider, spanning from 270 to 325 nm, instead of 270 - 290 nm in pyridine.

The absorption spectrum of the ligand 4-tert-butylcatechol (Figure 16 D) has characteristic peaks located at 217 nm ($\epsilon = 39.4$), 231 nm ($\epsilon = 108.8$), 281 nm ($\epsilon = 105.0$), 287nm ($\epsilon = 89.2$ m²/mol). The peak located around 281 nm has been assigned to a $\pi \rightarrow \pi^*$ transition, and is observed to be insensitive to the secondary ligand¹⁶⁷.

In the spectrum of the $CuPyr4TBC$ complex (Figure 16 A), the pyridine ligand has the highest molar absorptivity coefficient of the ligands and therefore dominates over the absorption of other ligands. The absorption spectra of the $CuPyr_2Cl_2$ complex show characteristic absorption bands in the region 239 nm to 262 nm these bands of pyridine shift slightly once it is bound to copper. The pyridine peak located at 202 nm disappears presumably because it is shifted below the detection range of the instrument. In the case of the 4TBC ligand the bands located at 217, 231 and 281 nm are hidden by the bands of pyridine, the only band from 4TBC that remains clearly visible, is the band located at 287 nm. A band in the range of 430 to 550 nm which has been attributed to a interligand charge transfer²⁰⁰ is absent in this complex, it is assumed then that

there is no LLCT in the CuPyr4TBC complex.

The peak at 287 nm is attributed to the 4-tert-butylcatechol (4TBC) and the peaks at 202, 240, 245, 251, 257 and 263 nm be attributed to the pyridine ligand. The absorption from 214 to 266 nm have been attributed to $\pi \rightarrow \pi^*$ transitions in the catechol ligand and a LMCT from pyridine to catechol²⁰¹. The presence of the ligands pyridine and 4TBC is proven directly from the UV-Vis spectra of the CuPyr4TBC complex and the bond of the ligand and the central atom can be proved with the IR spectra of the complex.

4.5.1.6 Energy transitions in CuPyr₂Cl₂ simulated spectra

The transitions observed in the simulated spectrum are located at 318, 288 and 260 nm while in the experimental spectrum one distinguishable peak can be observed around 292 nm. The simulated spectrum is shifted in order to resemble the experimental spectra and find a relation between them.

The most intense transition in the simulated spectra at 318 with a maximum amplitude (79%) involves the ligand centered orbital 69 (77% Pyr 6% Cl) and the metal centered 74 (63%), the wavefunction function changes suggest a density transition from the Cl atoms to be towards the Cu atom, yet the change of electron distribution can not be clearly seen.

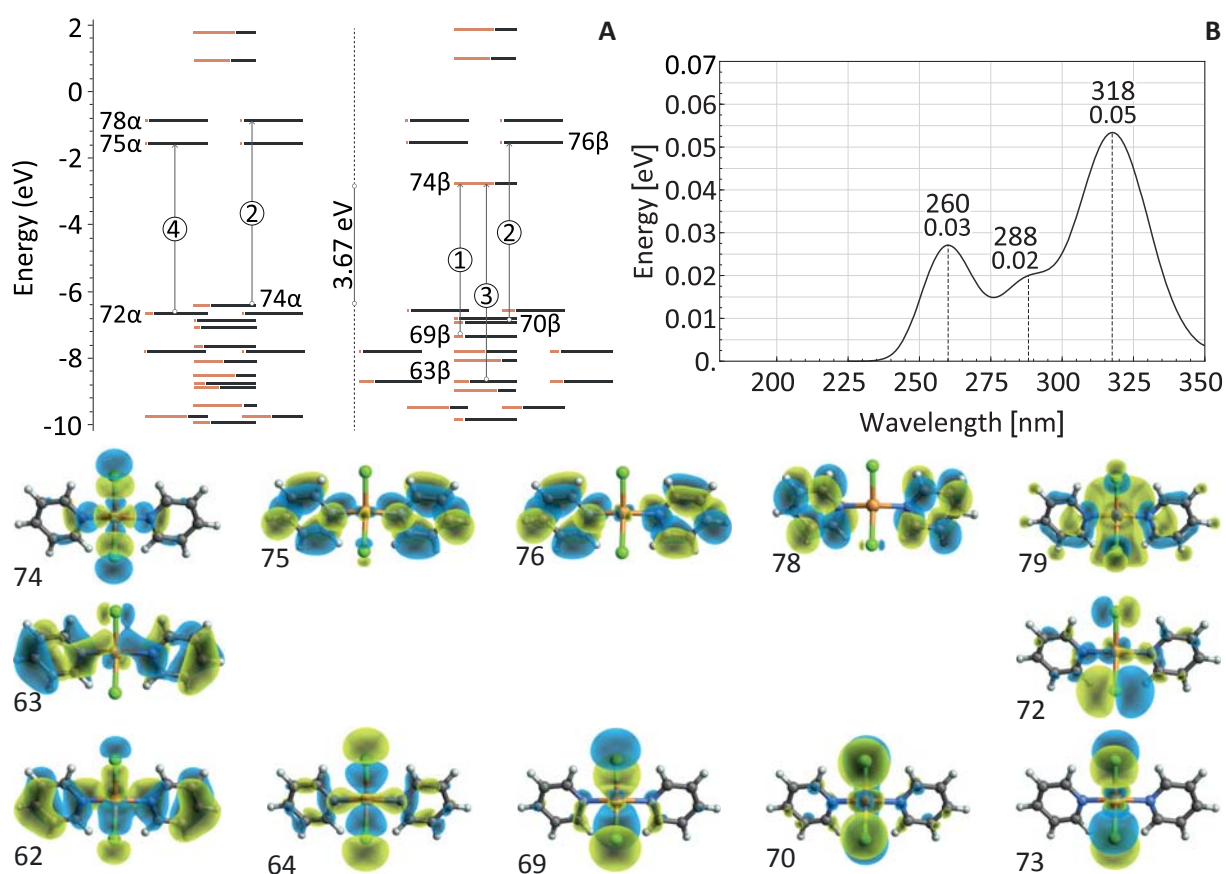


Figure 17: A. Molecular orbital diagram of CuPyr₂Cl₂. ■ = %Cu⁺², ■ = %[(Pyridine, Cl)₂]⁻². B. Simulated UV-Vis spectra and molecular orbitals involved in the transitions.

The other transition that could be correlated with the experimental spectra is located at 260 nm and has a maximum amplitude (48%) involving the ligand centered molecular orbitals 70 (78% Pyr, 6%Cl) and 76 (92% Pyr, 2% Cl). The transitions corresponds to a interligand transition involving the Cl ligand and the pyridine ligands where the density is shifted towards the pyridine ligand as seen in the wavefunction image of the orbital.

The simulated spectra of $\text{CuPyr}_2\text{Cl}_2$ and $\text{Cu}(\text{acac})_2$ show that the calculated energies for the transitions are higher than the experimental values. Increased energies of simulated transitions compared with experimental is well known to happen when the *Hartree-Fock* method is used, whereas the DFT method has the tendency to give transitions that are lower in energy than the experimental ones. The correlation introduced in the B3LYP approach mixes both calculations in order to correct the systematic error of both approaches. Nevertheless the correction done by the correlation, the calculated energies are still high when compared with the experimental values.

4.6 Infrared spectra

The objective of this section is first to prove experimentally the coordination of the organic ligands with copper for the CuPyr_4TBC , $\text{Cu}(\text{acac})_2$ and $\text{Cu}(\text{hfacac})_2$ complexes. The measured IR spectra of the complexes will be compared with literature reported spectra, when available, to confirm the bands and peaks expected within these complexes. Once the measured spectra has been confirmed, it can be compared with the DFT simulated spectra, first to check if the DFT simulations reproduce the most important vibrations and approximate to the molecular structure of the complexes. The peaks in the simulated IR spectra will be analyzed searching for any imaginary frequencies, which would indicate that the geometry does not correspond to an energy minimum geometry.

Most of the peaks present in the IR spectra of copper complexes come from the organic ligands. Due to the heavy atom effect the frequencies of the metal atom and the ligand bonding atom are found at higher wavenumber or lower frequencies. The shift of the peaks between the coordinated and the uncoordinated ligand and the change of the vibrational modes due to the change in the configuration and the bonding are indicative of the coordination. The following section presents the experimental IR measurements compared with literature values, when available, and the simulated IR spectra of the most relevant copper coordination compounds in this work. Simulations were performed at the DFT B3LYPV5/6-31G(d,p) level of theory for the ligands and at the DFT B3LYPV5/cc-TZV for the coordination compounds infrared analysis.

4.6.1 Infrared spectra of $\text{Cu}(\text{acac})_2$

The IR spectra of the copper complexes are independent of the oxidation of the central atom, for example in copper acetylacetonate ²⁰², the IR spectra of black particulate $\text{Cu}(\text{I})(\text{acac})_2$ has the same IR spectrum as $\text{Cu}(\text{II})(\text{acac})_2$ complex ¹⁵.

The region $1777 - 1668 \text{ cm}^{-1}$ corresponds to a carbon oxygen stretching band ²⁰³, observed in Figure 18 A; due to the electron resonance in the coordination ring, the $\nu\text{C}=\text{O}$ peak has a lower frequency than the $\nu\text{C}=\text{O}$ peaks in the uncoordinated ligand within the band, the uncoordinated $\nu\text{C}=\text{O}$ vibration is found around 1720 cm^{-1} ²⁰⁴, it is present in the uncoordinated ligand IR spectra but not in the coordination compound spectra (Figure 18 A & B). The absorption peaks at 1520 and 1590 cm^{-1} disclose the formation of a five-membered chelate ring containing copper and the oxygen atoms, and correspond to $\nu\text{C}=\text{C}$ and $\nu\text{C}=\text{O}$ respectively ^{205 162}. The $\nu\text{C}=\text{C}$ and $\nu\text{C}=\text{O}$ peaks are found in the experimental spectrum in Figure 18 B at 1520 and 1574 cm^{-1} .

The peaks located, for the uncoordinated ligand, at 1302 , 1246 and 777 cm^{-1} in Figure 18 A, which correspond to the wagging ω , twisting τ and stretching ν vibrational modes of CH_2 disappear once the ligand is coordinated. One hydrogen is lost from CH_2 leaving CH and the ligand negatively charged and ready to coordinate with the copper cation; the vibrational modes of the CH are an in-plane δ and an out-of-plane γ deformation at 1188 and 781 cm^{-1} respectively in Figure 18 B.

The peaks located at 611 and 453 cm^{-1} in Figure 18 B are mixed modes involving the deformation of the coordination ring $\delta\text{Ring}(**)$ and the methyl stretching $\nu\text{C}-\text{CH}_3(*)$ with the copper oxygen stretching $\nu\text{Cu}-\text{O}$, thus these peaks are a direct observation of the coordination environment. The band located at 453 cm^{-1} is the purest $\nu\text{Cu}-\text{O}$ stretching mode.

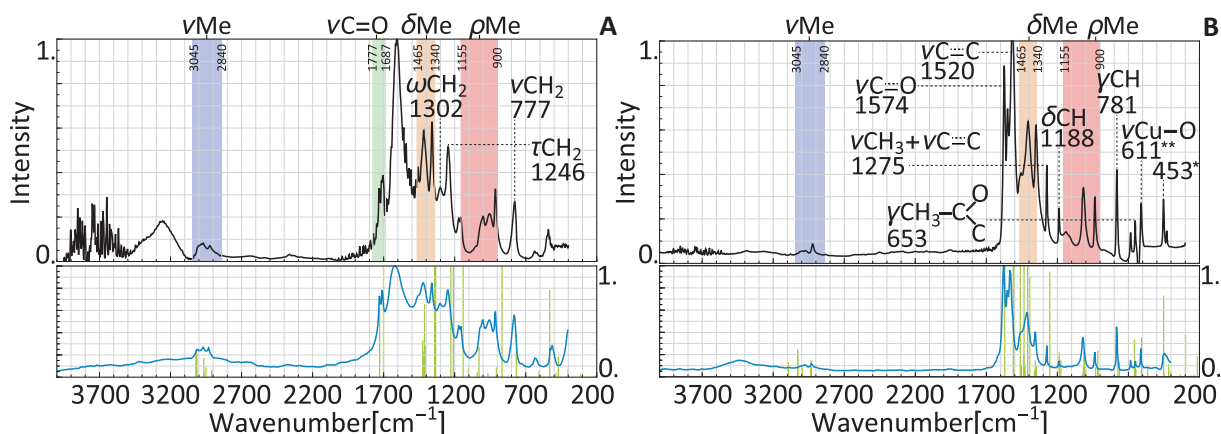


Figure 18: Infrared spectra of **A.** acetylacetonate and **B.** $\text{Cu}(\text{acac})_2$. Experimental (—), literature (—) and simulation (—).

4.6.2 IR spectra of $\text{Cu}(\text{hfacac})_2$

The IR spectrum of copper hexafluoroacetylacetonate has unique peaks, when compared with the non-coordinated ligand, those located at 417, 359 and 324 cm^{-1} corresponding the first two to the asymmetric and symmetric in-plane deformation of the ring δRing and stretching of the metal oxygen $\nu\text{Cu}-\text{O}$, and the last to the in-plane deformation of the metal oxygen $\delta\text{Cu}-\text{O}$, similar signals are found in its homologue complex $\text{Cu}(\text{acac})_2$. The torsion of the CH_2 group is present in the free ligand at 1269 cm^{-1} and, just as it happens in the case of acetylacetonate and its complex, the CH_2 disappears upon coordination and new associated vibrations with the CH group appear in the spectra of the copper complex Figure 19 B. The carbon oxygen symmetric and asymmetric stretching in the ligand in $\nu\text{C}=\text{O}$ are located at 1631 and 1690 cm^{-1} respectively, these are predicted by the simulations but very much shifted to higher wavenumbers, the antisymmetric stretching intensity of the simulation has been rescaled for better observation.

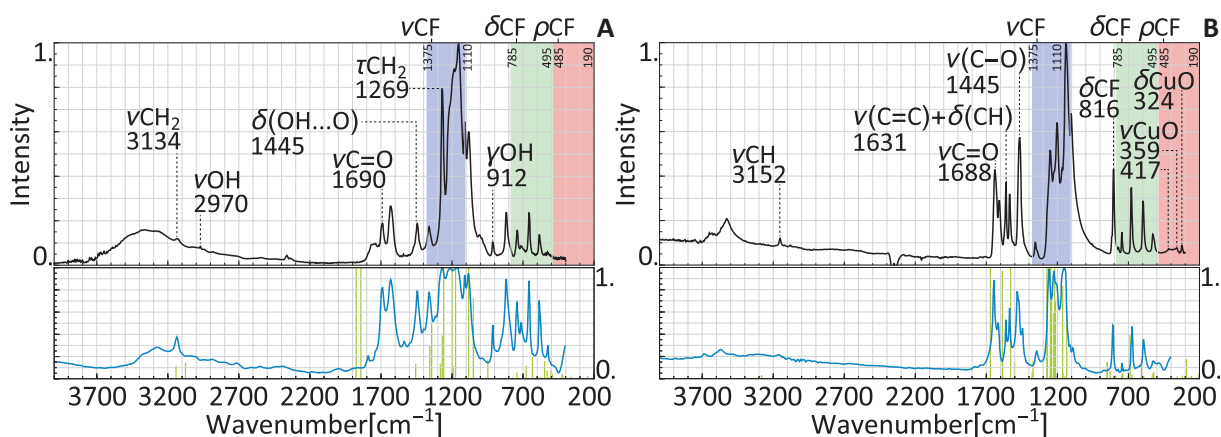


Figure 19: Infrared spectra of **A.** hexafluoroacetylacetonate (hfacac) and **B.** copper hexafluoroacetylacetonate hydrate ($\text{Cu}(\text{hfacac})_2/\text{H}_2\text{O}$). Experimental (—), literature (—) and simulation (—).

The methyl transition is located at 3152 cm^{-1} in the complex, at 3134 cm^{-1} for the free ligand, both values are similar to those reported in the literature of 3134 cm^{-1} ²⁰⁶. As seen in Figure 19 A and B the bands of the CF_3 group are the most intense in the spectra ²⁰⁷. There is completely concordance between measurements and literature peaks, simulations of the IR peaks of the ligand and the complex show all the experimental bands although some slightly shifted. The two most intense peaks in the simulated acetylacetonate spectra were multiplied by one third and used to renormalize the intensity of the smaller peaks for better observation, similar operation was performed on the $\text{Cu}(\text{hfacac})_2$ simulated spectra.

4.6.3 IR spectra of $\text{CuPyr}_2\text{Cl}_2$ and $\text{CuPyr}4\text{TBC}$

The peaks corresponding to the stretching of copper and coordinated nitrogen $\nu\text{Cu}-\text{N}$ for a $\text{Cu}(\text{II})$ di-pyridine complex should be located in the band 180-290 cm^{-1} ²⁰⁴, this region could not be measured with the available instruments to give direct indication of the coordination of

pyridine with copper, results from the *ab-initio* simulations predict such stretching at 249 cm^{-1} .

The copper-pyridine coordination can be proved indirectly by the shifts in the peaks of the bound and the unbound ligand. For pyridine the peaks at 604 cm^{-1} and 405 cm^{-1} which correspond to the in-plane and the out-of-plane ring deformation are shifted to higher frequencies upon complexation^{204 208 209}, the mentioned peak are shown in the IR of free pyridine in Figure 20 A.

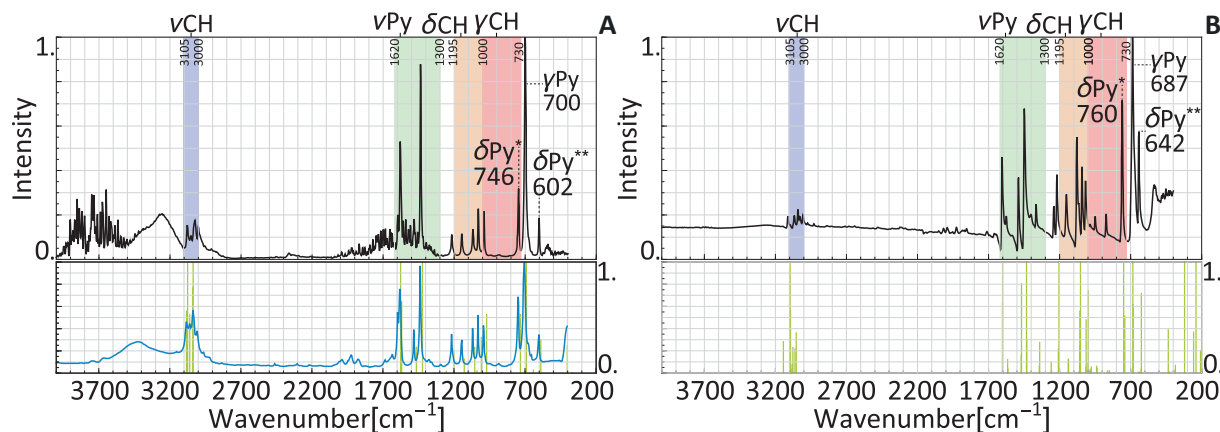


Figure 20: Infrared spectra of **A.** pyridine and **B.** $\text{CuPyr}_2\text{Cl}_2$. Experimental (—), literature (—) and simulation (—).

The IR spectra of the precursor complex $\text{CuPyr}_2\text{Cl}_2$ in Figure 20 B shows the Cu-Pyr peak displaced at 642 cm^{-1} which is in full agreement with what is reported in the literature. The in-plane ring deformation is predicted by the *ab-initio* calculations to be located at 613 cm^{-1} for the free pyridine and to 649 cm^{-1} for the coordinated pyridine. The peak occurring at 747 cm^{-1} is typical of uncoordinated pyridine and is diagnostic of the presence of free pyridine in the complex, the peak is shifted to around 760 cm^{-1} when all pyridine is coordinated, the absence of free pyridine has been observed in similar complexes like $\text{CuPyr}_4(\text{NCS})_2$ 757 cm^{-1} , $\text{CuPyr}_4(\text{I}_3)_2$ 753 cm^{-1} and $\text{CuPyr}_2\text{Br}_2$ 755 cm^{-1} , this criterion coupled with thermogravimetric analysis in literature indicates the non existence of $\text{CuPyr}_4\text{Cl}_2$ ¹⁶¹. The *ab initio* calculations predict the vibrations of the $\nu\text{Cu}-\text{Cl}$ are located at 267 cm^{-1} and 333 cm^{-1} for the symmetric and the asymmetric stretch respectively.

The peaks in the IR spectra of the complex $\text{CuPyr}4\text{TBC}$ has many vibrations of the tert-butyl group and the phenyl ring. The bonding of copper with 4TBC can be indirectly addressed by the disappearance of the peaks that correspond to the OH in-plane deformation located at 1367 and 1342 cm^{-1} . The coordination with pyridine, just as in the precursor complex $\text{CuPyr}_2\text{Cl}_2$ discussed above is indicated by the presence of the shift in the pyridine peaks located at 760 and 644 cm^{-1} . The presence of both coordinated ligand peak is due to either the presence of a heteroleptic copper complex or the mixture of two homoleptic copper complexes $\text{CuPyr}_2\text{Cl}_2$ and $\text{Cu}4\text{TBC}_2$.

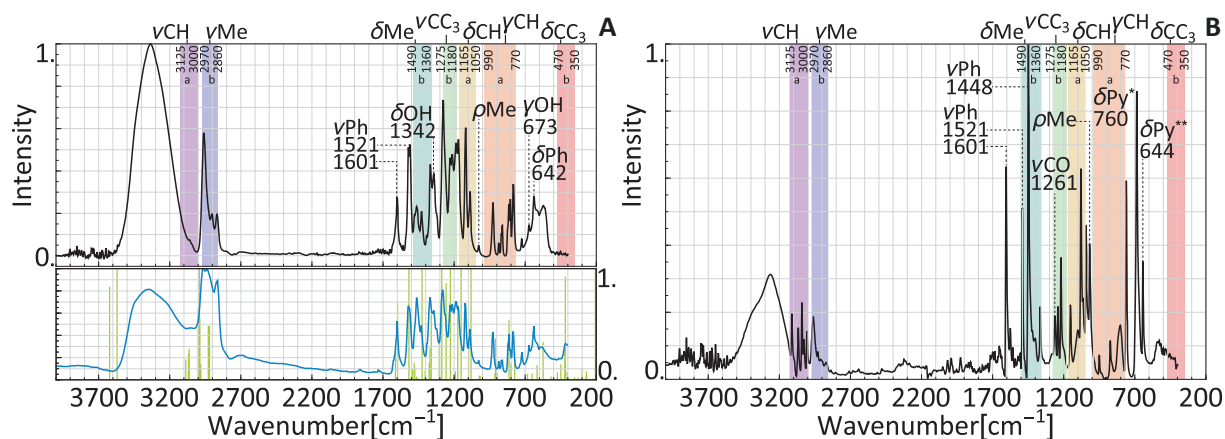


Figure 21: Infrared spectra of **A.** 4 tert-butyl catechol (4TBC) and **B.** Copper pyridine 4 tert-butyl catechol (CuPyr4TBC). Experimental (—), literature (—) and simulation (—).

The peaks at 1464 and 1259 cm^{-1} have been reported in literature as characteristic peaks of a similar complex Cu bipyridine 3,5 di-tert-butylcatechol dimer (CuPyr_2 3,5TBC)₂¹⁶⁶. The peaks appear characteristically and consistently in a variety of catechol complexes and therefore are considered a direct proof of its coordination with transition metals, the peaks correspond to the phenyl stretch (νPh) and the catechol stretch ($\nu\text{C-O}$) respectively¹⁶⁷. In the experimental IR spectra of the CuPyr4TBC similar peaks with high intensity are found at 1448 and 1261 cm^{-1} . The peak at 1261 cm^{-1} in the experimental spectra of CuPyr4TBC is not present in the precursor complex CuPyr₂Cl₂ IR spectra; but the peak at 1261 cm^{-1} in the experimental spectra of CuPyr4TBC can also be attributed to a νPy vibration. No depicted literature spectra to be digitized could be found for the CuPyr4TBC complex to compare with. All attempts to find and energy minimum geometry for this complex failed as well, all the geometries contained at least one imaginary frequency.

Resuming some important results of this section. The most important result concerning the analysis of IR measurements is the confirmation of the complexation of pyridine and 4TBC with the copper atom. The coordination of pyridine is confirmed by the peaks at 642 and 760 cm^{-1} while the coordination with 4TBC is confirmed by the peaks at 1448 and 1261 cm^{-1} . The simultaneous coordination of the ligands with one copper atom cannot be yet claimed and will be proved later with a mass spectroscopy analysis. The analysis of IR measurements of Cu(acac)₂ and Cu(hfacac)₂ is consistent with the literature reported measurements and bands.

Concerning the simulations of the IR spectra of the complexes CuPyr₂Cl₂, Cu(acac)₂ and Cu(hfaca)₂, it has been shown that all the IR simulated spectra do not contain imaginary frequencies, therefore the geometries found for the complexes are an energy minima and not a saddle point in the molecule energy curve. The geometry found for the complexes CuPyr₂Cl₂, Cu(acac)₂ and Cu(hfaca)₂ are valid structures for further calculation of electronic transitions with TD-DFT.

4.7 Mass Spectroscopy

The main objective of this section is to inquire into the nature of the synthesized complex CuPyr4TBC, to try to determine its molecular mass since the pyridine neutral ligand may be present more than once and to study if the main peak in the MS spectra corresponds with the molecular mass of the a heteroleptic copper complex containing pyridine and 4TBC. The MS spectra can be also used to try to elucidate some possible products of the photochemical reaction.

Mass spectroscopy (MS) analysis of the complex shows the peaks of the ligands, peaks of the complex moieties and products of the reaction involving the cleavage of the ligands. Several literature reports show the possibility of measuring organometallic complexes in the gas phase using electro spray ionization ESI^{210,211}, and it has been attributed to the “soft” ionization provided by ESI²¹², specific detection of other copper complexes have been proved with this technique²¹³. The ESI ionization conditions used in this work are reported in the methods section 3.4.4.

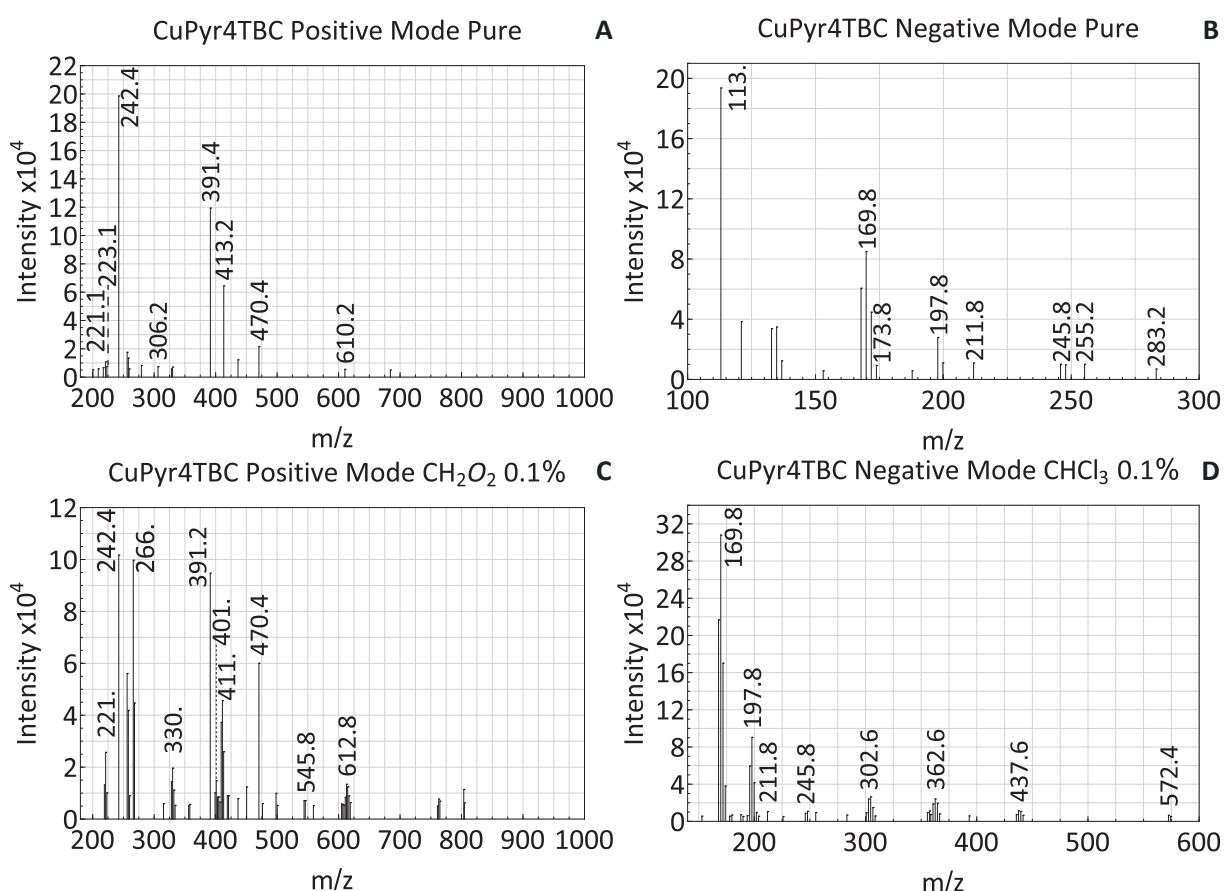


Figure 22: MS spectra of copper(II) pyridine 4-tert butyl catecholate CuPyr4TBC **A.** positive mode **B.** negative mode **C.** positive mode with 0.1% v/v formic acid **D.** negative mode with 0.1% v/v chloroform.

The MS spectrogram shows that most probably the CuPyr4TBC complex results as an equilibrium between the homoleptic complex of copper with 4TBC and the heteroleptic copper complex with pyridine and chloride. The two complexes take part in a complex equilibrium in

which the ligands are interchanged, such behavior has been seen in similar heteroleptic copper complexes¹⁶⁴.

The analysis also confirms that there are also copper dimer complexes as part of the equilibrium and that this equilibrium is sensitive to the change of solvent polarity and pH, because some complex peaks disappear upon addition of chloroform and acetic acid. The sensitivity of the instrument is high enough to detect the isotopes of copper ⁶³Cu and ⁶⁵Cu; as expected most of the copper effluents contain ⁶³Cu. The small decimal differences (of the order ± 0.5) between the ideal molecular weights and the measurement signals is due to the isotope effect, this is particularly true for complexes involving Cu and Cl. The catechol ligand can be bound to copper either as dehydrogenated catechol or semiquinone, in such cases the net charge of the ligand would be -2 and -1 respectively..

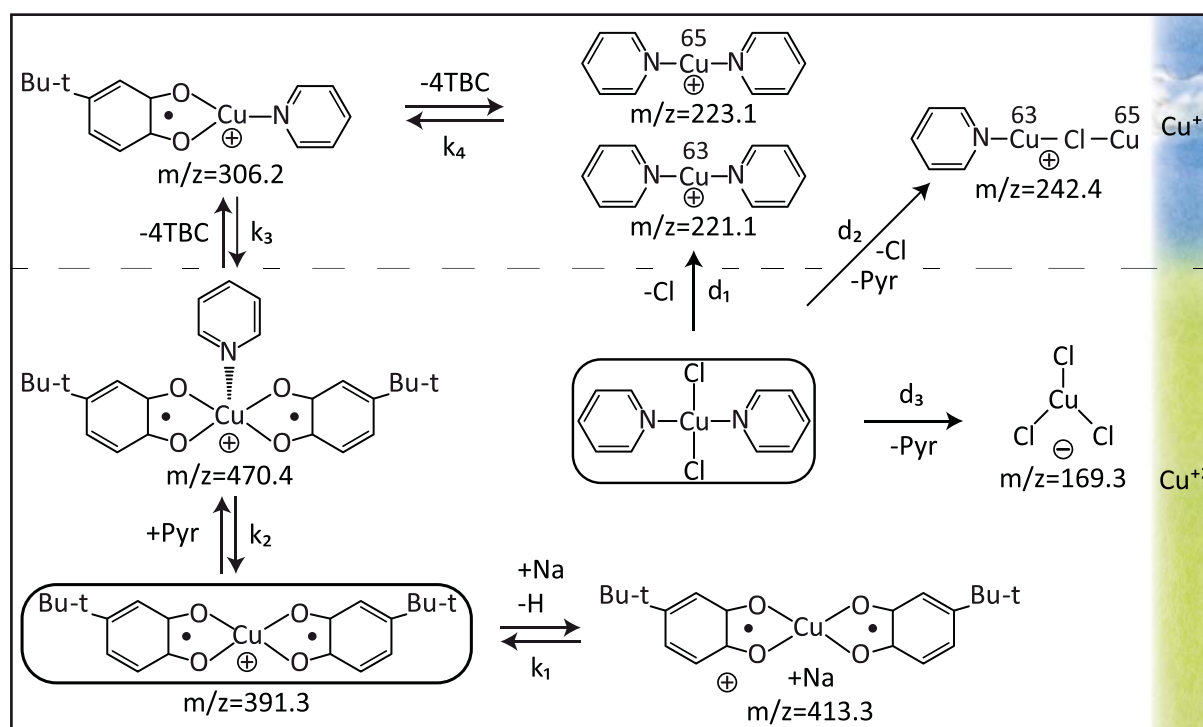


Figure 23: Effluents of the equilibrium between $\text{CuPyr}_2\text{Cl}_2$ and $\text{Cu}(4\text{TBSQ})_2$ complexes. Effluents detected in positive \oplus and negative \ominus mode in mass spectroscopy analysis.

In the MS positive mode, Figure 22 A and C, one of the highest peaks of the spectrogram corresponds to a molecular mass of 391 m/z, which is in very good agreement with the ideal molecular weight of the homoleptic $\text{Cu}(4\text{TBSQ})$ ion. The presence of the $\text{Cu}(4\text{TBSQ})$ ion is further confirmed, first by the peak at 413 m/z which is the product of deprotonation of the complex and addition of Na, leading to $\text{NaCu}(4\text{TBSQ})_2$, and secondly by the addition of formic acid, which triggers the appearance of the mono aqua complexes, $\text{Cu}(4\text{TBSQ})_2\text{H}_2\text{O}$, located at 409 m/z and 411 m/z for the two isotopes of copper.

The pH change of the solution caused by the addition of formic acid, in Figure 22 C, triggers the appearance of the peaks at 221 m/z and 223 m/z, associated with the complex $[\text{CuPyr}_2]^+$ for both copper isotopes. The complex $\text{CuPyr}_2\text{CHO}_2$ is also formed upon addition of formic acid with peaks located at 266 m/z and 268 m/z for both copper isotopes. The presence of the complex containing two pyridines is confirmed also in the negative spectra with the peak observed at 283.2 m/z corresponding to the complex $[\text{CuPyr}_2(\text{OCH}_3)]^-$, which reaffirms that coordination of copper with pyridine favors the +1 oxidation state.

The addition of chloroform triggers the formation of other copper complexes. In the negative spectra the complex peak detected at 197 m/z and 199 m/z in Figure 22 B and D are attributed to isotopes complexes $[\text{Cu}_2\text{Cl}_2]^-$. The complex formation is increased by the addition of Chloroform, as seen when comparing Figure 22 B and D. This complex is complex can be is again an initial stage of a copper cluster.

It can be seen in Figure 23 that the ionization process of $\text{CuPyr}_2\text{Cl}_2$, leads to several dissociation reactions d_1 , d_2 and d_3 ; its molecular ion cannot be detected in the MS spectra and only its dissociation products are detected. The fragment Cl forms, under the experimental conditions, the trichloro cuprate complex $[\text{CuCl}_3]^-$, showing readily the Cl dissociation, which can be detected at 169 m/z in the negative mode in Figure 22 B and D. The dissociation of the pyridine and the chloride ligands, either two chlorides (d_1) or three chloride and three pyridine of two complex molecules (d_2); from the $\text{CuPyr}_2\text{Cl}_2$ complex leads to the peaks observed at 221 m/z, 223 m/z and 242 m/z, these products are depicted in the upper part of Figure 23 because they are reduced. The dissociation of these ligands can then be associated with a charge transfer from the ligands to the central copper atom, leaving copper in +1 oxidation state. The peak located at 242 m/z corresponds with the molecular weight of binuclear copper pyridine chloride, Cu_2PyrCl , and can be seen as the initial stage of a copper cluster formation. The presence of the dimer confirms the tendency of these copper complexes to form copper dimers, as has been reported in literature ⁸⁶. The presence of the peak at 242 m/z is also direct evidence that pyridine is also dissociated from the $\text{CuPyr}_2\text{Cl}_2$ complex under the ionization conditions, and most importantly shows Cl acting as a bridging ligand between two Cu(I) centers.

The peaks located at 470 m/z and 306 m/z clearly show the complex equilibrium between the ligands 4TBC and pyridine, the peaks correspond to the molecular weight of $\text{CuPyr}(4\text{TBSQ})_2$ and $\text{CuPyr}4\text{TBSQ}$ molecular ions, respectively. Showing at first that the coordination of the $\text{Cu}(4\text{TBSQ})_2$ complex with a neutral pyridine occurs most probably in the axial positions in a square pyramidal configuration, which is in agreement with the idea that the chelation of copper by two 4TBC or 4TBSQ ligands leads to a square planar complex. The second conclusion that can be drawn from the presence of these two complexes is that although thermodynamically the complex with the bidentate ligand is favored over the monodentate ligand, the products of the substitution reaction

by pyridine are noticeable. Although a +2 oxidation state for copper in the peak at 306 m/z is possible if coordination with catechol instead of semiquinone is assumed, it is deemed as highly probable that the oxidation state of copper in this complex is +1 and it is coordinated with the semiquinone, based on the argument the coordination with nitrogen ligands favors the formation of Cu(I) complexes²¹⁴. The absence of the CuPyr₂4TBC₂ complex can be attributed also to the preference of Cu(I) to be bi-coordinated in the presence of nitrogen ligands. Similarly tetrahedral coordinated Cu(II) is prevalently observed with catechol or semiquinone chelates.

The fact that a high peak of Cu(4TBC)₂ molecular ion appears in the mass spectra shows that the complex containing 4TBC is more stable than CuPyr₂Cl₂.

CuPyr₂⁺ complexes are also detected single charged in the MS spectra, this result confirm the experimental observation in literature that pyridine actively does not withdraws charge from the copper ion. All the fragments containing pyridine are single charged, the donation of charge from nitrogen is easier than in the case of oxygen most probably due to their electronegativity, 3.04 and 3.44 respectively, compared with copper, 1.90 in the Pauling scale.

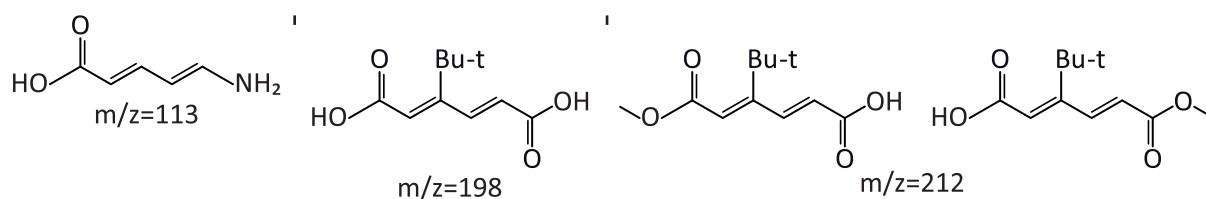


Figure 24: Possible products of the reaction detected with MS.

The MS spectra also shows some possible products of reaction which are shown in Figure 24. In the negative spectra, Figure 22 B and D the detection limit is lower than in the positive spectra. The peak at 113 m/z corresponds with the molecular weight of 5-amino-2,4-pentadienoic acid which would be a product of the bond cleavage of the aromatic ring of pyridine, similarly to what has been observed in catechol. The pyridine bond is broken in the α -position resembling the reaction observed in aryl ketones excited in the $^3(n,\pi^*)$. It cannot be stated, similarly to catechol, that the pyridine ring is cleavage specifically during the photochemical reaction, the presence of the peak at 113 m/z is considered and artifact of the measurement itself.

Other possible products are those coming from the cleavage of the ring in catechol molecules with peaks observed at 198 m/z corresponding with 3-(1,1-dimethylethyl)-2,4-hexadienedioic acid, and the peak at 212 m/z corresponding to the isomers 4-tert-butylmuconic acid monomethyl ester and 3-tert-butylmuconic acid methyl ester. The presence of these oxidized species in solution suggest that the electron in the aromatic ring might be serving also as a mechanism to reduce copper metal, as already observed by¹⁴⁸ the cleavage oxidation of catechol molecules lead to reduction of copper complexes. The ring cleavage of catechol might be considered to take place during the photochemical reaction although not necessarily triggered by it.

The most important conclusion of the MS spectra analysis shows that the CuPyr4TBC complex is an intermediate of the complex equilibrium between the complexes $\text{Cu}(4\text{TBSQ})_2$ and $\text{CuPyr}_2\text{Cl}_2$, and that this equilibrium is, as expected, sensitive to the pH and the solvent. The change in pH or solvent causes the appearance of other multi-coordinated copper pyridine 4TBSQ complexes.

Although literature reports show that products of the photochemical reaction with copper complexes containing aromatic ligands might be the result of the cleavage of the aromatic ring¹⁴⁸, these substances might be as well artifact in the measurement, because the cleavage might be also triggered by the ionization conditions.

4.8 Charge decomposition analysis on complexes

Single energy calculations on all complexes at a B3LYP/6-31G(d,p) level of theory, performed in Gaussian-09¹⁷³ were used in conjunction with the software package Multiwfn analyzer to perform the extended charge decomposition analysis (ECDA) and molecular orbitals diagrams and electrostatic potential maps^{175 215}. Extended charge decomposition analysis was carried out instead of charge decomposition analysis (CDA), because the complexes considered are open-shell which means different electronic configuration for the alpha and the beta electrons.

The charge decomposition analysis was performed to provide deep insight on how charges are transferred between fragments in a complex to achieve charge equilibrium²¹⁶. The more charge is transferred to the copper atom the higher the probability of the charge remaining on the copper atom when a covalent bond is broken.

The extended charge decomposition analysis expands the complex molecular orbital, either occupied or unoccupied, alpha or beta, using linear combination of fragment orbitals. In Table 8 the contribution to the complex molecular orbital by the virtual and occupied orbitals of each fragment are found in columns 3 – 6. The charge transfer is calculated from the polarized fragment, which are shown in Table 8 columns 7 – 10. Finally, the total charge transfer is the difference between the charge transferred from each fragment to one another in each polarization. Detailed information about the calculations can be found in literature^{216 175 215}.

The analysis ECDA was done considering the copper central atom as first fragment and the ligands as the second fragment of the complex. The ECDA analysis shows that there is more charge transferred to the copper central atom in the case of copper pyridine in comparison with the other complexes. The total charge transfer and the sequence from more to less charge transfer from the

organic ligands is $\text{CuPyr}_2\text{Cl}_2$ (-1.33) > $\text{Cu}(\text{acac})_2$ (-1.14) > $\text{Cu}(\text{hfacac})_2$ (-1.09), the value in parenthesis is the sum of the column CT for each complex in Table 8.

Table 8: Extended charge decomposition analysis of copper complexes $\text{Cu}(\text{acac})_2$, $\text{Cu}(\text{hfacac})_2$ and $\text{CuPyr}_2\text{Cl}_2$.

Complex/ Orbital	Occupancy	Frag.(1): copper		Frag.(2): ligands		A ^a	B ^b	C ^c	D ^d	CT ^e
		Occ. [%]	Virt. [%]	Occ. [%]	Virt. [%]					
$\text{Cu}(\text{acac})_2$										
Alpha	Occupied	1230.9	140.6	5313.8	14.6	0.69	1.41	0.15	0.86	-0.72
	Virtual	69.1	2159.4	86.1	22585.4					
Beta	Occupied	1388.0	54.0	5343.2	14.8	0.12	0.54	0.15	0.57	-0.42
	Virtual	12.0	2145.9	56.8	22585.2					
$\text{Cu}(\text{hfacac})_2$										
Alpha	Occupied	1231.3	137.8	10117.3	13.6	0.69	1.38	0.14	0.83	-0.69
	Virtual	68.7	2162.3	82.7	29786.4					
Beta	Occupied	1388.4	51.4	10146.7	13.6	0.12	0.51	0.14	0.53	-0.40
	Virtual	11.6	2148.6	53.4	29786.4					
$\text{CuPyr}_2\text{Cl}_2$										
Alpha	Occupied	1224.1	158.3	5905.2	12.4	0.76	1.58	0.12	0.95	-0.82
	Virtual	75.9	2141.8	94.8	20787.6					
Beta	Occupied	1389.2	61.8	5936.6	12.5	0.11	0.62	0.12	0.63	-0.51
	Virtual	10.8	2138.2	63.4	20787.5					
PL= Polarization CT= Charge Transfer ^a : PL(1) + CT(1→2), ^b : PL(1) + CT(2→1), ^c : PL(2) + CT(1→2), ^d : PL(2) + CT(2→1), ^e : CT(1→2) - CT(2→1).										

The larger charge transfer in $\text{CuPyr}_2\text{Cl}_2$ can be explained as follows. The presence of a shifted charge toward the central atom in the $\text{CuPyr}_2\text{Cl}_2$ complex can be attributed to the presence of the Cl^- ligand which can be easily oxidized, thus displacing more of its charge toward the central atom. The shift in the charge towards the central atom can also be attributed to the fact that the pyridine energy levels are lower in energy when compared to the acac and hfacac ligands. The interaction between copper and pyridine, in terms of the charge transfer, has also been observed experimentally and is attributed to two mechanisms: first the donation of the pyridine lone electron pair, which is the major contribution to the bond and second a small backdonation of the metal to the fourth π -antibonding orbital of pyridine ¹⁹⁸.

Although it is not known how much of the large charge transfer in $\text{CuPyr}_2\text{Cl}_2$ comes from the Cl and from the pyridine ligand, revision of literature result comparing ligand where the bonding atom is nitrogen with other where C, P and As are bonding atoms, suggest that the nitrogen ligands is a good choice for transferring more charge towards the copper atom as shown in the ECDA analysis.

Studies by *Bagus et al.* with CO and NH_3 copper complexes showed that although both CO and NH_3 have lone pairs available for bonding with transition metals, the charge transfer of their

interaction is different ²¹⁷. In their report they show that the amount of the σ - and π -donation in the copper complex with nitrogen are displaced toward the metal while in the case of CO complex, the π -donation was displaced towards the ligand. These results are consistent with the results obtained in this work and suggest that in order to reduce the central copper atom by mobilizing more charge from the ligand, N containing ligands should be used.

Galiano et al. performed theoretical studies with ethynylamine, ethynylphosphine and ethynylarsine at the B3LYP/6-311+G(2df,2p)/B3LYP/G-311G(d,p) and reported that the binding energy with Cu(I) is lower when the heteroatom is nitrogen, followed by arsenic and phosphorus ²¹⁸, thus not following the trend of their calculated relative basicities 189.8, 184.0 and 192.5 ²¹⁹ ²²⁰, respectively. Such results also suggest the advantages of using nitrogen as heteroatom in the ligand over other atoms of the same group, arguing that a lower binding energy with Cu(I) will lead to an easier detachment of the ligand.

Even when the copper surface is already formed the use of nitrogen containing ligands for copper photo deposition seem to be advantageous. Theoretical studies performed by *Rodriguez* shows that oxygen containing ligands acetate, methoxy and thiomethoxy have a higher electron acceptor character than nitrogen ligands, such as pyridine when bound with surfaces of metallic copper ²²¹. The mentioned results have a direct influence in the recomplexation reaction once a metal film has been formed. If free ligands are left intact in solution after the deposition of metallic copper, the back oxidation reaction of the metal can be lowered if the ligands behave more as electron donor, as in the case of pyridine. In resume, the electron donating character of the ligand is desirable because the aim of the whole process is to diminish the oxidation number of copper towards zero in any stage of the deposition process, either by favoring the reduction upon coordination or by subduing the oxidation when metallic deposition has already happened.

Resuming this section. It has been shown by extended charge decomposition analysis that there is more charge mobilized towards the central atom by Cl and pyridine ligands than by acetylacetone and hexafluoroacetylacetone ligands. The higher charge mobilization is thought to increase the probability of reduction of the central atom when the complex is formed as well as to increase the probability of the charge to remain in the copper atom once the bond between the ligand is broken. Some studies suggest an advantage of some ligands containing N over C, P and As to mobilize more charge towards the central, of course this advantage cannot be broadly assumed and more investigation in this matter is required.

5 Kinetic of the reaction

The progress of the reaction was measured with UV-Vis spectroscopy with a broad range of measurement between 200-1000 nm. The main point of interest was to address the production of metallic copper. The peak of metallic copper particles can be found at a wavelength of 574 nm, which corresponds with the plasmonic resonance of metallic copper^{222 223 224 225}. The spectra of the photoreaction were measured every 15 minutes after irradiation with a 200 W Hg lamp.

The rate of photodeposition recorded in this work at 574 nm represents the rate of the whole process, this is the rate of photochemical reaction and the rate of material deposition. The deposition process is diffusion controlled. The general mechanism of deposition is assumed to involve, the breaking of the bonds between copper and the ligand, the successive reduction of copper to metallic copper, the absorbance of metal atoms in the substrate of deposition, the nucleation of copper particles and its growth to form a film.

5.1 Kinetic of copper complexes in alcohol solutions with alkyl and aryl sensitizers

5.1.1 Kinetic of $\text{Cu}(\text{acac})_2$ with acetone as sensitizer

Experiments were performed at saturation conditions of the complex and 1:3 v/v ratio of acetone as sensitizer, in a quartz cuvette of total volume 3 mL, with methanol, ethanol and 2-propanol as solvents.

UV-Vis of the photoreaction of $\text{Cu}(\text{acac})_2$ complex (Figure 25) shows peaks at 574 nm and 680 nm, the last peak is only evident in ethanol and 2-propanol. The first peak corresponds to the plasmon resonance of copper particles produced during the irradiation of the $\text{Cu}(\text{acac})_2$ complex¹¹⁸, the second peak at 680 has been attributed to another copper complex that involves $\text{Cu}(\text{I})$ ^{118 28}. The $\text{Cu}(\text{I})$ complex is in the form of black particles²⁸ that are clearly visible in solution, the particles are visible after approximately 45 minutes of irradiation after which particles have agglomerated to a size in which they are visible¹¹⁸; the $\text{Cu}(\text{I})$ complex particles are nucleated in the inter-phase between the quartz window and the solution, specifically in the area of irradiation.

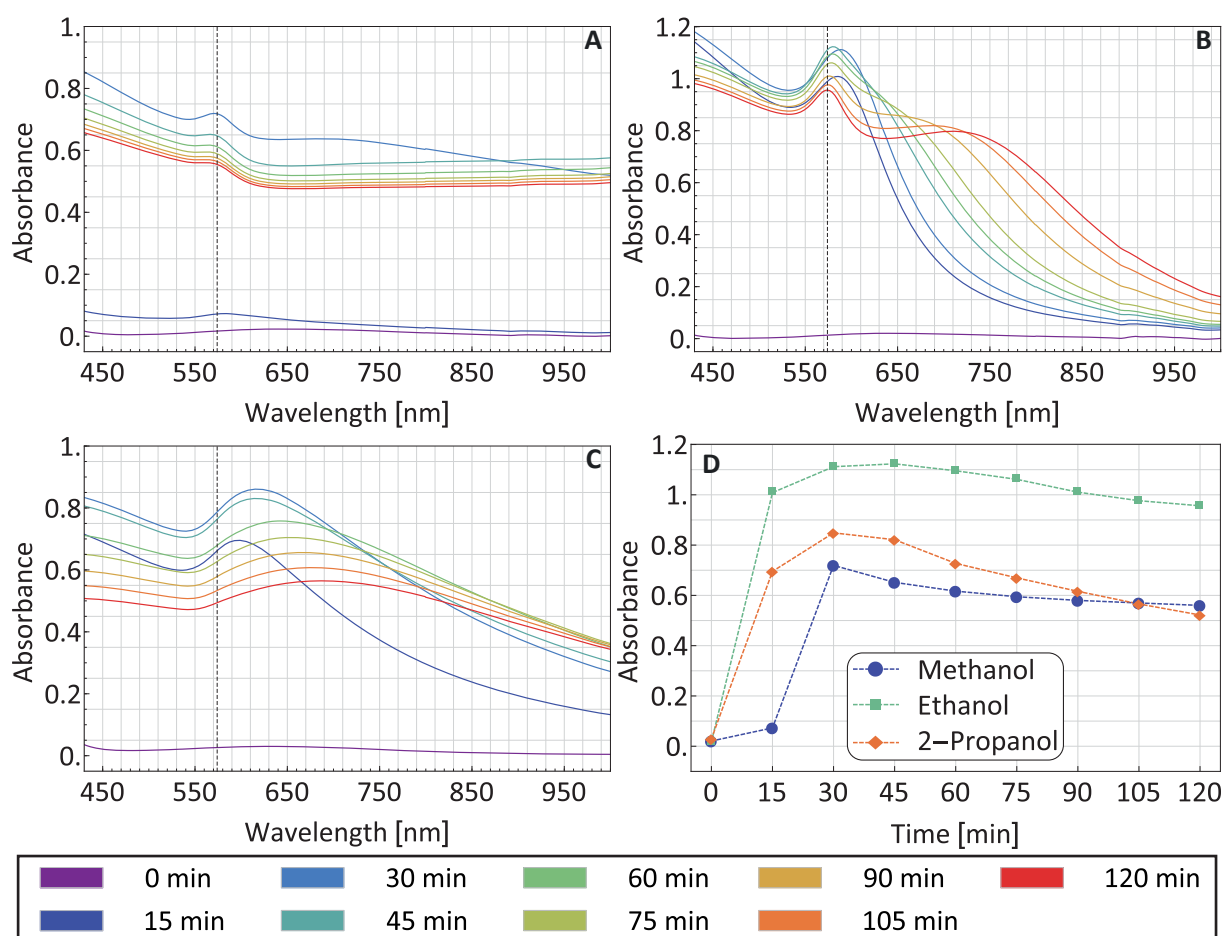


Figure 25: Kinetic of the reaction of $\text{Cu}(\text{acac})_2$ with acetone in **A.** methanol **B.** ethanol and **C.** 2-propanol **D.** kinetic of deposition of copper followed with UV-Vis spectroscopy. The dashed line at 574 nm represents the plasmon resonance of metallic copper.

The formation of a Cu(I) complex is an intermediate step in the reduction towards metallic copper. In the UV-Vis spectra of ethanol and 2-propanol, (Figure 25 B and C), it is evident that the decrease in the absorbance of the peak located around 574 nm is related with the increase of the peak at 680 nm, the peak at 680 nm seems to increase after at least 45 min of irradiation. Such observation is coherent with the results observed by ¹¹⁸, where further irradiation of intermediate Cu(I) complex lead to photodeposition of metal.

The peak associated with metallic copper particles at 574 nm increases initially within 30 minutes of irradiation as evident in the UV-Vis spectra Figure 25; after approximately 45 minutes of irradiation the peak begins to decrease. To the naked eye a visible deposition of a lustrous film on the irradiated window is detectable at 45 minutes of irradiation. The detection of the copper peak at the early stages of the irradiation can be due to production of copper nanoparticles in solution without coalescence to form a metallic film. The whole spectra is shifted upwards as the irradiation time increases, this is caused by the deposition of metallic copper on the wall of the cuvette that attenuates the incoming light therefore increasing the absorbance in the whole

spectral range.

The comparison between the different spectra suggest that the efficiency of the reaction is dependent on the solvent used. Associating the value of maximum absorbance at 574 nm with the efficiency of copper metallic deposition in Figure 25 D , the maximum efficiency is observed when ethanol is used, the change of the efficiency of deposition seem to follow the tendency EtOH>2-PropOH>MetOH.

5.1.2 Kinetic of $\text{Cu}(\text{acac})_2$ with benzophenone as sensitizer

Experiments were performed at saturation conditions of the complex and a concentration of 5×10^{-4} M of benzophenone, in a quartz cuvette of total volume 3 mL, with methanol, ethanol and 2-propanol as solvents.

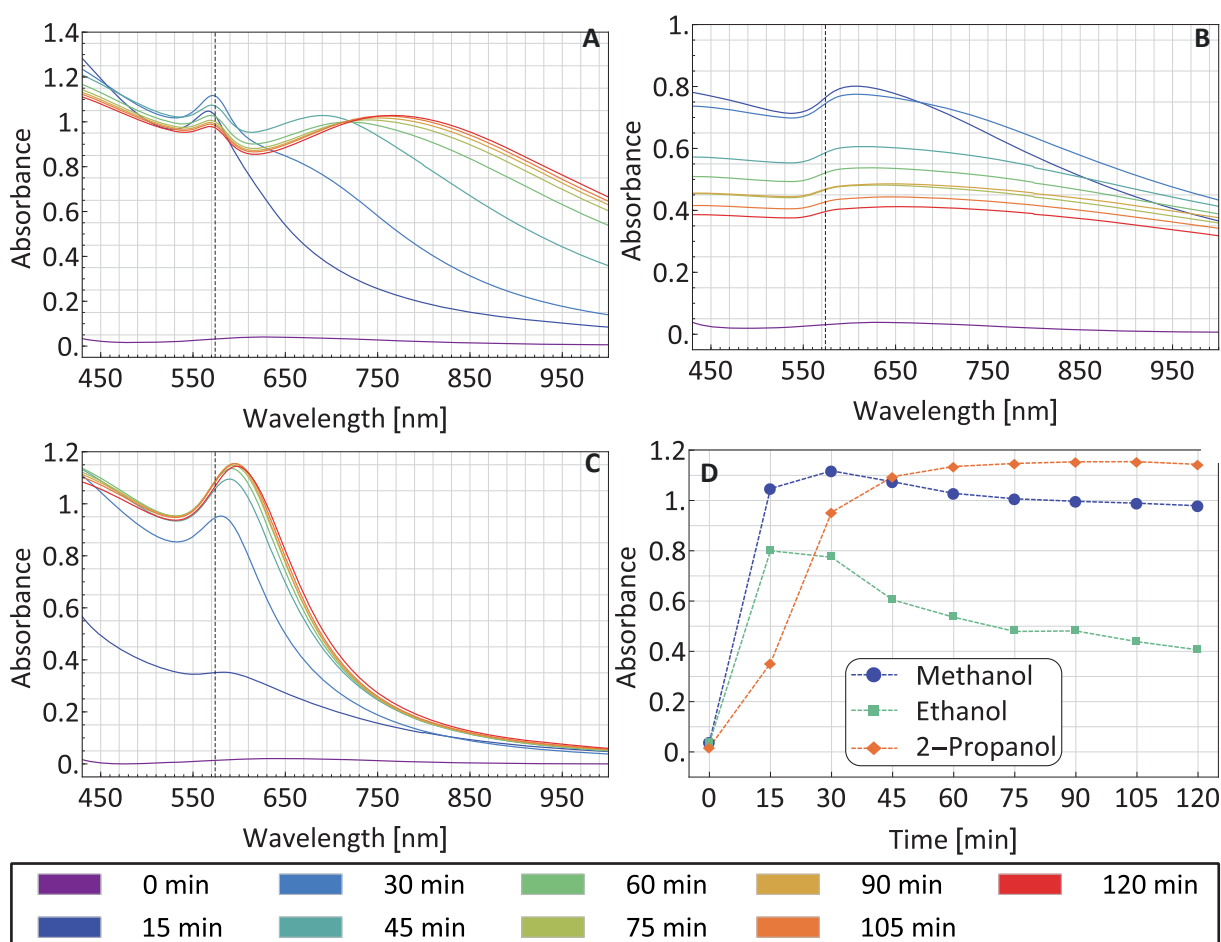


Figure 26: Kinetic of the reaction of $\text{Cu}(\text{acac})_2$ with benzophenone in **A.** methanol **B.** ethanol and **C.** 2-propanol, **D.** kinetic of deposition of copper followed with UV-Vis spectroscopy. The dashed line at 574 nm represents the plasmon resonance of metallic copper.

Irradiation experiments with benzophenone show deposition of metallic copper by the appearance of the peak at 574 nm. In methanol and ethanol the peak increases within 45 minutes of irradiation followed by a decrease in the absorbance, the decrease is observed till the end of

the irradiation experiment. The descent of the 574 nm peak is more pronounced in ethanol than in methanol (Figure 26 A & B).

The highest absorbance in the 574 nm peak is observed when 2-propanol is used as solvent (Figure 26 C), the reaction in this solvent with benzophenone is characterized by a rapid increase of the peak within 45 minutes followed by a slow increase till a maximum absorbance value; deposition of metallic copper film was observed on the irradiated window at the end of the experiment. The deposition in methanol and ethanol with benzophenone just as when acetone is used as a sensitizer (Figure 25), occurs during the first 30 to 45 minutes of irradiation and later starts to decrease in time. Contrary to what is observed in the 2-propanol-acetone system, in 2-propanol-benzophenone the deposition of copper is maintained during the whole irradiation time, seen as a steady rise in the peak at 574 nm till saturation is reached. The saturation in these experimental conditions is reached when enough copper metal has been deposited forming a film that hinders light from triggering the reaction and going through the cuvette.

With benzophenone the reaction seems to be more efficient in 2-propanol; following the tendency 2-PropOH>MetOH>EtOH (Figure 26 D), different from the tendency reported in literature 2-PropOH>EtOH>MetOH²⁸.

As observed in the cases of the sensitized reaction with acetone a second peak increases with time in the UV-Vis spectra of methanol and ethanol Figure 21 A & B, when benzophenone is used the peak seems to be located further away from the metallic peak of copper compared with the results with acetone as sensitizer.

5.1.3 Kinetic of CuPyr4TBC with acetone as sensitizer

Experiments were performed at saturation concentration as in the complex $\text{Cu}(\text{acac})_2$ shown previously.

During the irradiation CuPyr4TBC no production of particles or precipitates was observed in solution and a copper mirror was observed after 15 minutes of irradiation.

The kinetic of reaction of CuPyr4TBC shows some important differences when compared with the reactions of the complex $\text{Cu}(\text{acac})_2$. First, the peaks located at wavelengths higher than 574 nm have disappeared in the UV-Vis spectra of the irradiated complex solution in ethanol and 2-propanol (Figure 27 B and C); a very broad band is observed in the kinetic with methanol around 740 nm (Figure 27 A). Secondly, a continuous deposition of copper is observed as the absorbance at 574 nm always increases as irradiation time increases.

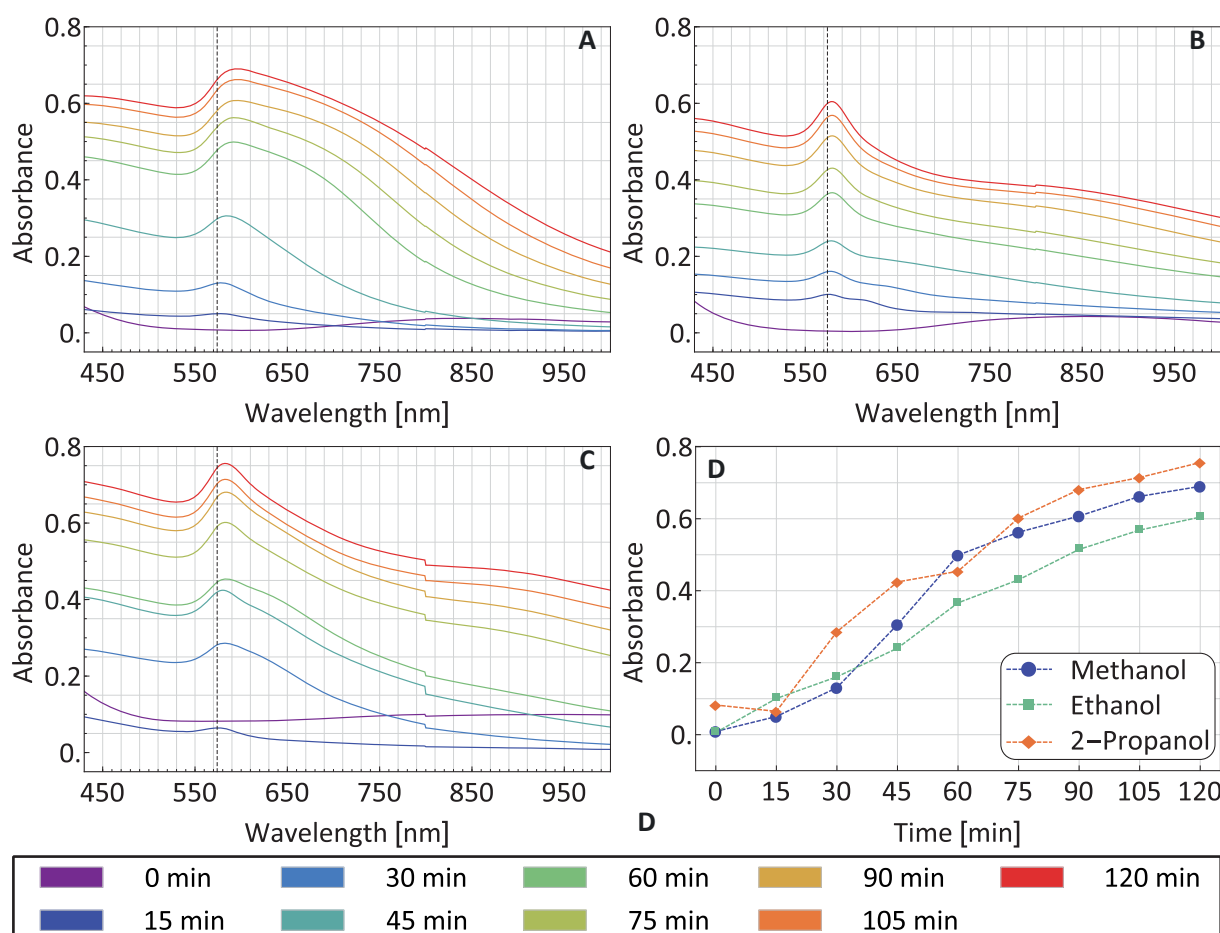


Figure 27: Kinetic of the reaction of CuPyr4TBC with acetone in **A.** methanol **B.** ethanol and **C.** 2-propanol **D.** kinetic of copper photodeposition followed with UV-Vis spectroscopy. The dashed line at 574 nm represents the peak of metallic copper.

Focusing in the presence of copper complexes in solution, the fact that no secondary peak is observed in with this complex when ethanol and 2-propanol are used as solvents can be clarified as follows. A Cu(I) complex must be an intermediate in the photoreduction of copper, the absence of other peaks than that at 574 nm for metallic copper, suggest that any Cu(I) complex does not absorb in the irradiated wavelength or that the Cu(I) complex absorbs in the irradiated wavelength but it is not found in higher concentrations in solution. It is expected hat the Cu(I) complex has some kind of absorption and since there are some small absorptions around 620 nm, it is believed that no high concentrations of Cu(I) complex are found during the reaction, which implies that the reaction from Cu(I) to metallic copper is fast, and therefore there is not enough Cu(I) complex to be detected in solution. The presence of a peak located around 660 nm is detected when the reaction is done in methanol Figure 27 A.

Comparison of the deposition of copper in Figure 25 and Figure 27 shows that, for the Cu(acac)₂ complex the irradiation leads to an increase of a peak at 574 nm within 30 minutes followed by a steady decrease of the peak intensity whereas for the CuPyr4TBC complex a steady

increase of the signal is observed for the whole irradiation time. It was observed on multiple times that the deposited copper material on the cuvette wall was always found more inhomogeneous for $\text{Cu}(\text{acac})_2$ than for CuPyr4TBC , the spots deposited with the first had a black coloration and the film was found to have many spots without copper deposition. The maximum absorbance at 574 nm was always higher for $\text{Cu}(\text{acac})_2$ than for CuPyr4TBC , yet less material was observed deposited in the cuvette wall. The photodeposition of a copper film involves the reduction of copper in solution to metallic copper and its nucleation on a substrate surface. It is though that the peak in the kinetic of $\text{Cu}(\text{acac})_2$ within 30 minutes of irradiation causes rapid formation of metallic particles in solution, but this rapid nucleation of particles does not lead to more deposited material. The steady production of copper in the kinetic of CuPyr4TBC on the other hand leads to a better growth of an homogeneous copper film.

As seen in Figure 27 D, the kinetic curves for 2-propanol, ethanol and methanol are very irregular and very similar, there is not a significant difference between the kinetic of reaction in any of the three used solvents, leading to the practical conclusion that the reaction is equally efficient in these solvents and that any of them can be indifferently used.

5.1.4 Kinetic of $\text{CuPyr}_2\text{Cl}_2$ with acetone as sensitizer

Experiments were performed at saturation conditions of the complex and 1:3 v/v ratio of acetone as sensitizer.

As seen in Figure 28 the kinetic of the precursor complex is very similar to the kinetic of the CuPyr4TBC complex, characterized by the steady increase of the metallic copper absorption peak at 574 nm. The graphics in Figure 28 A and B are equivalent to Figure 27 A and B of the mixture complex CuPyr4TBC . In the graphic with methanol a similar shoulder is observed in both complexes $\text{CuPyr}_2\text{Cl}_2$ and CuPyr4TBC , such close similarities constitute another argument, apart from the one discussed in the MS spectra analysis, to state that the CuPyr4TBC is a mixture complexes comprising the $\text{CuPyr}_2\text{Cl}_2$ complex. Moreover, this results suggest that the most active specie for photoreduction in the CuPyr4TBC mixture is $\text{CuPyr}_2\text{Cl}_2$.

Ethanol as well as methanol are deemed to be equivalent for the photoreduction of this complex. The curves run nearly parallel to one another. Although no experiment with 2-propanol is available, it is expected to see a similar result of what it has been observed in the CuPyr4TBC , given the similarities of the kinetic curves in ethanol and methanol.

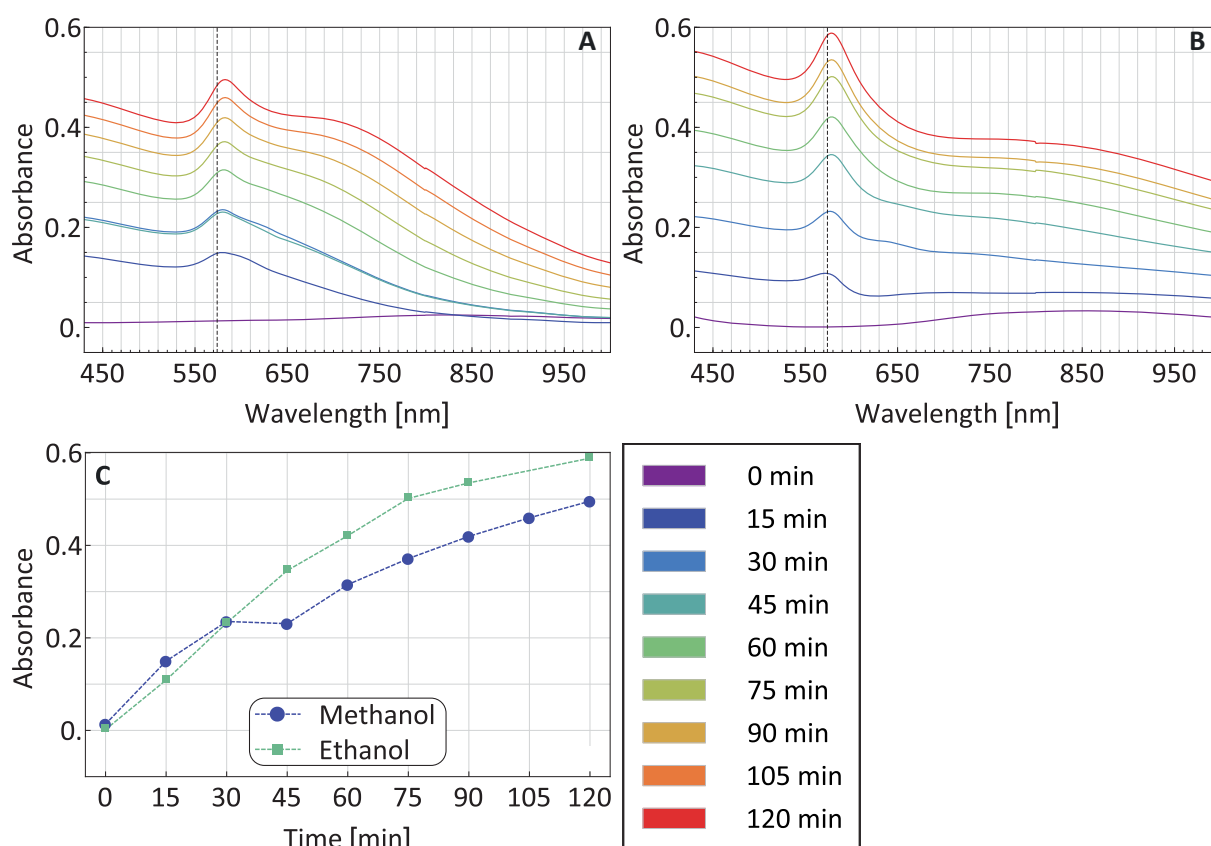


Figure 28: Kinetic of the reaction of $\text{CuPyr}_2\text{Cl}_2$ with acetone in **A.** methanol and **B.** ethanol, **D.** kinetic of copper photodeposition followed with UV-Vis spectroscopy. The dashed line represents the peak of metallic copper.

5.1.5 Kinetic of CuPyr4TBC with acetone in solvents with less hydrogen donating ability

Reactions were carried out in non-polar aprotic solvents, polar aprotic solvents and polar protic solvents. The solubility of the complex was observed experimentally to be lower in non polar solvents.

A saturated solution of the CuPyr4TBC complex was prepared in chloroform-acetone in a 3:1 ratio. Irradiation of the solution leads to deposition of a white powder on the irradiated window. The product was stable in air and has a high adherence to the glass surface. No formation of particles or deposition of material with copper appearance was detected. Similar results were observed when a saturated solution of CuPyr4TBC was irradiated in a n-hexane - acetone 3:1 ratio solution. No significant changes in the solution were observed, no deposition of particles or films were detected during the whole irradiation time. For the non-polar aprotic solvents, n-hexane and chloroform, no deposition of metallic copper was observed whatsoever during the irradiation experiments which can be evidenced in Figure 29 B and C, where no peak near 574 nm can be observed. In the experiment with chloroform a white substance with high adherence to the quartz

window was observed, the substance was not further investigated. The lack of deposition in the case of chloroform can be attributed to the activation of a secondary reaction competing with the copper deposition reaction that deposits a white substance. The substance could not be further analysis because it could not be recovered due to its low solubility and the small amount of material formed.

As polar aprotic solvents acetonitrile and DMSO were tried, no changes in the solution of formation of films or particles was observed in both experiments for the whole irradiation time, the results with acetonitrile are shown in Figure 29 A, were no peak at 574 nm was observed. The solutions of the complex in acetonitrile and DMSO were prepared as the solutions mentioned above.

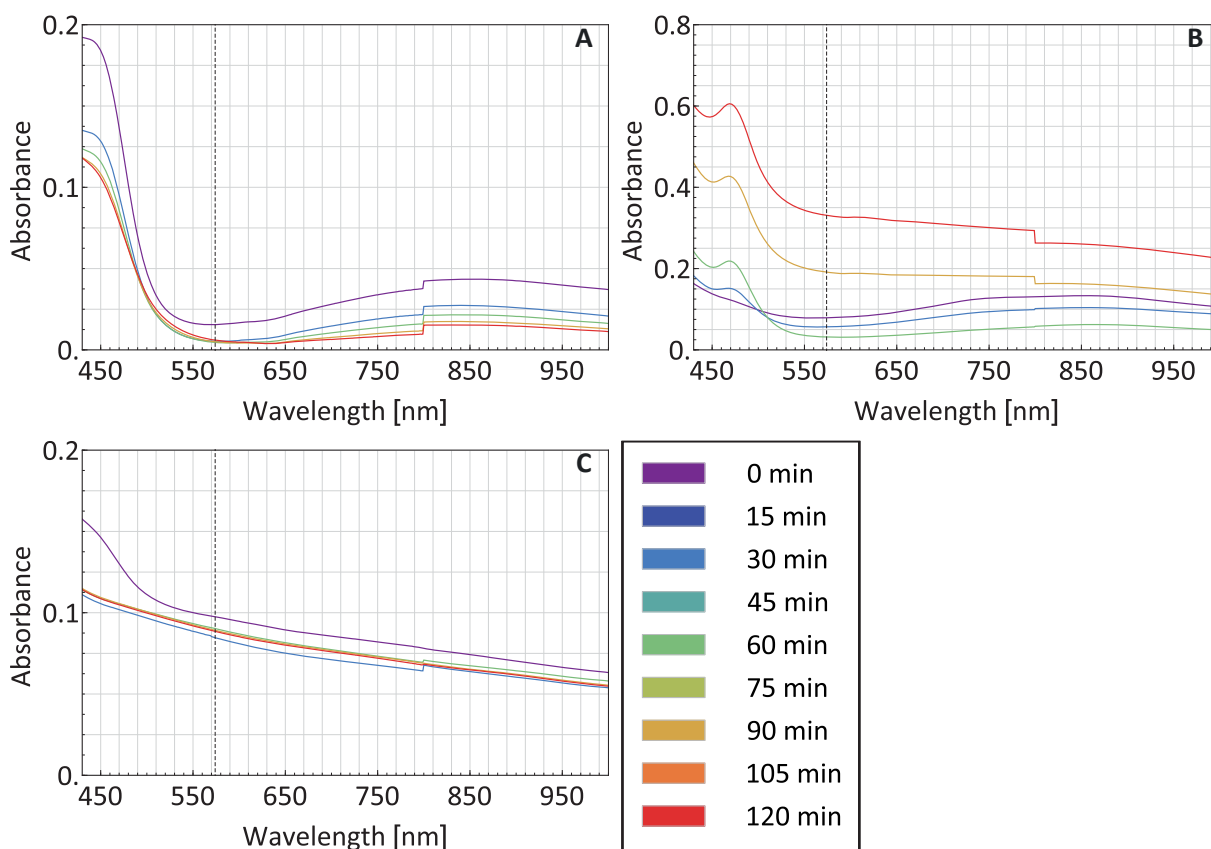


Figure 29: Kinetic of the reaction of CuPyr4TBC with acetone in **A.** acetonitrile, **B.** chloroform and **C.** n-hexane followed with UV-Vis spectroscopy. The dashed line represents the peak of metallic copper.

A comparison of Figure 29 and Figure 27, where protic solvents were tried, shows that the deposition reaction is favored by the presence of hydrogen donating solvents. The hydrogen α donating parameter for methanol, ethanol and 2-propanol are 0.93, 0.83 and 0.76 respectively^{226 227}, meaning that the solvent that works best as a hydrogen donor is methanol. While for acetonitrile, n-hexane and chloroform the hydrogen α donating parameter are 0.19, 0.00 and 0.44. Although chloroform is a fair hydrogen donor, the reaction in this solution was observed to produce a white precipitate instead of a copper film.

5.1.6 Kinetic of CuPyr4TBC without acetone in a TiO₂ layer over PET

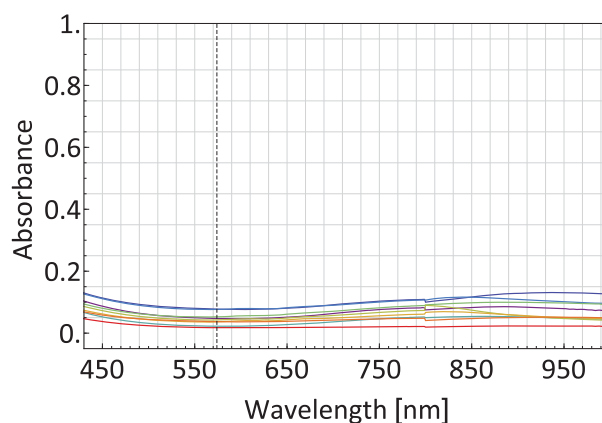


Figure 30: Kinetic of the reaction of CuPyr4TBC in ethanol with a TiO₂ layer over PET as sensitizer.

TiO₂ was tried as photo catalyst of the reaction. Solutions of CuPyr4TBC 5×10^{-4} M in ethanol without acetone were irradiated for 120 min with a 200 W Hg lamp. As seen in Figure 30 no deposition was observed during the whole irradiation time. This experiment show that the potential of TiO₂ might not been sufficient for the reduction of the copper complex or most importantly the complex does not couple with the excitation and reduction mechanism of TiO₂. On the contrary it was observed consistently that the reduction of the copper complexes to metallic copper was achieved when a ketone sensitizer was in solution which indicates that the reduction mechanism of TiO₂ and the ketone sensitizer are radically different, and only the mechanism of the ketone sensitizer can reduce the copper complexes effectively.

5.2 Kinetic of reaction at different wavelengths

The kinetic of the reaction of the synthesized complex was compared with the kinetic of the reactions of commercial complexes at different wavelengths. The wavelengths of reactions where the reaction predominantly happened are shown for comparison in Figure 31. The wavelength where the reaction proceeded the fastest was at 260 nm, this is thought to be mainly because of two combined reasons directly related with the principles of photochemical reactions, first benzophenone is used as sensitizer and the absorption coefficient at 260 nm ($\epsilon = 2086.4 \times 10^3$) is the second highest when compared with the other wavelengths 245 ($\epsilon = 2153.8 \times 10^3$), 275 ($\epsilon = 756.056 \times 10^3$), 285 ($\epsilon = 383.4 \times 10^3$) and 300 nm ($\epsilon = 51.7 \times 10^3$ m²/mol); secondly the optical power at 260 nm is 4.3 times larger than at 245 nm, where the absorption coefficient is higher.

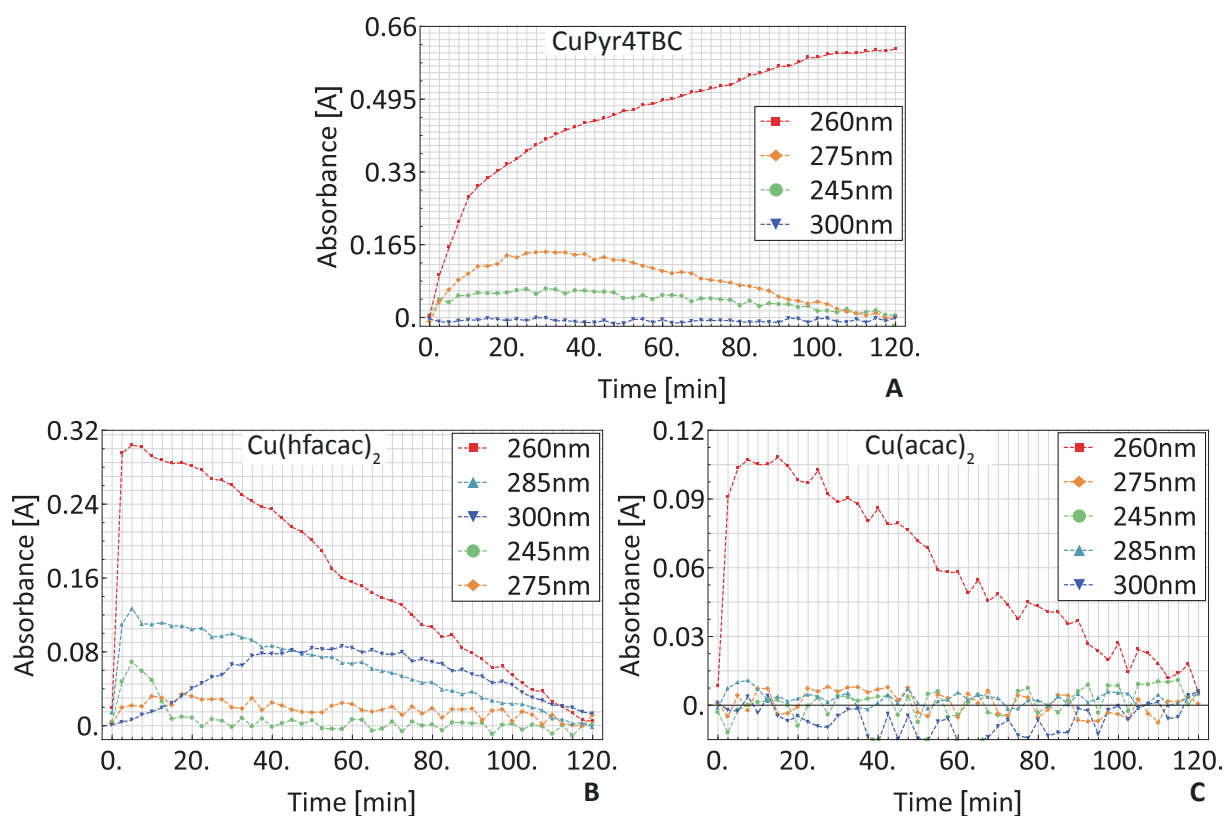


Figure 31: Kinetic of copper complexes irradiated with different wavelengths in methanol sensitized with benzophenone **A.** CuPyr4TBC **B.** Cu(hfacac)₂ **C.** Cu(acac)₂.

The absolute value of the absorbance of metallic copper in Figure 31 for CuPyr4TBC complex is higher at every wavelength when compared with Cu(hfacac)₂ or Cu(acac)₂, except at 300 nm when compared with Cu(hfacac)₂. The reaction at 300 nm for Cu(hfacac)₂ in Figure 31 B shows a deposition of copper, at this wavelength the sensitizer has a low molar absorption coefficient ($\epsilon = 51.2$) but the absorption of the complex is high ($\epsilon = 1168.2 \text{ m}^2/\text{mol}$). Suggesting that the direct absorption of light by the complex might be causing the loss of the ligand and reduction to metallic copper, following the reaction



Efficient ligand loss reactions are most commonly caused by ligand field, metal to ligand or ligand to metal transitions²²⁸, because they entail an electron transfer from or to the metal, which formally change the oxidation state of the metal and destabilize the coordination geometry. As previously reported in the section explaining the simulated energy transitions, several LMCT transitions were found in this complex.

5.2.1 Stages of the reaction kinetic

The reaction rate in Figure 32 A and B seem to be fast initially then it decreases reaching a minimum and then increase to an almost constant rate. Based on this behavior it was assumed that a counter reaction to the desired reaction of metallic copper deposition was taking place. The kinetic in Figure 32 A was carried out with similar concentrations of complexes in solution, CuPyr4TBC [2.61×10^{-3}] M, Cu(hfacac)₂ [5.30×10^{-3}] M and Cu(acac)₂ [6.11×10^{-3}] M, with the same concentration of benzophenone, [2.41×10^{-5}] M, in methanol.

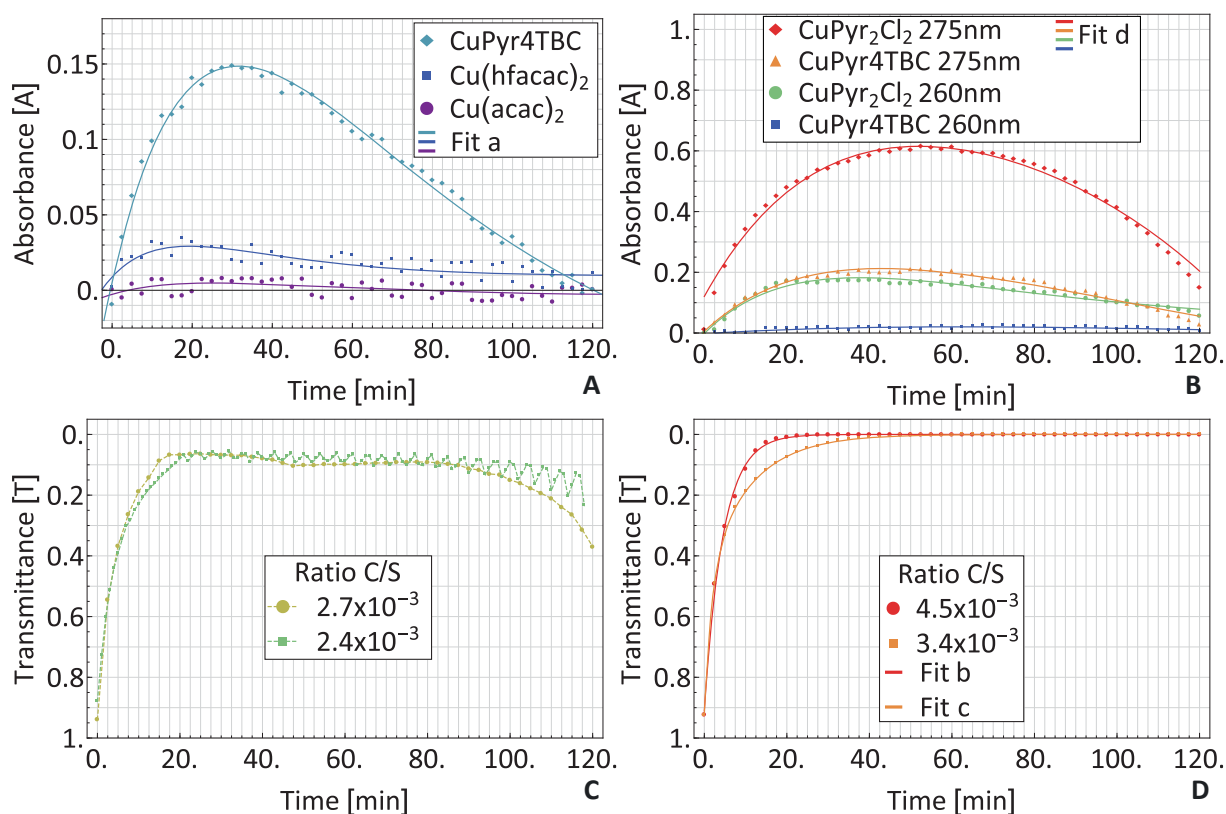


Figure 32: Reaction kinetics at 574 nm irradiated with 275 nm UV-LED with different CuPyr4TBC/benzophenone (C/S) ratios **A.** concentration of complex 4.4×10^{-4} M and **B.** 3.6×10^{-4} M **C.** reaction kinetics of CuPyr4TBC/benzophenone (C/S) ratio below optimal **D.** reaction kinetics of CuPyr4TBC/benzophenone (C/S) ratio near optimal value.

As the results show in Figure 32 A, the synthesized complex CuPyr4TBC shows better performance in the deposition of metallic copper than the commercial complexes Cu(acac)₂ and Cu(hfaca)₂. CuPyr4TBC yields higher rates of reaction, as the initial slope of the kinetic curve is more pronounced, and seven to fifteen times more deposition (ratio between the maximal absorbance) than commercial complexes Cu(hacac)₂ and Cu(acac)₂ respectively.

The kinetic in Figure 32 B was carried out at saturation conditions of CuPyr4TBC and CuPyr₂Cl₂, with the same concentration of benzophenone in methanol. It shows that the precursor complex CuPyr₂Cl₂ has even higher rates and yields of photodeposition than the complex CuPyr4TBC although the solubilities are in the same order of magnitude. Thus CuPyr₂Cl₂ constitutes the complex that deposits copper most efficiently. The kinetic of deposition in Figure 32 B still shows

that at some point after the maximum absorbance has been reached the deposited copper spot dissolves.

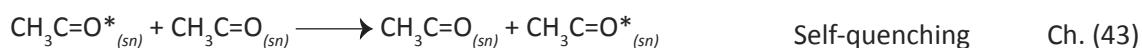
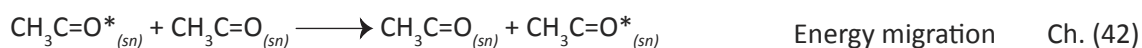
The decrease in the reaction after some point is not understood completely. It is thought that the sensitizers do not regenerate during the reaction, meaning it does not act as a catalyzer. At some point the sensitizer its depleted and a counter reaction competing with the reduction reaction dissolves the deposited metal. Based on this idea the ratio of complex to sensitizer was modified to study its impact on the kinetic of metallic deposition. The aim of the optimization was to reach complete coverage of the sampled spot with copper and maintain the deposited metallic spot.

$$\text{ratio } \frac{C}{S} = \frac{\text{moles of sensitizer in solution}}{\text{moles of complex in solution}} \quad \text{Ch. (41)}$$

The C/S ratio was decreased to optimize the reaction, as shown in Figure 32 C and D. The reactions seems to be divided in different phases, this becomes evident in the set of experimental results. The reaction kinetic in Figure 32 C shows that the reaction kinetic can be divided into three phases in terms of the transmittance, a starting phase of the reaction with no lag phase, a steady state phase and a depletion phase. Assuming that the relation between the reaction rate and the transmittance are linear, the reaction rate in the starting phase is characterized by an exponentially decrease of the transmittance, the upper limit of this first phase is reached when the transmittance is zero and it is not possible to transmit more light because the metallic spot reflects all incoming light. Next comes the steady region of the reaction, characterized by a constant value of the transmittance; the steady state phase of the reaction is long lasting compared with the starting and the ending phases, detailed analysis of this phase shows that we need to discern two trends. As seen in Figure 32 C the steady state can be characterized as a straight line or a unsteady line. The serrated trend was always observed when the solutions were not fresh, the straight trend was always observed when the solutions were fresh. The jagged line is the result of changes in the thickness and homogeneity of the film due to a counter-reaction. The deposition and dilution of the copper spot caused by the reaction and counter reaction are responsible of the jagged line, deposition and dilution recourse till the amount of sensitizer in the system is depleted, leading to the death phase of the reaction. In the death phase the velocity of reaction increases with time, perceived as an almost step decrease in the transmittance. When the reaction was done with lower concentrations of sensitizer in solution as in Figure 32 A and B the steady state of the reaction could not be reached. Which means that the sensitizer is key to the process of reduction to metallic copper, the total the equilibrium of the reaction is only shifted by the presence of the excited sensitizer in solution.

Comparison of Figure 32 C and D, shows that the steady state phase of the reaction is dependent on the concentration of the sensitizer and that the optical density of the deposited film, which is proportional to the amount of deposited metallic copper, is also affected by this variable.

The transmittance reached in Figure 32 C is lower than the transmittance reached in Figure 32 D although the amount of sensitizer in C was higher. The lower reaction rate at higher amounts of sensitizer can be attributed to a self-quenching mechanism of the sensitizer. In the self-quenching mechanism the concentration of the sensitizer is too high, leading to the point where is more probable that the sensitizer reacts with itself than finding a molecule of the complex to react. The reaction of an excited molecule of sensitizer with itself would lead to an energy transfer (Ch. (42)) or a self-quenching mechanism (Ch. (43)), the later would be followed by deactivation of the excited state though luminescent or thermal decay, as represented in the following reactions



6 Metallic depositions

Copper depositions was carried out mainly in quartz cuvettes. Deposition of metallic copper happened on the irradiated window of the cuvette. The depositions were analyzed with microscopic images as well as the content of the deposition was determined with EDX.

6.1 EXD analysis of the deposited material on quartz and TiO_2

Deposition experiments were performed on a separated slide of quartz glass and a TiO_2 layer over PET placed inside the cuvette and next to the irradiated window, as shown in Figure 33, with the objective to have a sample of the photodeposition while preserving the integrity of the quartz cuvette.

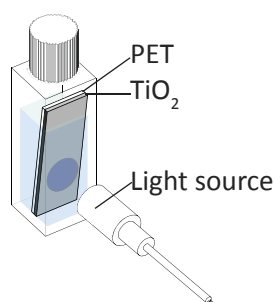


Figure 33: Experimental setup for deposition of metal over a substrate piece inside the cuvette.

The complex solution consisted of a saturated solution of CuPyr4TBC in methanol sensitized with benzophenone. This experimental setup was used to analyze the chemical composition of the deposition by EDX. Results of this experimental setup are showed in Figure 34.

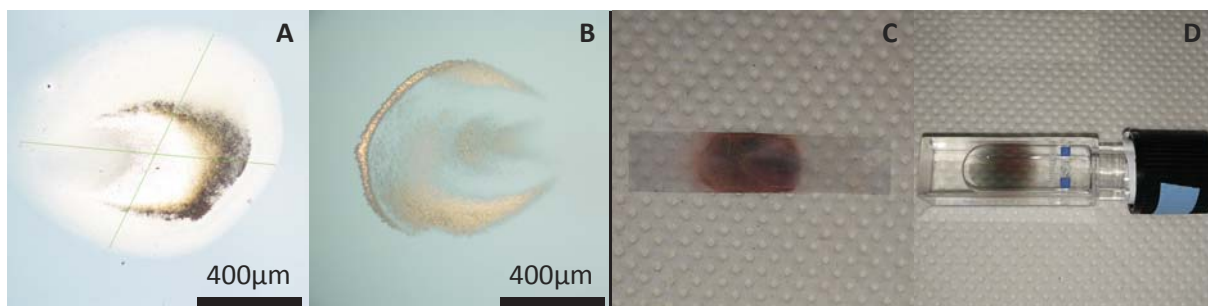


Figure 34: Ketone sensitized metallic deposition on **A.** irradiated window of a quartz cuvette **B.** removable quartz glass slide **C.** removable PET piece with TiO_2 layer **D.** irradiated window next to the PET piece.

Deposition of copper particles or copper films was easily done on quartz substrates, the use of polymeric material, such as pure PET, as substrate resulted in fewer particle deposition and

no compact deposition. This can be explained due to the low adhesion of metals to polymers. The affinity of the metal with the substrate is also a key technical aspect for the deposition of metallic copper. Deposition was also successfully achieved on TiO_2 layers. If deposition of copper is desired on polymeric material, the material should be coated previously with a glassy material.

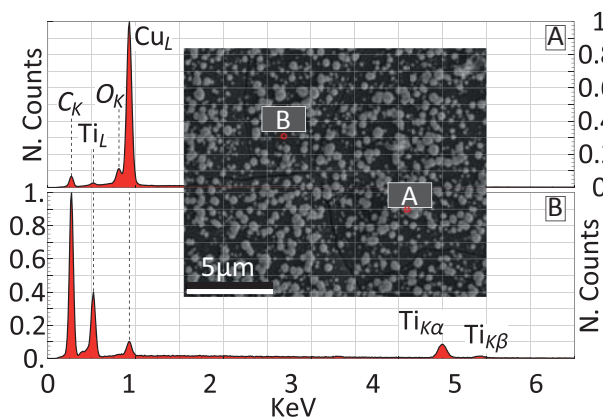


Figure 35: EDX analysis of deposited particles on TiO_2 layer over a piece of PET. CuPyr4TBC complex in methanol sensitized with benzophenone **A**. sample spot on a copper particle **B**. sample spot on the substrate.

The EDX analysis was performed on the metallic deposition over a TiO_2 layer on PET. As seen previously in section 5.1.6 the TiO_2 does not catalysis the reduction of the copper complex. The EDX analysis was performed in two positions, one where particles where deposited and the other on the bare substrate of TiO_2 (Figure 35). The EDX of the spot containing particles (Figure 35 A) shows up to 90% of copper content with very low oxygen content, the signal of the TiO_2 substrate below is barely detected. This result shows that the deposited spots are mostly metallic copper and not copper oxide. The oxide present in the analyzed spot, evidenced as a small oxygen peak, can be due to the exposure to oxygen in air as well as copper oxide that has formed with the remaining oxygen in the degassed solution. In contrast the sampled spot where no particles are observed (Figure 35 B) shows a high content of carbon and oxygen, titanium and a negligible copper peak; the carbon oxygen and copper peaks most probably come from complex dried on the surface of the sample.

In conclusion, the EDX analysis confirms that the observed spots with metallic appearance are indeed metallic copper and that the copper content is high, although some carbon and oxygen are detected it cannot be clarified if these contaminants are present in the interior or external layer of the particles or are just detected because of the interaction volume of the X-ray beam.

6.2 Depositions of systems irradiated with UV-LED's

The deposition of metallic copper spots were successfully obtained with low intensity light sources, i.e. UV-LEDs. As show in earlier chapters the energy of the light sources never surpasses 0.4 mW. The total time of the experiment was 120 min of irradiation. The concentrations of the complexes in each column were equivalent as well as the solvent and concentration of the sensitizer, benzophenone. The images of deposited copper spots from various complexes at different wavelengths is shown in Figure 36.

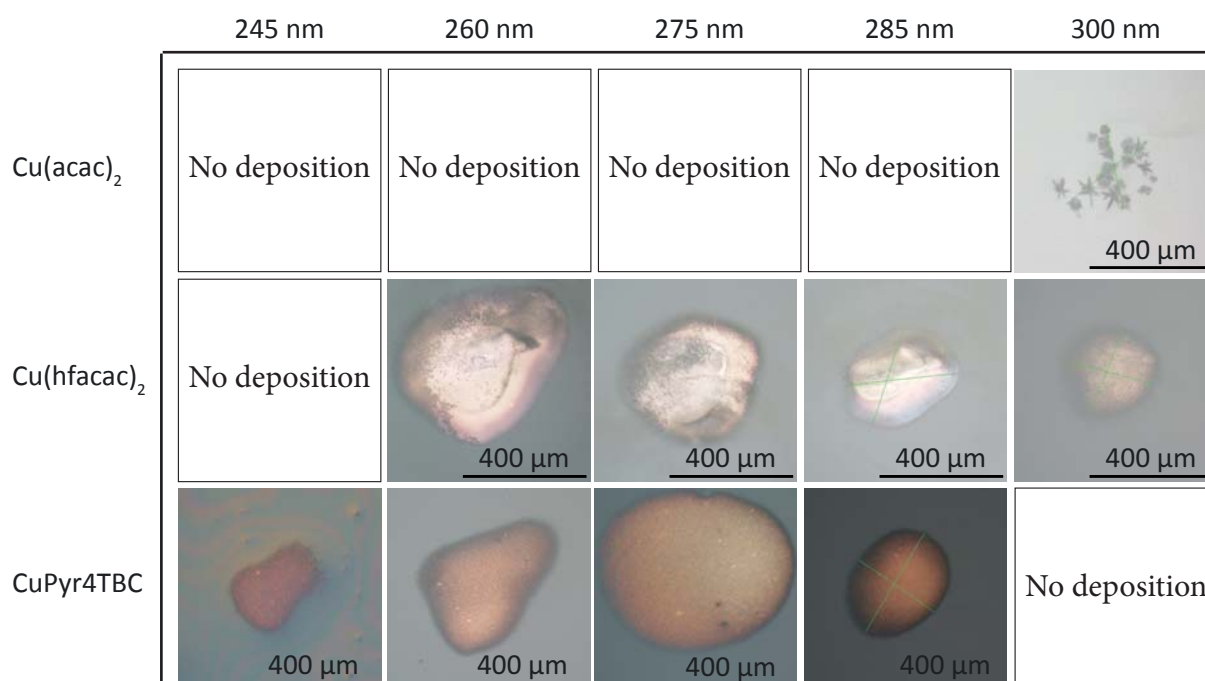


Figure 36: Deposition of metallic copper at different wavelengths at equivalent concentration of complex and sensitizer. Total irradiation time 120 min.

Independently of the rates of deposition it is evident that the best deposition spot was obtained for CuPyr4TBC at 275 nm (Figure 36). The copper spot is homogeneous in form and color, and the deposited spot show low signs of contamination. Differently, the copper spot deposited with the commercial complexes shows some dark coloration in the deposited spots in all cases, which evidences the contamination of the film. In all deposited spots presented in Figure 36 there is a black deposition surrounding the deposited metal spot, this black halo is thought to be copper oxide or a Cu(I) complex which has deposited, the intensity of the light at the borders was not enough achieve the complete reduction to metallic copper.

If the deposited copper spot is left in solution without irradiation, the deposited metallic copper disappears in solution, most probably because of a complexation reaction. At the end of the irradiation time the copper spot could be maintained in the cuvette by replacing the complex

solution with a reducing solution, as used in photography development. The reducing solution consisted of a Rodinal from Afga prepared with a 1:25 ratio to deionized water. Rodinal contains p-aminophenol as reducing agent. The fact that the spot can be maintained in the cuvette by a reducing solution suggest first, that the technique is equivalent to photography techniques where the deposition of metallic silver is maintained with these solutions and second that the disappearance of the metallic spot if it is left in contact with the original reaction solution is due to oxidation involving probably a recomplexation reaction.

A difference in the wavelength range where deposition is possible is observed for each complex, deposition takes place for the CuPyr4TBC complex from 245 to 285 nm, while for the Cu(hacac)₂ complex the range is more shifted to longer wavelengths and spans from 260 to 300 nm. Interestingly, some deposition is achieved for the complexes Cu(hfacac)₂ and Cu(acac)₂ at 300 nm where the absorption of the sensitizer is very low, which suggest that maybe at this wavelength another mechanism rather than a mechanism activated by the sensitizer is taking place. Although less energy is necessary for deposition of Cu(hfacac)₂ and Cu(acac)₂ at 300 nm, there is not enough deposition and the quality of the deposition is not satisfactory. For the Cu(acac)₂ complex no satisfactory deposition was observed in the explored wavelength range, this is consistent with published results on this complex, where 3 to 16 hours of irradiation with a 200 - 400 Hg Watt UV lamp were necessary to achieve a large copper deposition^{118 28}. The results obtained here agree with the literature^{118 28} in the sense that irradiation for long time is necessary to deposit copper with Cu(acac)₂. On the other side this agreement is also a strong suggestion that the results obtained here are scalable and that the use of a more intense light source with a wider irradiation area at a defined wavelength, but with the use of CuPyr4TBC or better with CuPyr₂Cl₂, would lead to a large area of deposited copper metal. Deposition was observed with the CuPyr4TBC complex after irradiation for around 15 minutes with a 275 nm UV-LED, it is expected that the use of a light source with higher optical output and higher concentration of energy at this wavelength, like a laser could be used for direct writing of copper structures.

It has been also observed that some oxide was deposited on the front of the irradiated spot, as if the oxide was first to deposit when there is oxygen in solution (Figure 37 A). It seems that after the remnant oxygen in solution is consumed, the product of deposition is metallic copper. As seen in Figure 37 C, there is a variation in the amount of deposited oxide on irradiated spot, clearly visible in the dark field microscope images as indigo. The different oxygen content in the cuvettes represents the technical difficulty to degas the cuvettes which cannot be subjected to vacuum and can only be degassed by displacing the oxygen in the empty cuvette and bubbling the inert gas in the solution. More interestingly the back light images (Figure 37 B) show that the copper spot is compact at its center where the intensity of light is greater.

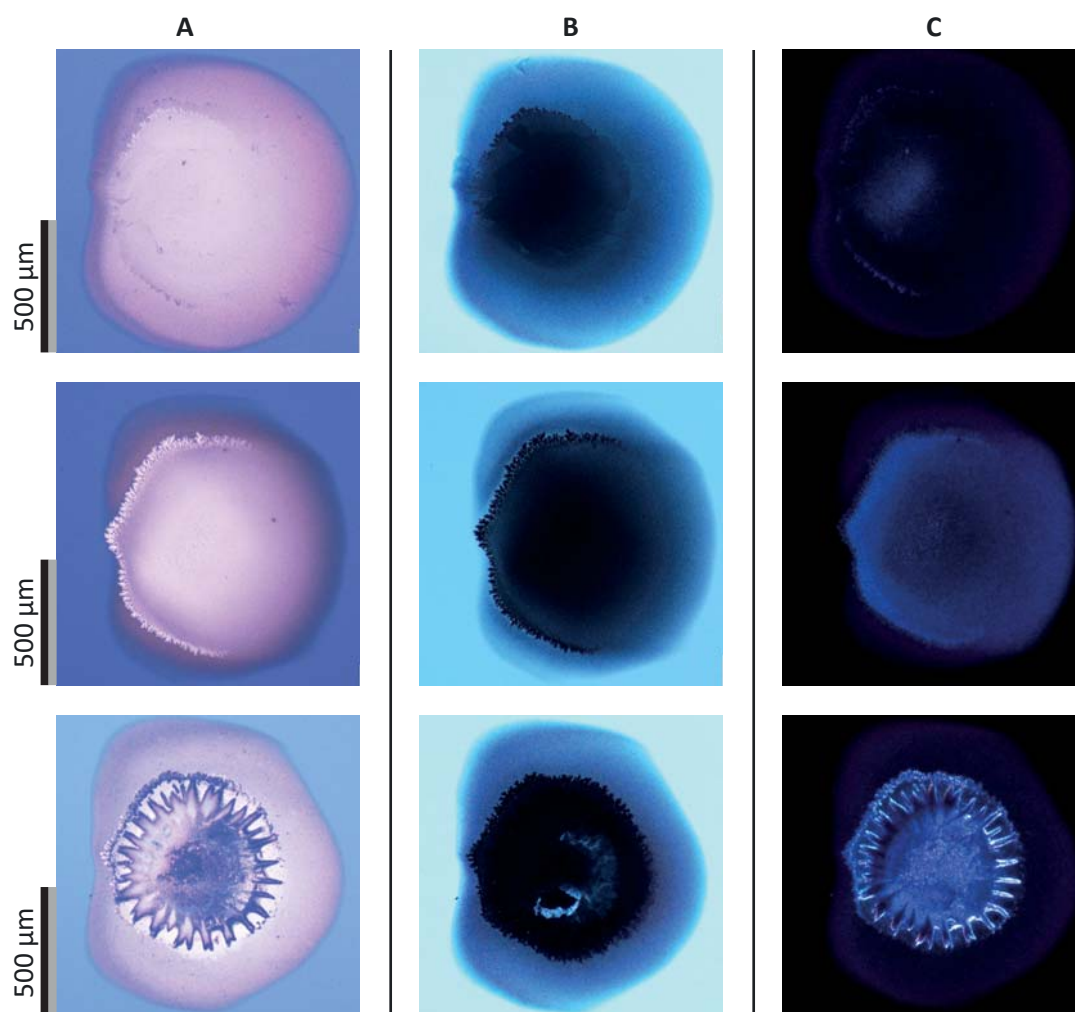


Figure 37: Microscopic images in **A.** bright field **B.** back light and **C.** dark field of deposited copper spots with different content of oxide.

6.3 Upscaling depositions of bigger areas

Irradiation with a 1000 W Hg lamp was also investigated, trying to achieve larger copper film depositions. The experiments were done with the $\text{Cu}(\text{acac})_2$ complex trying to reproduce the result by *Chow and Buono-core*^{28 15}. The irradiation time was restricted to 120 min. The reported deposition by Buono-core with $\text{Cu}(\text{acac})_2$ were done with a Rayonet reactor with a high emission wavelength at 245 and 365 nm; the 1000 W Hg lamp used in this work could only deliver the wavelength at 365 nm. Experiments were carried out using a system containing the homogeneous and the heterogeneous catalyst. The liquid phase were saturated solutions of $\text{Cu}(\text{acac})_2$ and CuCl in methanol sensitizer with acetone. The heterogeneous catalyst was a TiO_2 anatase layer over a PET film.

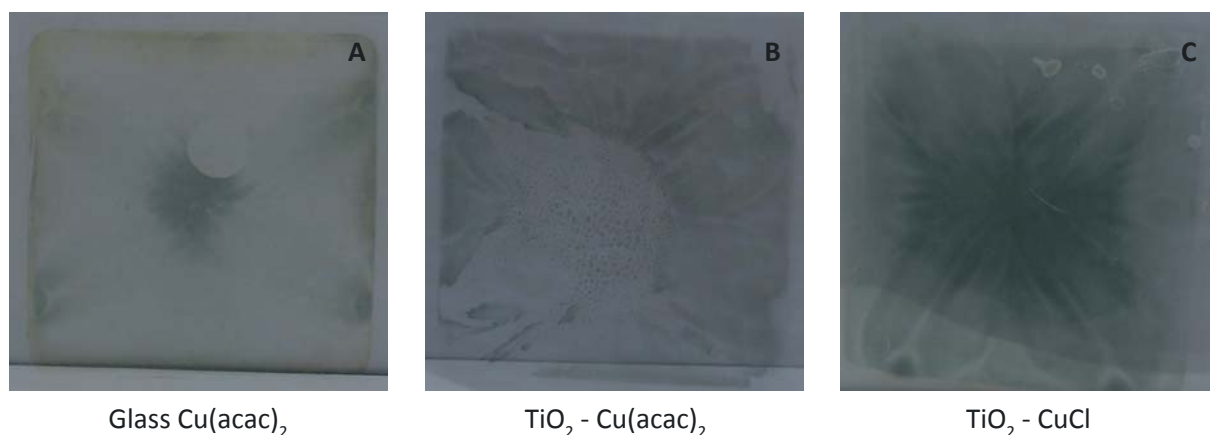


Figure 38: Irradiation of $\text{Cu}(\text{acac})_2$ and CuCl with 1000 W Hg lamp sensitized with benzophenone.

The reaction was first performed at ambient temperature (19°C) with little deposition. It was observed that the spectra of the 1000W Hg lamp has a high emission in the infrared region and the solvents used were not dehydrated. Considerable heating of the solution was observed during the first irradiations, for this reason the later experiments were done irradiating the solution from above with the photoreactor partially submerged in an ice bath. The results presented here are the ones performed with the ice bath.

The results in Figure 38 show that the deposition with the heterogeneous catalysts were improved with respect to the use of only the homogeneous catalyst, as more particles were deposited on the substrate. The black particles are thought to be copper oxide. Copper chloride deposited more material than the $\text{Cu}(\text{acac})_2$ complex. Despite more material being deposited with CuCl , this material is not metallic copper. In fact, the same results were obtained when CuCl solutions were irradiated in quartz cuvettes sensitized with acetone, more material was deposited but this material always had a black color. At similar conditions, other copper complexes deposit a metallic film. More interestingly than the deposition itself are the conditions of the depositions. When the photoreactor was cooled in an ice bath, more deposited material was observed. It is thought that the reaction proceeds faster at lower temperatures because the reaction is exothermic.

Experiments with the best working complexes could not be performed due to time constraints and are considered to belong to a project centered in the up scaling of the process.

6.4 Reduction mechanism

The short lifetimes of the excited states of transition metal complexes of $<10^{-6}$ s force that bimolecular processes must be fast enough to compete with intermolecular deactivation, with rates near the diffusion constant. The outer sphere mechanism can usually fulfill this condition, differently from ligand substitution reactions, coordinated ligand reactions and inner-sphere redox reactions. Consequently the most important quenching processes of excited transition metal complexes are outer-sphere electron and energy transfer²²⁹. There is a propensity of transition metal complexes to react in those fashions usually by formation of an exciplex, an excited complex where one of the molecules is in the excited state.

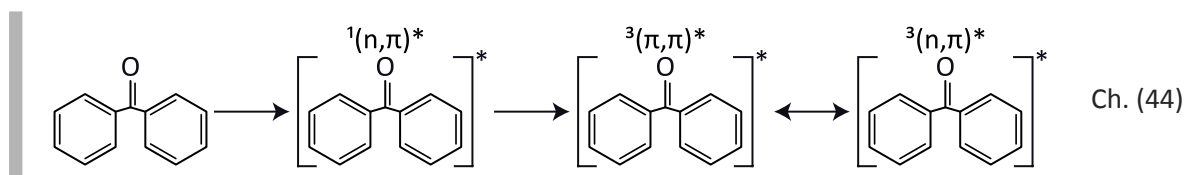
Based on experimental observation and published literature result, possible reaction mechanism for the copper complexes $\text{CuPyr}_2\text{Cl}_2$ and CuPyr_4TBC will be explained. During the reduction of the copper complex to metallic copper some reactions proceed photochemically while others are redox reactions without the involvement of an excited state, based on the facts that copper is reduced to metallic copper upon irradiation and that some products of the excision of bonds in the aromatic ring have been detected by mass spectroscopy. The reduction reactions for the $\text{CuPyr}_2\text{Cl}_2$ complex are thought to be only of photochemical nature while the mechanism of CuPyr_4TBC would involve similar photochemical reactions as in the $\text{CuPyr}_2\text{Cl}_2$ complex and additionally a redox reaction.

The highlight of the analysis will be the reactions directly involved in the photoreduction, mostly those involving the complex and the sensitizer. Therefore analysis of the reaction mechanism will focus on the reduction of the complex while interacting with the sensitizer or secondly generated species, and not on reactions involving deactivation of secondary species when not interacting with the complex.

6.5 Reaction mechanism of the reduction of the $\text{CuPyr}_2\text{Cl}_2$ complex

The irradiated complex in presence of a sensitizer (Sens.) decomposes into its ligands anions or radicals and metallic copper. The reaction was always observed to take place in the presence of a ketone sensitizer and when the absorption of the sensitizer matched that of the used light. Similar sensitized accelerated reactions have been reported in literature with $\text{Cu}(\text{acac})_2$

Given the high ISC efficiencies of the ketones used, acetone and benzophenone, the primary process of the photoreaction undoubtedly involves the formation of a triplet state of the sensitizer. In the case of benzophenone the primary photochemical process is



The highest rates of photoreduction were observed when using light with a wavelength of 260 or 275 nm where the absorption coefficients of the sensitizers are high; for acetone the molar absorption coefficients at these wavelengths are 1223.86 and 1480.11 m²/mol respectively, for benzophenone 2086.40 x 10³ and 756.06 x 10³ m²/mol. The wavelength of light absorption by the sensitizer, its triplet state formation and the accelerated reduction rate of the complex are then related.

After the triplet state of the sensitizer has been formed, the complex and the sensitizer can form an excited complex. Once the exciplex is formed several pathways for the reduction are available, the possibilities are that there is an electron transfer from the sensitizer to the copper complex either by direct transfer, backelectron transfer or that there is an energy transfer either radiative or radiationless. Another mechanism of reduction is through radicals, which does not involve the formation of an exciplex.

6.5.1 Considering a radiative energy transfer mechanism

The radiative energy transfer involves the emission of light by the excited molecule and the absorption of that emitted light by the complex, expressed in the following reactions



The excited molecule emitting in Ch. (45) would be the ketone sensitizer and the absorbing molecule A the copper complex. The ideal circumstances in which the reaction Ch. (45) would proceed through this mechanism are: a high quantum yield emission ϕ_D^e of the excited molecule D*, a high concentration of molecules A in the path of emission, a high molar extinction coefficient ϵ_A of the absorber A and good overlap between the emission spectrum of D* and the absorption spectrum of A¹⁸².

The digitized emission spectra of the acetone^{230 231} and benzophenone²³² as well as the absorption spectra of the complexes are presented in Figure 39.

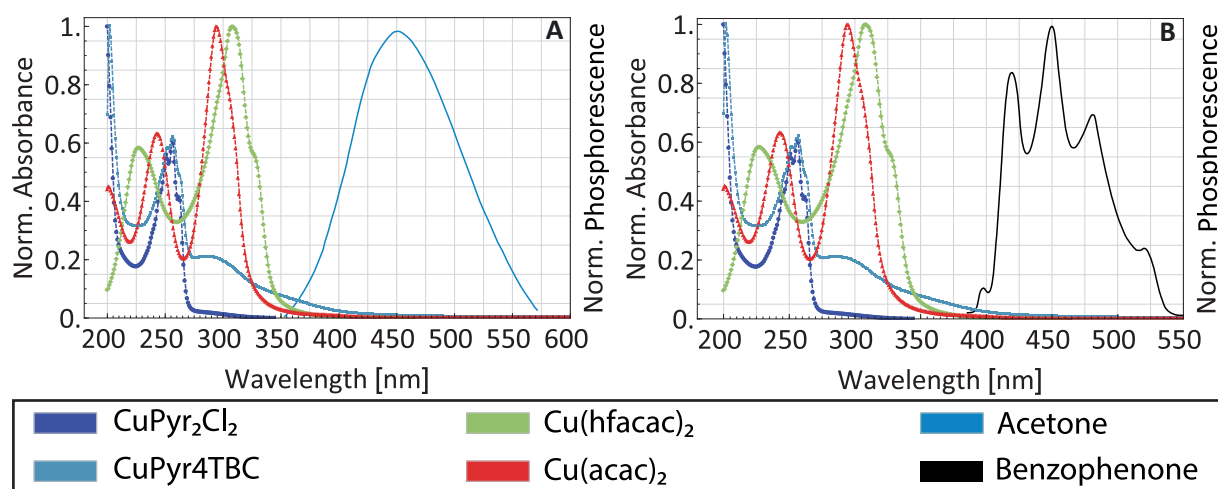


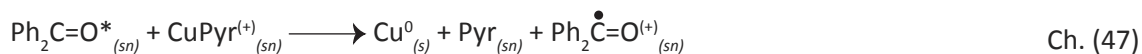
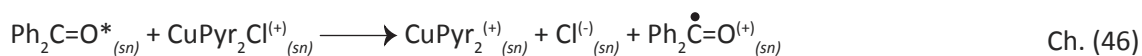
Figure 39: Absorption spectra and phosphorescent spectra of **A.** acetone and **B.** benzophenone taken from literature.

Although the absolute values of the emission spectra are not known in Figure 39, there are several observations that permit to conclude that the energy transfer is not radiative. First, the fluorescence and phosphorescence quantum yield of acetone and benzophenone are very low at working temperatures, $\phi_{fl}=8.4 \times 10^{-4}$ ²³³ and $\phi_{ph}<0.003$ (at 200K)²³⁴ for acetone and $\phi_{fl}=4 \times 10^{-6}$ and $\phi_{ph}=0.01$ (at 298K) for benzophenone³¹. Second and most important, there is considerable low superposition between the complex absorption and the sensitizer emission, as represented in Figure 39; only the tail region of the absorbance spectra of the complexes overlaps with the emission spectra of the sensitizers. The highest superposition happens between CuPyr4TBC and the lowest superposition with CuPyr₂Cl₂, yet the fastest reaction rate is observed with CuPyr₂Cl₂ followed by CuPyr4TBC. It is expected that the higher the superposition, the higher the reaction rate. Since the expected behavior is not followed, it is concluded that there is no correspondence between the superposition with the emission of the sensitizer and the rate of reaction, consequently, the reaction mechanism by radiation energy transfer is not plausible.

6.5.2 Considering a direct electron transfer mechanism

Since there is no information available of the redox potential of the complexes that can be compared with those of the sensitizers, it cannot be asserted undoubtedly if the complex is reduced, oxidized neither the direct electron transfer mechanism can be dismissed. The oxidation potentials of the sensitizers lie around 0.129 V for acetone and 0.129 V for benzophenone^{235 183} and the reduction potentials are -2.84 V for acetone and -1.80 V for benzophenone⁴³. Neither the direct oxidation or the direct reduction reaction of the sensitizers is favored in the ground state of the sensitizer. In the excited state as shown previously in Table 4 the oxidation reaction would

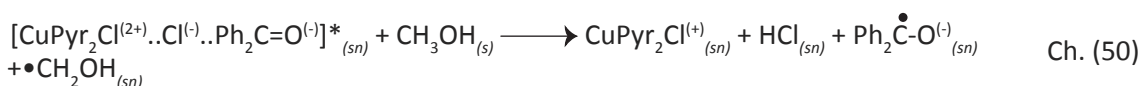
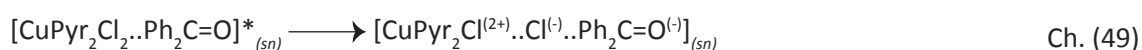
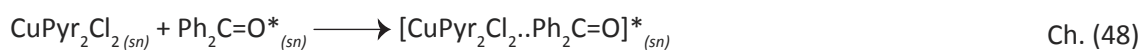
be more probable than the reduction reaction. However a sensitized direct electron transfer mechanism as that proposed by ¹¹⁸ would be



In the direct transfer scheme the electron source would be the sensitizer, and the ligands would be ejected from the complex in the ionic form. Ch. (46) is particularly not probable, since the products of the reaction, the remnant complex and the expelled ligand, are in the ionic form which most probably would lead to a recomplexation reaction without effective reduction of the metal center. Although the triplet state of the ketone sensitizers lies high in energy, due to the aforementioned argument of recomplexation, a direct electron transfer is deemed as less probable than other mechanisms.

6.5.3 Considering a back electron transfer mechanism

As a back electron transfer mechanism, the following reactions can be highlighted based on similar reactions proposed by ¹⁵ for the sensitized reduction of $\text{Cu}(\text{acac})_2$.



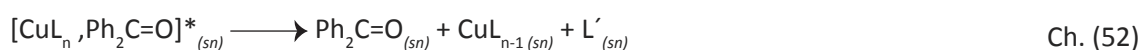
In this set of reactions Ch. (48) - Ch. (50) the sensitizer acts as a temporary electron acceptor while forming an exciplex with the copper complex Ch. (48) surrounded by solvent molecules. The sensitizer assist the loss of the ligand in the complex by destabilizing the complex extracting an electron Ch. (49). After the ligand has been loss, the electron is back-transferred to the remaining complex Ch. (50). The sensitizer is regenerated immediately by the back electron transfer reaction. It is believed that the direct electron transfer and back electron transfer in Ch. (48) and Ch. (50) are favored by the solvent cage in which the exciplex is formed. In this mechanism the transient copper complex $\text{CuPyr}_2\text{Cl}^{(2+)}$ has been oxidized temporary and the oxidation is though to trigger the decomposition reaction of the complex. The sensitizer is thought to assist in the in the reduction of the complex and ligands with the aid of the solvent, the solvent is thought to be the final electron donor.

The oxidation of the complex can be thought to be localized in the central atom or delocalized in the whole complex. The central atom is coordinated with atoms of higher electronegativity and no conjugative stabilization of an intermediate radical ion is possible. In Ch. (49), the electron is thought to come from the metal center, the copper has oxidized from Cu(II) to Cu(III) and the coordination number has been reduced. It is worth mentioning that copper Cu(III) complexes are almost never observed²³⁶. Cu(III) has been observed as intermediate but only with very strong oxidizers, such as $\bullet\text{OH}$ ²³⁷. Also, it is expected that the oxidation would lead to an increase in the coordination number rather than a decrease, as the mechanism proposed. As an example the oxidation from Cu(I) to Cu(II) complexes leads to an increase in the coordination number and the change in the coordination geometry from linear to tetrahedral or square planar. Such experimental observations discourage holding this mechanism as probable.

6.5.4 Considering an energy transfer mechanism

An energy transfer mechanism has been proposed as a predominant quenching mechanism for coordination complexes, still it is not completely understood²⁸.

An energy transfer mechanism could proceed, either a triplet-triplet or a triplet-singlet transfer, from the sensitizer to the copper complex. Independently of the type of energy transfer, the copper complex is destabilized by the excitation causing the successive loss of the ligands. An LMCT transition was found during the TD-DFT analysis of the complex. The LMCT leads to a redox reaction between the ligand and the metal where the metal acts as an oxidizer and the ligand as a reducer²³⁸. The mechanism of reaction of the copper complex in solution its thought to proceed as in the gas phase, as explained individually by literature results on $\text{Cu}(\text{Pyr})_n$ and $\text{CuPyr}_2\text{Cl}_2$ complexes^{130 125 138}. The mechanism of reaction illustrated for $\text{CuPyr}_2\text{Cl}_2$ in the gas phase, is sufficient to explain the reduction of copper in these complex in solution if the same mechanism of reaction is assumed.



The reduction reaction is thought to proceed after the complex has been activated by the sensitizer, forming an exciplex Ch. (51). As a general reaction pathway of the ligands loss the reaction Ch. (52) is proposed. The Cl ligands are lost as first steps of the process, because their

bond energy is lower than that of pyridine. The reduction of Cu(II) to Cu(I) in $\text{CuPyr}_2^{(+)}$ takes place when the last Cl ligand is lost. The reaction is thought to proceed similarly with the pyridine ligand, and just as with the Cl ligand the reduction from Cu(I) to Cu^0 takes place when the last pyridine ligand is lost.

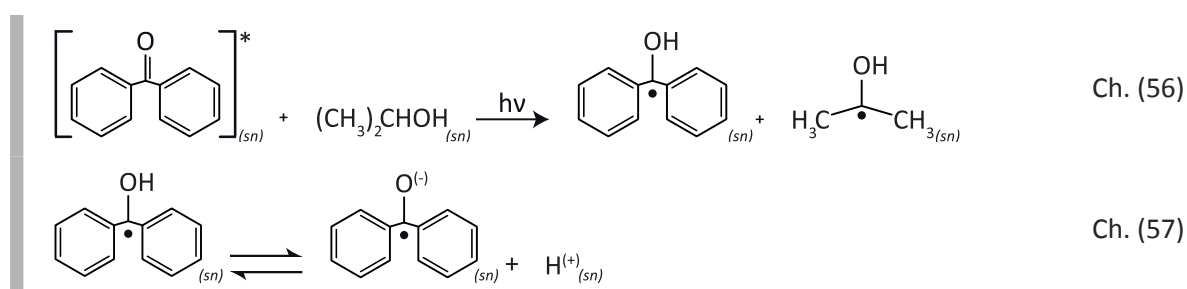
Energy transfer has been commonly observed from triplet excited state of benzophenone and acetone to aromatic moieties and amines, the organic species act as a quencher²³⁹. Some reports show that CuCl_2 salts are also efficient quenchers of the triplet states of anthracene, in fact CuCl_2 was found to have the highest quenching constant among transition metal chloride salts²⁴⁰. The quenching constant was determined in THF and pyridine, being the quenching constant around 50% higher in pyridine. In fact, the quenching constant of the transition metal salts was always higher when pyridine was used as a solvent. It seems the authors did not take into consideration the fact of complex formation between the salt and pyridine and attributed the quenching rate solely to the CuCl_2 salt. Considering the complex formation, it can be concluded from the cited study that the formation of a copper pyridine chloride complex increases the quenching constant of the triplet state of anthracene²⁴⁰. Given the experimental observation of copper reduction, it can then be claimed that the quenching of the triplet state triggers a redox reaction in the complex and that the ligands act of an energy conductor between the triplet of the sensitizer and the metal²⁴¹. The $\text{CuPyr}_2\text{Cl}_2$ complex absorbs in the wavelength of irradiation, it can be also assumed that the complex itself is activated by the light to an excited state. Nevertheless, experiments where complex solutions in acetonitrile, acetonitrile-acetone and 2-propanol-acetone where irradiated for 120 min showed no copper deposition. Literature results in the gas phase show that the complex photodissociates, meaning that indeed the excitation of the complex leads to ligand loss. It will be assumed then that the reaction in the condensed phase proceeds at very low rates without the sensitizer. No reaction was observed when the reaction was performed in acetonitrile and sensitized with acetone, which means that although the sensitizer was present to transfer energy and assist the decomposition, the reaction did not take place. The fact that the system only works when a suitable solvent and sensitizer are in solution, although the excited state of the sensitizer and the complex can be reached shows the decisive role of the solvent. The decisive role of the solvent in the reaction is more represented in the radical reaction mechanism and for this reason the energy transfer mechanism is regarded as less probable than the radical mechanism.

6.5.5 Considering a radical mechanism

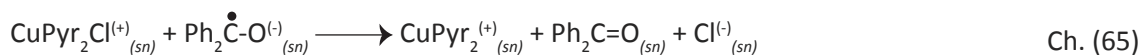
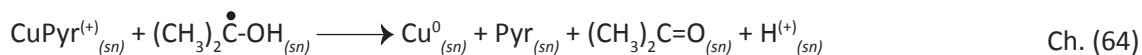
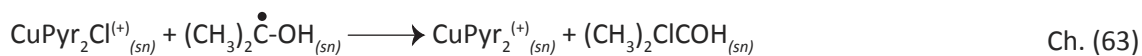
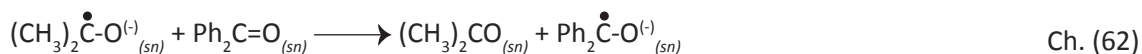
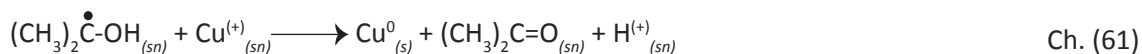
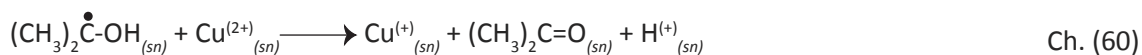
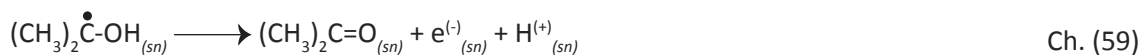
The majority of literature studying carbonyl compounds involve an electron transfer or hydrogen donation to the carbonyl triplet²⁴², because the carbonyl group is a good electron and hydrogen acceptor due to its low lying vacant orbitals. But it seems there is no direct electron or proton transfer but a concerted proton and electron transfer, specially probable in hydrogen

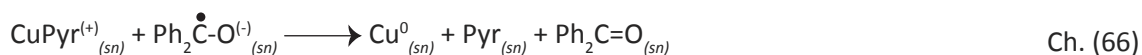
donating solvents, which yields the same anion radical, Ch. (56) and Ch. (57), as the direct electron transfer ²⁴³.

An electron transfer from a methyl or phenyl radical from acetone or benzophenone is disregarded based on the fact that the photofragmentation of these ketones is inefficient at the working conditions. Photofragmentation of these ketones is efficient when using vacuum ultraviolet (V-UV) or double photon excitation to excite the molecules to a higher triplet state than T_1 . In the case of acetone 193 nm wavelength is necessary for nonsynchronous fragmentation of both Methyls ²⁴⁴ and in the case of benzophenone double excitation at 308 nm is necessary ²⁴⁵.



The ketone triplet state in presence of an hydrogen donating solvent will readily abstract an hydrogen ^{246 247} and lead to radical formation. In Ch. (56) the triplet excited state benzophenone abstracts an hydrogen from the 2-propanol, but this reaction is equivalent for ethanol and methanol ^{248 249}, and the product is the corresponding alkoxy radical. Although, for ethanol it is also possible to have the 2-Hydroxyethyl. For 2-propanol, 86% of generated radicals will be secondary and 13% will be primary ²⁵⁰. The hydrogen abstraction reaction is very fast and efficient for ketones in alcohol solutions ^{251 252}. Radicals formed in secondary steps Figure 25 and Ch. (57) by the sensitizer reaction with the solvent, one from benzophenone and the other from the alcohol, can reduce the copper complex.





Ch. (57) reaction is equivalent to reaction Ch. (58) where the radical ions are in equilibrium with its protonated form. The protonated radical can further oxidize and produce an hydrogen cation and a solvated electron Ch. (59)²⁵³, which immediately informs of the capabilities of these intermediates to act effectively as electron donors. The formation of alkoxy copper complexes with Cu(II) and Cu(I) is also possible nevertheless the complexation reaction has to compete with the reduction reactions Ch. (60) and Ch. (61) which are considerably efficient, specially with the methoxy radical where the rates of reduction for Cu(II) and Cu(I) can reach 1.6×10^8 and $1 \times 10^{10} \text{ L mol}^{-1} \text{ s}^{-1}$ respectively, the Cu(I) rate constant in methanol is two orders of magnitude higher than the reaction with ethoxy and 2-propoxy radicals²⁵⁰. Conversion from alkoxy anion radical and benzophenone radical anion is also possible and it is represented in Ch. (62). The set of reactions Ch. (63) - Ch. (66) constitute the reduction reaction between the $\text{CuPyr}_2\text{Cl}_2$ complex and the reducing radicals. In some reactions there is a two electron transfer, one electron it responsible for the Cu reduction while the other electron is responsible for the pyridine reduction and alcohol regeneration. Reactions Ch. (63) and Ch. (65) are the first to take place since the Cu-Cl bond (BDE $\text{Pyr}_2\text{Cu}^+\text{-Cl}=125 \text{ kJ/mol}$) is weaker than the Cu-Pyr bond (BDE $\text{PyrClCu}^+\text{-Pyr}=194 \text{ kJ/mol}$) as proved in gas phase photodissociation experiments¹³⁸. Once the Cl ligands have been lost the reduction reaction Ch. (66) would take place, where the Cu-Pyr bond breaks and the metal is reduced in the process.



The rate constants of the reduction of other copper complexes with alkoxy radicals is of the order of 10^6 - 10^8 while the rate constant of O_2 quenching with the alkoxy radicals is of the order 10^9 . Which shows the reason why O_2 should be excluded from the system, the reaction with oxygen in Ch. (67) is very fast and efficient²⁵⁴; if oxygen is present in solution in sufficient quantity it will quench the radical before any reduction reaction with the complex takes place. Moreover the formed peroxide radicals or 1-hydroxy-1-methylethyldioxy radical are able to reduce any copper ion present in solution equivalently to reaction with ferrous ions in literature²⁵⁵.

6.5.6 Analysis on the best solvent for radical mechanism

Analyzing further the above presented reaction in terms of the best solvent for radical production, in Table 9 the reaction constant of hydrogen abstraction (k_r) by benzophenone, the

reaction Activation Energy (E_a) and the alpha hydrogen donation parameter (α_H) is presented for the used alcohol solvents. The Ionization Potential (IP) and Electron Affinity (EA) of the produced alkoxy radical are also presented.

Table 9: Data of hydrogen abstraction reaction by benzophenone and potentials of the produced alkoxy radical.

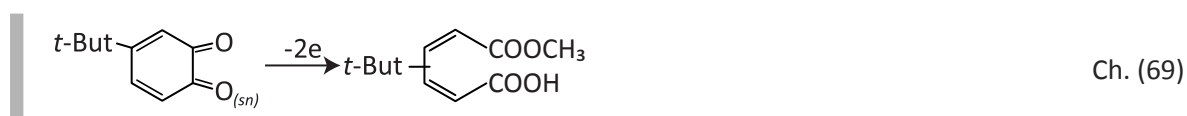
Alcohol	k_r^a	E_a [Kcal/mol] ^a	α_H^b	Alkoxy Radical		
				IP [eV] ^c	EA [eV] ^d	E_{ox} [V] ^e
CH ₃ OH	3x10 ⁵	3.5	0.93	10.72±0.008	1.57±0.004	-0.98
CH ₃ CH ₂ OH	8x10 ⁵	2.8	0.83	9.11±0.05	1.71±0.004	-1.18
(CH ₃) ₂ CHOH	1x10 ⁶	2.6	0.76	9.20±0.05	1.85±0.004	-1.30

a 182 , b 226 227 , c 181 , d 256 , e 257 .

The more negative the oxidation potential the more probable it is to oxidize and transfer an electron. The alkoxy radical with higher reduction capability is ethoxy radical closely followed by the radical from 2-propanol; but the hydrogen abstraction kinetic is the fastest in 2-propanol, nevertheless the difference between the reaction kinetic of ethanol and 2-propanol is not very significant. Although the best suitable solvent is 2-propanol in terms of the reduction capability of its alkoxy radical the complex is not very soluble in it. As seen in the chapter comparing the kinetic of reaction in the three solvents the low solubility of the complex in 2-propanol seems to be compensated by the rate of radical production and its reduction potential, and the deposition rate of the three solvents is equivalent.

6.6 Reaction mechanism of the reduction of the CuPyr4TBC complex

Apart from the photochemical reactions involving radicals for CuPyr₂Cl₂, which are also expected for CuPyr4TBC, another mechanism is expected to take place for the CuPyr4TBC. The isomer compounds 4-tert-butylmuconic acid monomethyl ester and 3-tert-butylmuconic acid methyl ester were detected in the results of mass spectroscopy, these are the products of the cleavage of the aromatic ring and oxidation of 4-tert-butylcatechol. Since there is enough literature that support the cleavage reaction of catechol in the presence of copper chloride and pyridine it is fair to assume that the same reaction is taking place in this work¹⁴⁸. The cleavage reaction taking place is



No consensus has been found in the literature regarding the exact mechanism of reaction. The cleavage reaction has been observed in aerobic and anaerobic conditions. Most importantly under aerobic conditions O_2 was identified as the final electron acceptor of the reaction. The oxygen has been found to re-oxidize the copper complex involved in the cleavage to a Cu(II) oxidation state, configuring a cyclic Fenton reaction. In anaerobic conditions it is thought that the final electron acceptor of the reaction is copper and since the cleavage reaction involves a two electron transfer, the cleavage reaction offers a new reaction path for copper to be reduced when oxygen is absent.

Although the reduction of CuPyr4TBC is more efficient than that of the commercial complexes, it is less efficient than that of the CuPyr₂Cl₂ complex. This lower efficiency has been attributed to a higher stability of the complex, due to the chelate effect and to the coordination with oxygen. The reduction process of the organometallic copper to copper complex means directly that the bonds with the ligand have to be broken, the easier the bonds are broken the easier the copper atom will be free, nevertheless as can be already expected the breaking of the bonds in the ligand is not enough to ensure that the metal will be reduced, as observed in the carbonyl photoreaction with copper, the photoreaction of such complexes mostly produces copper cations. Electrons should be available for copper to reduce while the bond breaking with the ligands is happening, there the importance of the presence of the Cl and the pyridine ligands in the complex are demonstrated. Although the Cl ion is highly electronegative, the electronegativity seems to be well compensated by the presence of the pyridine ligands. This last point can be illustrated when comparing the total charge transfer of the ligand fragments to the central atom, for CuPyr₂Cl₂, Cu(acac)₂ and Cu(hfacac)₂ presented previously. The presence of two Cl and two pyridine ligands account for a better charge donated to the central atom than the atom with the same coordination number surrounded by oxygen.

7 Conclusions

In this study copper coordination complexes were synthesized in the search for an efficient compound that deposits metallic copper after irradiation with light. The synthesized complexes were compared with commercial complexes reported in literature for copper photodeposition, $\text{Cu}(\text{acac})_2$ and $\text{Cu}(\text{hfacac})_2$. Among the complexes sensitizer $\text{CuPyr}_2\text{Cl}_2$ and CuPyr4TBC showed the most promising results for metallic copper deposition. Photochemical reactions of the aforementioned complexes were studied by varying the reaction conditions such as solvent, sensitizer and irradiation wavelength, which lead to the proposal of a reaction mechanism.

Infrared analysis of the synthesized complexes shows the coordination of copper with the pyridine and the 4TBC ligands in CuPyr4TBC . For the $\text{CuPyr}_2\text{Cl}_2$ coordination with the pyridine was confirmed and no free pyridine was encountered in the complex.

Mass spectroscopy analysis identify CuPyr4TBC as a mixture compound, comprising complexes $\text{Cu}(4\text{TBC})_2$ and $\text{CuPyr}_2\text{Cl}_2$. The heteroleptic copper complex CuPyr4TBC could be detected by mass spectroscopy and it is believed to exist as an equilibrium between the complexes $\text{Cu}(4\text{TBC})_2$ and $\text{CuPyr}_2\text{Cl}_2$.

Energy dispersive X-ray spectroscopy shows that the deposited material of the irradiations of complex CuPyr4TBC is in fact metallic copper with up to 90% copper content. Microscopic images of the deposited spots show that the formation of oxide can be avoided by degassing of the solution and suggest that if oxygen is present the oxide formation reaction precedes the reduction reaction that form metallic copper.

The CuPyr4TBC mixture complex showed better performance for copper photodeposition at wavelengths 260 and 275 nm than literature reported complexes $\text{Cu}(\text{acac})_2$ and $\text{Cu}(\text{hfacac})_2$. The pure complex $\text{CuPyr}_2\text{Cl}_2$ showed better performance for copper deposition than mixture complex CuPyr4TBC at 260 and 275 nm irradiation experiments synthesized with benzophenone. The quality and rate of copper deposition follows the tendency $\text{CuPyr}_2\text{Cl}_2 > \text{CuPyr4TBC} > \text{Cu}(\text{hfacac})_2 > \text{Cu}(\text{acac})_2$ for irradiation wavelengths between 245 and 285 nm in methanol, ethanol and 2-propanol sensitizer with benzophenone. Less amount of complex in sensitized solutions was necessary with $\text{CuPyr}_2\text{Cl}_2$ and CuPyr4TBC in comparison with $\text{Cu}(\text{acac})_2$ and $\text{Cu}(\text{hfacac})_2$ to deposit metallic copper when irradiated at wavelengths 260 and 275, which indicates as higher metallic copper deposition efficiency.

TD-DFT simulations of the complex $\text{CuPyr}_2\text{Cl}_2$ shows that some transitions in the UV-Vis spectra of the complex can be associated with LMCTs. The LMCTs found in the simulated spectra of complexes $\text{Cu}(\text{acac})_2$ and $\text{Cu}(\text{hfacac})_2$ are thought to be responsible for the reduction of the copper complex at 300 nm. The charge decomposition analysis done on the TD-DFT results of the

complexes show that more charge is transferred to copper upon coordination with the chlorine and pyridine ligand than with the acetylacetonate and the hexafluoroacetylacetonate ligands.

The rate of photodeposition of metallic copper complexes is increased when a sensitizer with an active triplet state capable of hydrogen abstraction is in solution. The ratio between the sensitizer and the amount of complex in solutions affects the rate of copper deposition and side reactions. For the $\text{CuPyr}_2\text{Cl}_2$ complex, the ratio of complex to benzophenone sensitizer should be higher than 4.5×10^{-3} .

The maximal rates of reaction were encountered when benzophenone is used as sensitizer and when the irradiated wavelength lies around the maximum absorbance of it at 260 and 275 nm. The reaction is thought to proceed through a radical mechanism involving the triplet state of the sensitizer and alkoxy radicals developed in solution. The photoreduction reaction could only be observed in polar protic solvent with high alpha hydrogen donating capability.

8 Outlook

The reaction mechanism can be clarified by measuring the redox potential of the complex and comparing it with the redox potential of the sensitizer in its excited state. The reaction mechanism can be discerned from an electron transfer mechanism by comparing the free energies of reduction, oxidation or liberation from an energy transfer. If the triplet state of the complex lies near and lower in energy with the triplet energy state of the sensitizer and the excited state LUMO and HOMO of the complex is “surrounded” by that of the sensitizer, an energy transfer mechanism is favored. Another strategy to discern an electron transfer from an energy transfer driven reaction is to plot of the quenching constant with the free energy of the system, as explained elsewhere²²⁹.

The task of gaining more insight about the radical reaction mechanism of the photoreduction of copper complexes can be addressed by making more photochemical experiment concerted to prove the presence of radicals during irradiation. Inspection of the radical mechanism can be done by performing the photoreaction in the presence of stable radicals, such as 2,2,6,6-tetramethylpiperidinyloxy (TEMPO), t-butyl nitroxide or p-dinitrobenzene²⁵⁸, which will tend to react with the radicals produced in solution by the photoreaction. The products of the radicals interaction can be later measured by mass spectroscopy. Since other reaction mechanisms, like the backelectron transfer mechanism, also involves the radical formation and it can always be possible for several reaction mechanisms to be functioning simultaneously; this kind of experimentation will bring more information and certainty about the route of reaction and possible intermediates in the reaction.

Stern-Volmer plots could be also performed to establish the quenching done by the hydrogen donating solvent or by the complex on the sensitizer. The Stern-Volmer between the complex and the sensitizer should be performed in aprotic solvents polar and apolar, to gain more insight on the properties of the solvent in the photoreaction. If the quenching reaction constant is greater with the solvent than with the complex, this would lead to think that the main route of deactivation is through the interaction with the solvent which means that the radical mechanism of reduction would be more plausible than the backelectron reaction between the complex and the sensitizer.

Much more details of the reaction mechanism which are beyond the reach of this work can be addressed by making quenched and non-quenched transient absorption spectroscopy experiments. This tool is widely used to gain valuable information about the intermediates of reaction and whether there is a exciplex being formed. The fast spectroscopic detection of reaction intermediates and exciplexes is a direct evidence of the route of reaction, this combined with the possibility to establish the decay rate of the transients in the reaction would lead to narrowing

even more the possible reaction paths.

It would be interesting to study the reaction with some sensitizer that could be only be excited to the singlet state, as tried elsewhere ¹⁶, e.g. sensitizer which have a low intersystem crossing efficiency (ISC) as benzene, with this type of experiments the efficiency of electron transfers from a singlet vs a triplet state, such as the offered by the sensitizer presented in this work, can be done. This kind of experimentation would lead to gain more insight also on the mechanism of reaction since the reaction paths that are preferred in the triplet state and the singlet state are different because of its different electron distribution ²⁵⁹. Some studies have shown that reactivity of the ketones ¹(n,π*) singlet states are even more reactive than their ³(π,π*) triplet states for hydrogen abstraction reaction, thus the use of 2-pentanones and 2-hexanones as sensitizer could accelerate the reaction rate ²⁵¹. Incipient experiments were performed using commercial complexes in order to include other wavelengths for the photoreaction. The results seem promising, although due to the size of the sensitizer molecules, a higher degree of organic contamination is expected in comparison with smaller sensitizer molecules as acetone. The absorption coefficients of the commercial sensitizers are reported in „Annex C“.

The photodeposition of metallic copper might be improved by designing new complexes with higher deposition efficiencies and yields. It has been reported that the electron transfer to the central atom can be bridged by the ligands ²⁶⁰ possible copper complexes for further experimentation might be ones containing pyridine carboxylate complexes ²⁶¹. Gould et al. found that Co(II) coordinated with pyridinecarboxylato groups, especially for pyridine 2,5- and 2,6-dicarboxylic acids, could be reduced at immeasurable fast rates by Cr²⁺, and suggested the possibility that the ligand served as a bridge for electron transfer, connecting the electron deficiency of the coordinated Co with the electron coming from Cr²⁺, the pyridine was thought to accommodate the reducing electron in its ring; ideally the alkyl chain of the substituents should be unsaturated and contain alternated double bonds to increase the electronic resonance and possibly the electron bridging efficiency ²⁶⁰.

For copper pyridine complexes, it is suggested also that the use of substituted pyridines with electron donating substituents will reduce the complex stability, at least in its dimeric form, thus easing the excision process of the metal from the ligand and increasing the rate of complex reduction and deposition, suggestions of substituents are 4-CN, 4-CF₃, 3-CF₃ and 2-Cl ²⁶².

The formulation of the photoreducible solution could be further improved also by adding reducible metals that have also a high conductivity and improve the reduction of copper toward metallic copper. Aluminum, palladium and magnesium metal ions, which lie higher in the reactivity series, can be added in form of acetate, chloride or nitrate to improve the reduction speed of the process as observed in copper oxalate complexes ²⁶³.

The objective to deposit metallic copper in larger surfaces that could lead to a new novel way to fabricate microelectronic devices. Further characterization of the deposited copper material is also necessary. The objective of measuring the conductivity and thickness of deposited material was elusive in this work due to the absence of a suitable light source with high optical power in the UV range around 260 and 275 nm to deposit sufficient material for such investigation. Given the back complexation reaction observed during the use of this process, it is necessary to have a large area light source that can deliver a high energy input in the system in the UV-B region.

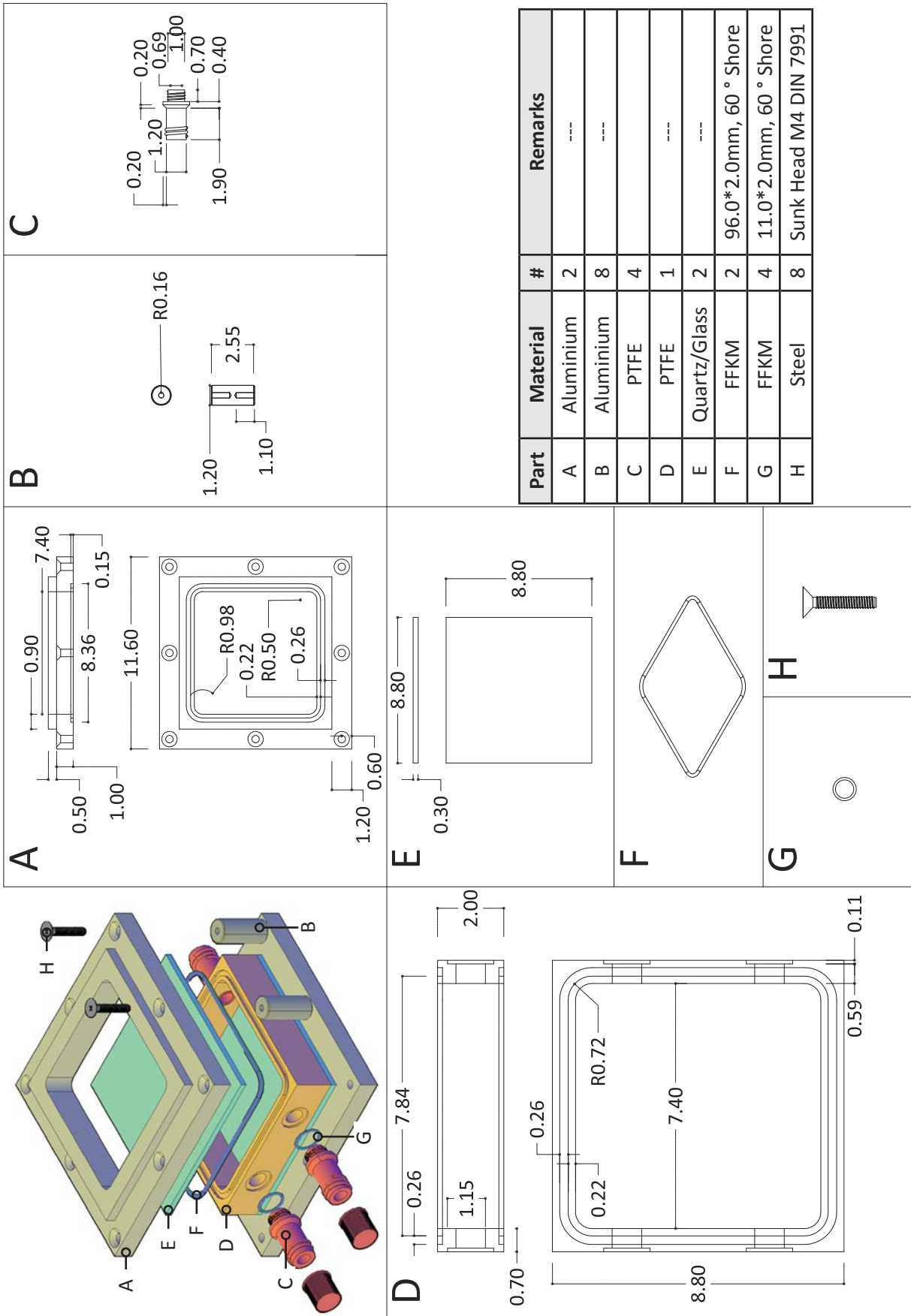


Figure 40: Schemes of techniques that can be implemented with different light sources **A.** direct laser writing **B.** photolithography.

A high output light source in the range of 245 to 275 nm is necessary to deposit metallic material as in photolithography technique. The use of a light source with a large irradiation area and higher energy output would lead to depositing metallic material on the irradiated areas. An array of UV-LED's would be one possibility of a large area light source, nevertheless this approach has the disadvantage of not being a single source of light which means that the intensity of irradiation might not be homogeneous and that the energy output is not as high.

A laser source, such as a Kr:F excimer laser (248 nm) or a Nd:YAG 4th harmonic (266 nm) could be used as light sources with the copper complexes in a direct writing technique. A solvent, where the complexes and sensitizer have a high solubility, with low volatility, good hydrogen donor ability and which radical has enough potential to reduce the copper complex is necessary if this technique is used.

Annex A



Part	Material	#	Remarks
A	Aluminium	2	---
B	Aluminium	8	---
C	PTFE	4	---
D	PTFE	1	---
E	Quartz/Glass	2	---
F	FFKM	2	96.0*2.0mm, 60 ° Shore
G	FFKM	4	11.0*2.0mm, 60 ° Shore
H	Steel	8	Sunk Head M4 DIN 7991

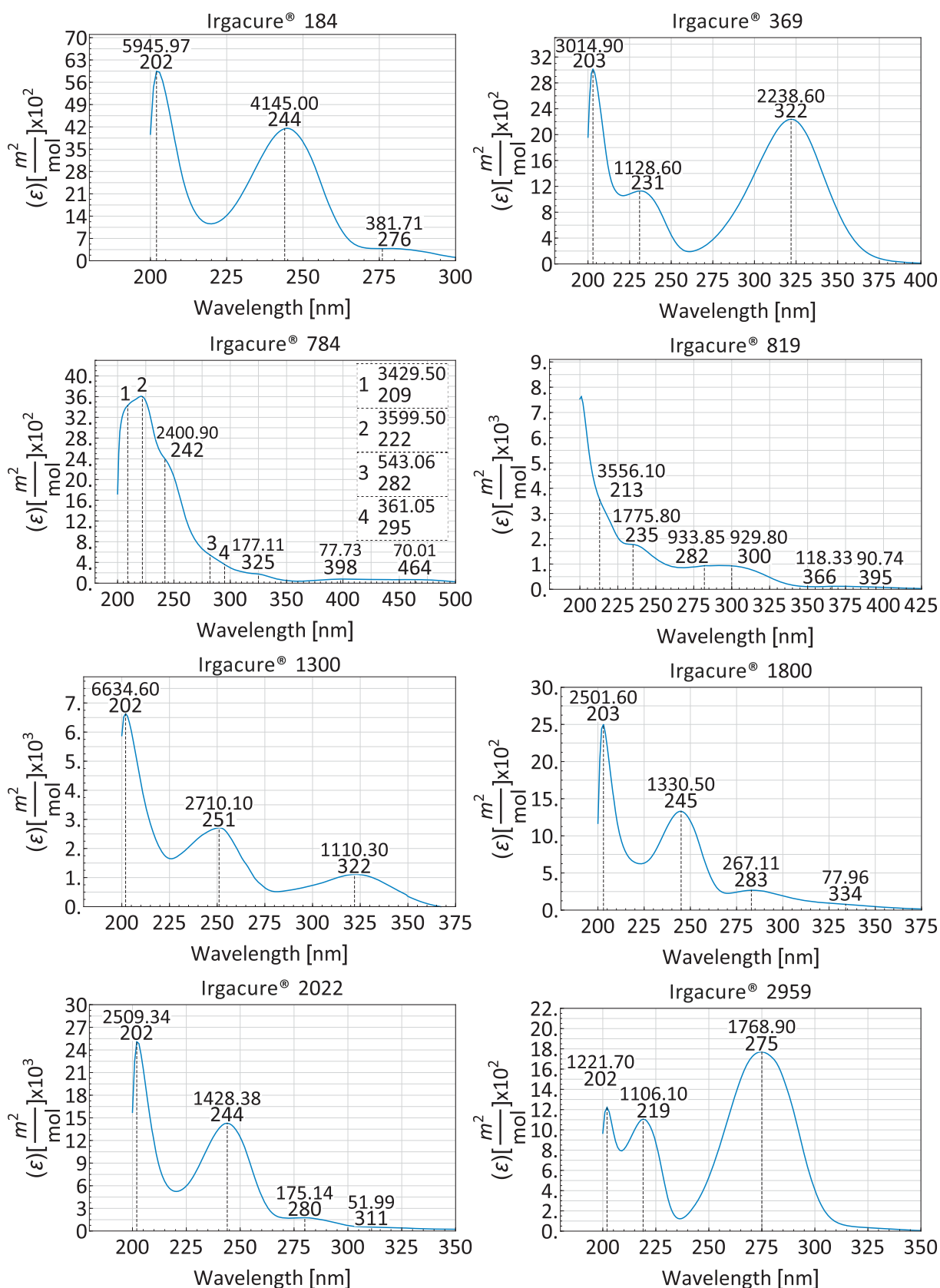
Annex B

XYZ files in of the optimized geometries of the complexes. Complexes where optimized using B3LYP/6-32G(d,p) level of theory using Software Gaussian09. The atom sequence corresponds with ordering in the tables.

Cu(acac) ₂			Cu(F ₆ acac) ₂			CuPyr ₂ Cl ₂					
Cu	-0.004067	-0.0095	-0.038046	Cu	0.003501	-0.042243	0.010334	Cu	0.002358	0.208289	0.29683
O	1.264742	1.311651	0.473832	O	-1.277034	1.306464	-0.376875	Cl	-0.004804	2.464822	0.221363
O	1.299896	-1.287391	-0.533338	O	-1.32017	-1.348797	0.380883	Cl	-0.003892	-1.639003	1.568927
O	-1.269946	-1.322955	0.483753	O	1.317697	-1.368682	-0.343475	N	-1.941652	-0.009766	-0.230202
O	-1.28699	1.294808	-0.528548	O	1.27914	1.306696	0.380226	C	-2.388602	-1.231192	-0.59147
C	3.320493	2.35007	0.98348	C	-3.306008	2.483134	-0.559775	C	-3.730134	-1.49165	-0.847099
C	2.533937	1.163198	0.474438	C	-2.535461	1.172434	-0.305166	C	-4.659598	-0.461542	-0.699011
C	3.212308	0.011953	0.038981	C	-3.248012	0.005739	-0.002383	C	-4.201309	0.796873	-0.314654
C	2.566398	-1.13654	-0.44731	C	-2.574063	-1.179576	0.297724	C	-2.840518	0.985286	-0.100033
C	3.383305	-2.31811	-0.91975	C	-3.383189	-2.463857	0.538758	N	1.945493	-0.009543	-0.226496
C	-3.339997	-2.337777	0.979421	C	3.386781	-2.462205	-0.546483	C	2.841118	0.990907	-0.116027
C	-2.537987	-1.161085	0.470418	C	2.571405	-1.182365	-0.290395	C	4.201489	0.799023	-0.319592
C	-3.204801	-0.006861	0.025338	C	3.245954	0.010562	-0.008224	C	4.661352	-0.460909	-0.694575
C	-2.553777	1.143022	-0.451991	C	2.536354	1.174891	0.299538	C	3.733196	-1.49166	-0.839045
C	-3.367709	2.328639	-0.91925	C	3.302444	2.487811	0.553575	C	2.391971	-1.235088	-0.575308
H	4.398063	2.17514	0.972096	F	-4.635851	2.283303	-0.644192	H	-5.718164	-0.641719	-0.868403
H	3.089159	3.226133	0.368365	F	-3.07685	3.335896	0.453811	H	-4.03238	-2.493936	-1.135017
H	3.002421	2.584626	2.004724	F	-2.897412	3.055513	-1.700525	H	-1.644049	-2.018906	-0.638001
H	3.08789	-3.209285	-0.356364	F	-3.134547	-3.34306	-0.446551	H	2.435108	1.960159	0.149436
H	4.457782	-2.158536	-0.809301	F	-4.708384	-2.224472	0.56206	H	4.872527	1.632884	-0.183232
H	3.155614	-2.516209	-1.972849	F	-3.037196	-3.02607	1.704605	H	5.721501	-0.642942	-0.861797
H	-3.146782	-3.210043	0.345746	F	3.178253	-3.333167	0.454436	H	-4.889105	1.625501	-0.171144
H	-3.003079	-2.595257	1.988812	F	3.007308	-3.036592	-1.696107	H	-2.431554	1.949228	0.183387
H	-4.413023	-2.136877	0.99725	F	4.70925	-2.213477	-0.61429	H	4.038351	-2.491182	-1.130186
H	-4.441719	2.180356	-0.790122	F	4.632255	2.294449	0.625517	H	1.646559	-2.02354	-0.610273
H	-3.156323	2.519198	-1.977108	F	2.896537	3.05078	1.702323				
				F	3.058466	3.348649	-0.451934				
				H	4.324504	0.03198	-0.021455				
				H	-4.326776	0.022447	-0.009688				

Annex C

Absorption coefficient of some commercial Irgacure® sensitizers.



References

- (1) Rickerby, J.; Steinke, J. H. G. Current Trends in Patterning with Copper. *Chem. Rev. (Washington, D. C.)* **2002**, *102* (5), 1525–1549.
- (2) Gladfelter, W. L. Selective Metalization by Chemical Vapor Deposition. *Chem. Mater.* **1993**, *5* (10), 1372–1388.
- (3) Tollens, B. Silver Solution as a Reagent for Aldehyde. *Berichte der Dtsch. Chem. Gesellschaft* **15**, 1635–1639.
- (4) Gysling, H. Photosensitive Copper (I) Complexes. 3989732, 1976.
- (5) Franco, J.; Patel, N. K. Electronic Property of Photosensitive Film on Copper in Solutions of Potassium Iodide. *J. Appl. Electrochem.* **1973**, *3* (4), 341.
- (6) Franco, J.; Patel, N. K. Photosensitive Film Formation of Copper in Aqueous Hydrofluoric Acid Solution. *Labdev, Part A Phys. Sci.* **1974**, *12* (4), 193.
- (7) Shimidzu, N.; Masuda, H.; Ohno, S. The Application of Photo-Reduction of Thin Cuprous Iodide Film for Metal Image Formation. *Chem. Lett.* **1984**, No. 6, 961–964.
- (8) Franco, J.; Patel, N. K.; Pathak, P. D. X-Ray Study of Photosensitive Film on Copper in Aqueous Solution of Ferric Chloride. *Indian J. Phys.* **1975**, *49* (5), 368–372.
- (9) Caldwell, R. S. Photosensitive Copper Halide Material for Use in Producing Photographic Images., February 21, 1989.
- (10) McKee, W. E.; Kaspaul, E. E. Image Recording Medium., February 5, 1974.
- (11) Sugita, K.; Ide, H.; Tamura, K.; Suzuki, S. Photosensitive Ionomer. VIII. Photosensitive copper(I and II) Carboxylates. *Bull. Soc. Photogr. Sci. Technol. Japan* **1974**, No. 23, 6–11.
- (12) Taylor, B. J. Photosensitive Film Formation on Copper. *J. Photogr. Sci.* **1974**, *22* (6), 305–306.
- (13) Buono-Core, G. .; Iwai, K.; Chow, Y. L. Sensitized Photolysis of Bis(acetylacetonato) copper(II); General Reaction Pattern. *Can. J. Chem.* **1979**, *57*, 8–16.
- (14) Chow, Y.; Buono-Core, G. Role of the Acetylacetonyl Radical in the Sensitized Photoreduction of Bis (acetylacetonato) Copper (II). *J. Am. Chem. Soc.* **1986**, 1234–1239.
- (15) Chow, Y. L.; Buono-Core, G. E.; Marciniak, B.; Beddard, C. Mechanistic Studies of Aromatic Ketone-Sensitized Photoreduction of bis(acetylacetonato)copper(II). *Can. J. Chem.* **1983**, *61* (5), 801–808.
- (16) Chow, Y. L.; Buono-Core, G. E.; Marciniak, B.; Li, H. Benzene-Sensitized Photoreduction of bis(acetylacetonato)copper(II) under Hydrogen. *J. Chem. Soc. Perkin Trans. 2 Phys. Org. Chem.* **1986**, No. 3, 365–369.
- (17) Buono-Core, G. E.; Klahn, A. H.; Aros, F.; Astorga, V. Benzophenone Sensitized Photochemistry of a copper(II) Polypyrazolylborate Complex. *Polyhedron* **1996**, *15* (2), 363–366.
- (18) Buono-Core, G. E.; Leon, G. Triplet State Ketone-Sensitized Photochemistry of copper(II) and nickel(II) Complexes with 4-Acylpyrazolones. *J. Coord. Chem.* **1990**, *21* (4), 323–332.
- (19) Hill, R. H.; Avey, A. A.; Blair, S. L.; Gao, M.; Palmer, B. J. Molecular Design for Photo- and Electron Beam Lithography with Thin Films of Coordination Compounds. *Mater. Chem. Phys.* **1996**, *43* (3), 233–237.
- (20) Chu, C. W.; Hill, R. H. Solid State Photochemistry of Thin Films of Cr, Mo and W Organometallic Compounds on Silicon Substrates. *Mater. Chem. Phys.* **1996**, *43* (2), 135–139.

- (21) Chu, Y.; Yang, Z.; Rodgers, M. T. Solvation of Copper Ions by Acetone. Structures and Sequential Binding Energies of $\text{Cu}^+(\text{acetone})_x$, $x=1,4$ from Collision-Induced Dissociation and Theoretical Studies. *J. Am. Soc. Mass Spectrom.* **2002**, *13*, 453–468.
- (22) Buono-Core, G. E.; Tejos R., M.; Klahn, A. H.; Cabello, G.; Lucero, A.; Hill, R. H. Solid State Photochemistry of Cu(II) Alkyltropolonate Complexes in Thin Films: The Photochemical Formation of High Quality Films of Cu(I) Oxide. *J. Chil. Chem. Soc.* **2007**, *52* (4), 1318–1321.
- (23) Buono-Core, G. E.; Tejos, M.; Lara, J.; Aros, F.; Hill, R. H. Solid-State Photochemistry of a Cu(II) β -Diketonate Complex: The Photochemical Formation of High Quality Films of copper(II) Oxide. *Mater. Res. Bull.* **1999**, *34* (14/15), 2333–2340.
- (24) Avey, A. A.; Hill, R. H. Solid State Photochemistry of $\text{Cu}_2(\text{OH})_2(\text{O}_2\text{C}(\text{CH}_2)_4\text{CH}_3)_4$ in Thin Films: The Photochemical Formation of High-Quality Films of Copper and Copper(I) Oxide. Demonstration of a Novel Lithographic Technique for the Patterning of Copper. *J. Am. Chem. Soc.* **1996**, *118* (1), 237–238.
- (25) Nawafune, H.; Akamatsu, K.; Uchida, M.; Arimura, H. Integrated Circuit Formation by UV-Induced Copper Deposition Using Auxiliary Reducing Agent., September 13, 2007.
- (26) Zhang, H. L.; Zhao, G. Y.; Xu, L. Z. Preparation of the Photosensitive Copper Complex and CuO Film Pattern. *Appl. Surf. Sci.* **2013**, *274*, 397–400.
- (27) Foster, N. S.; Lancaster, A. N.; Noble, R. D.; Koval, C. A. Effect of Organics on the Photodeposition of Copper in Titanium Dioxide Aqueous Suspensions. *Ind. Eng. Chem. Res.* **1995**, *34* (11), 3865–3871.
- (28) Buono-Core, G. E. Mechanistic Studies on the Sensitized Photochemistry of Bis(2,4-Pentanedionato) Copper(II). *Dissertation* **1981**.
- (29) Akamatsu, K.; Kimura, A.; Matsubara, H.; Ikeda, S.; Nawafune, H. Site-Selective Direct Photochemical Deposition of Copper on Glass Substrates Using TiO_2 Nanocrystals. *Langmuir* **2005**, *21* (18), 8099–8102.
- (30) Fenton, H. J. H. Oxidation of Tartaric Acid in Presence of Iron. *J. Chem. Soc.* **1894**, *65*, 899–910.
- (31) Montalti, M.; Credi, A.; Prodi, L.; Gandolfi, M. T. *Handbook of Photochemistry*, 3rd ed.; CRC Taylor & Francis, 2006.
- (32) Kutal, C. Spectroscopic and Photochemical Properties of d^{10} Metal Complexes. *Coord. Chem. Rev.* **1990**, *99*, 213–252.
- (33) Ballhausen, C. J. Jahn-Teller Configurational Instability in Square-Planar Complexes. *Theor. chim. Acta* **1965**, *3*, 368–374.
- (34) Lever, A. B. P. Charge Transfer Spectra of Transition Metal Complexes. *J. Chem. Educ.* **1974**, *51* (9), 612–616.
- (35) Ferraudi, G.; Muralidharan, S. Photochemical Properties of Copper Complexes. *Coord. Chem. Rev.* **1981**, *36*, 45–88.
- (36) Sýkora, J.; Sima, J. Photochemistry of Coordination Compounds. *Coord. Chem. Rev.* **1990**, *107*, 1–225.
- (37) Maiti, B. K.; Maia, L. B.; Pal, K.; Pakhira, B.; Avile, T.; Moura, I.; Pauleta, R.; Nun, J. L.; Rizzi, A. C.; Brondino, C. D.; et al. One Electron Reduced Square Planar Bis (benzene-1,2-Dithiolato) Copper Dianionic Complex and Redox Switch by O_2/HO^- . *Inorg. Chem.* **2014**, *53*, 12799–12808.
- (38) Rappoport, Z.; Marek, I. *The Chemistry of Organocopper Compounds*; Wiley: Chichester; Hoboken, NJ, 2009.

- (39) Jastrzebski, J. T. B. H.; Van Koten, G. Structures and Reactivities of Organocopper Compounds. In *Modern Organocopper Chemistry*; Norbert Krause, Ed.; 2002; Vol. 1, pp 1–44.
- (40) Krause, N. *Modern Organocopper Chemistry*; Wiley-VCH: Weinheim; Cambridge, 2002.
- (41) Lamsabhi, A. M.; Alcamí, M.; Mó, O.; Yáñez, M.; Tortajada, J.; Salpin, J. Unimolecular Reactivity of Uracil–Cu²⁺ Complexes in the Gas Phase. *ChemPhysChem* **2007**, *8*, 181–187.
- (42) Lamsabhi, A. M.; Alcamí, M.; Mó, O.; Yáñez, M.; Tortajada, J. Association of Cu²⁺ with Uracil and Its Thio Derivatives: A Theoretical Study. *ChemPhysChem* **2004**, *5*, 1871–1878.
- (43) Vanýsek, P. *CRC Handbook of Chemistry and Physics 91st Edition*; Haynes, W. M., Ed.; Taylor & Francis, 2010.
- (44) Holleman, A. F.; Wiberg, N. *Holleman-Wiberg's Inorganic Chemistry*; 2001; Vol. 1.
- (45) Bratsch, S. G. Standard Electrode Potentials and Temperature Coefficients in Water at 298.15 K. *J. Phys. Chem. Ref. Data* **1989**, *18* (1), 1–21.
- (46) El-Nahas, A. M.; Tajima, N.; Hirao, K. Binding Energies and Electronic Structures of Cu⁺(OH₂)_n and Cu⁺(NH₃)_n (n = 1-4): Anomaly of the Two Ligand Cu⁺ Complexes. *J. Mol. Struct. THEOCHEM* **1999**, *469*, 201–213.
- (47) Bauschlicher Jr., C. W.; Langhoff, S. R.; Partridge, H. The Binding Energies of copper⁺-Water and copper⁺-Ammonia Complexes (Cu⁺-(H₂O)_n and Cu⁺-(NH₃)_n (n = 1-4)). *J. Chem. Phys.* **1991**, *94* (3), 2068–2072.
- (48) Rosi, M.; Bauschlicher Jr., C. W. The Binding Energies of One and Two Water Molecules to the First-Row Transition Metal Positive Ions. II. *J. Chem. Phys.* **1990**, *92* (3), 1876–1878.
- (49) Rimola, A.; Constantino, E.; Rodriguez-Santiago, L.; Sodupe, M. Binding Properties of Cu^{+/2+}-(glycyl)_nglycine Complexes (n = 1-3). *J. Phys. Chem. A* **2008**, *112* (15), 3444–3453.
- (50) Shoeib, T.; Rodriguez, C. F.; Michael Siu, K. W.; Hopkinson, A. C. A Comparison of copper(I) and silver(I) Complexes of Glycine, Diglycine and Triglycine. *Phys. Chem. Chem. Phys.* **2001**, *3* (5), 853–861.
- (51) Bertran, J.; Rodriguez-Santiago, L.; Sodupe, M. The Different Nature of Bonding in Cu⁺-Glycine and Cu²⁺-Glycine. *J. Phys. Chem. B* **1999**, *103* (12), 2310–2317.
- (52) Rimola, A.; Rodriguez-Santiago, L.; Sodupe, M. Cation-π Interactions and Oxidative Effects on Cu⁺ and Cu²⁺ Binding to Phe, Tyr, Trp, and His Amino Acids in the Gas Phase. Insights from First-Principles Calculations. *J. Phys. Chem. B* **2006**, *110* (47), 24189–24199.
- (53) Hoyau, S.; Ohanessian, G. Absolute Affinities of α-Amino Acids for Cu⁺ in the Gas Phase. A Theoretical Study. *J. Am. Chem. Soc.* **1997**, *119* (8), 2016–2024.
- (54) Marino, T.; Russo, N.; Toscano, M. Interaction of Cu⁺ and Cu²⁺ Ions with α-Alanine. A Density Functional Study. *J. Mass Spectrom.* **2002**, *37* (8), 786–791.
- (55) Trujillo, C.; Lamsabhi, A. M.; Mo, O.; Yanez, M. The Importance of the Oxidative Character of Doubly Charged Metal Cations in Binding Neutral Bases. [Urea-M]²⁺ and [thiourea-M]²⁺ (M = Mg, Ca, Cu) Complexes. *Phys. Chem. Chem. Phys.* **2008**, *10* (22), 3229–3235.
- (56) Pulkkinen, S.; Noguera, M.; Rodriguez-Santiago, L.; Sodupe, M.; Bertran, J. Gas Phase Intramolecular Proton Transfer in Cationized Glycine and Chlorine Substituted Derivatives (M - Gly, M = Na⁺, Mg²⁺, Cu⁺, Ni⁺, and Cu²⁺): Existence of Zwitterionic Structures?. *Chem. - A Eur. J.* **2000**, *6* (23), 4393–4399.
- (57) Schwenk, C. F.; Rode, B. M. Influence of Electron Correlation Effects on the Solvation of Cu²⁺. *J. Am. Chem. Soc.* **2004**, *126*, 12786–12787.

- (58) Persson, I.; Persson, P. Structure of Jahn-Teller Distorted Solvated copper(II) Ions in Solutions, and in Solids with Apparently Regular Octahedral Coordination Geometry. *Dalt. Trans.* **2002**, 1256–1265.
- (59) Collings, M. D.; Sherman, D. M.; Ragnarsdottir, K. V. Complexation of Cu^{2+} in Oxidized NaCl Brines from 25°C to 175°C: Results from in Situ EXAFS Spectroscopy. *Chem. Geol.* **2000**, *167*, 65–73.
- (60) Wright, R. R.; Walker, N. R.; Firth, S.; Stace, A. J. Coordination and Chemistry of Stable Cu(II) Complexes in the Gas Phase. *J. Phys. Chem. A* **2001**, *105* (1), 54–64.
- (61) Walker, N. R.; Firth, S.; Stace, A. J. Stable Cu(II) Coordination Complexes in the Gas Phase. *Chem. Phys. Lett.* **1998**, *292*, 125–132.
- (62) Marino, T.; Toscano, M.; Russo, N.; Grand, A. Structural and Electronic Characterization of the Complexes Obtained by the Interaction between Bare and Hydrated First-Row Transition-Metal Ions (Mn^{2+} , Fe^{2+} , Co^{2+} , Ni^{2+} , Cu^{2+} , Zn^{2+}) and Glycine. *J. Phys. Chem. B* **2006**, *110*, 24666–24673.
- (63) Pavelka, M.; Shukla, M. K.; Leszczynski, J.; Burda, J. V. Theoretical Study of Hydrated Copper(II) Interactions with Guanine: A Computational Density Functional Theory Study. *J. Phys. Chem. A* **2008**, *112*, 256–267.
- (64) Dietrich-Buchecker, C. O.; Sauvage, J. P.; Kintzinger, J. P. New Family of Molecules: The Metallo-Catenanes. *Tetrahedron Lett.* **1983**, *24* (46), 5095–5098.
- (65) Pranowo, H. D.; Setiaji, A. H. B.; Rode, B. M. Cu^+ in Liquid Ammonia and in Water: Intermolecular Potential an Monte Carlo Simulation. *J. Phys. Chem. A* **1999**, *103*, 11115–11120.
- (66) Schwenk, C. F.; Rode, B. M. Cu(II) in Liquid Ammonia : An Approach by Hybrid Molecular Dynamics Simulation. *ChemPhysChem* **2004**, *5*, 342–348.
- (67) Pranowo, H. D.; Rode, B. M. Solvation of Cu^{2+} in Liquid Ammonia: Monte Carlo Simulation Including Three-Body Corrections. *J. Phys. Chem.* **1999**, *103*, 4298–4302.
- (68) Gómez-Balderas, R.; Raffa, D. F.; Rickard, G. A.; Brunelle, P.; Rauk, A. Computational Studies of Cu(II)/Met and Cu(I)/Met Binding Motifs Relevant for the Chemistry of Alzheimer's Disease. *J. Phys. Chem. A* **2005**, *109*, 5498–5508.
- (69) Raffa, D. F.; Gómez-Balderas, R.; Brunelle, P.; Rickard, G. A.; Rauk, A. Ab Initio Model Studies of Copper Binding to Peptides Containing a His–His Sequence : Relevance to the B-Amyloid Peptide of Alzheimer's Disease. *J. Biol. Inorg. Chem.* **2005**, *10*, 887–902.
- (70) Raffa, D. F.; Rickard, G. A. Ab Initio Modelling of the Structure and Redox Behaviour of Copper (I) Bound to a His – His Model Peptide : Relevance to the B -Amyloid Peptide of Alzheimer ' S Disease. *J. Biol. Inorg. Chem.* **2007**, *12*, 147–164.
- (71) Sýkora, J.; Brandsteterová, E.; Jabconová, A. Photoredox Reactivity of Copper Complexes and Photooxidation of Organic Substrates. *Adv. Chem. Ser.* **1993**, *238*, 377–397.
- (72) Koppenol, W. H. The Centennial of the Fenton Reaction. *Free radica Biol. Med.* **1993**, *15*, 645–651.
- (73) Sakaki, S.; Koga, G.; Sato, F.; Ohkubo, K. New Photoreduction Catalysis by $[\text{Cu}(\text{NN})\text{PPH}_3]_2^+$ (NN=2,9-Dimethyl-1,10-Phenanthroline or 4,4',6,6'-Tetramethyl-2,2'-bipyridine) and Its Application to cobalt(III) Complexes. *J. Chem. Soc. Dalt. Trans.* **1985**, 1959–1962.
- (74) Sakaki, S.; Koga, G.; Ohkubo, K. Successful Photocatalytic Reduction of Methylviologen (MV^{2+}) with $[\text{Cu}(\text{NN})(\text{PPh}_3)_2]^+$ (NN = 2,9-Dimethyl-1,10-Phenanthroline or 4,4',6,6'-Tetramethyl-2,2'-Bipyridine) upon near-UV-Light Irradiation and a Novel Solvent Effect on Its Catalytic Activity. *Inorg. Chem.* **1986**, *25* (14), 2330–2333.

- (75) Brackman, W.; Havinga, E. Oxidation of Phenols with Copper-Amine Catalysts and Its Relation to the Mode of Action of Tyrosinase. III. Kinetics of Oxidation of Monohydric Phenols with Copper-Morpholine Complex as Homogeneous Catalyst. *Recl. des Trav. Chim. des Pays-Bas la Belgique* **1955**, *74*, 1070–1080.
- (76) Brackman, W.; Havinga, E. Oxidation of Phenols with Copper-Amine Catalysts and Its Relation to the Mode of Action of Tyrosinase. I. Catalytic Oxidation of Monohydric Phenols to O-Quinone Derivatives. *Recl. des Trav. Chim. des Pays-Bas la Belgique* **1955**, *74*, 937–955.
- (77) Hsu, C. Y.; Lyons, J. E. Oxidizing Phenol to P-Benzoquinone., October 23, 1984.
- (78) Hay, A. S.; Blanchard, H. S.; Endres, G. F.; Eustance, J. W. Polymerization by Oxidative Coupling. *J. Am. Chem. Soc.* **1959**, *81*, 6335–6336.
- (79) Gargano, M.; Ravasio, N.; Rossi, M. Reactivity of Metallic Copper with Acidic Compounds in the Presence of Molecular Oxygen. Crystal Structure of $[\{\text{Cu}(\text{NCO})(\text{Py})_2\}_2]\text{H}_2\text{O}$. *Dalt. Trans.* **1989**, 921–925.
- (80) Morisaki, S.; Komamiya, K.; Naito, M. Wet Oxidation of Phenol in Aqueous Solution with Oxygen Catalyzed by copper(II) Sulfate. *Nippon Kagaku Kaishi* **1980**, No. 7, 1191–1193.
- (81) Matsushima, R.; Ichigawa, Y.; Kuwabara, K. Photooxidation of 2-Hydroxy Acids by copper(II) in Aqueous Solution. *Bull. Chem. Soc. Jpn.* **1980**, *53* (7), 1902–1907.
- (82) Morimoto, J. Y.; Degraff, B. A. Photochemistry of the copper(II)-Malonate System. A “Sensitized” Reaction. *J. Phys. Chem.* **1972**, *76* (9), 1387–1388.
- (83) Morimoto, J. Y.; DeGraff, B. A. Photochemistry of Copper Complexes. Copper(II) Malonate System. *J. Phys. Chem.* **1975**, *79* (4), 326–331.
- (84) Kerr, J. A.; Lloyd, A. C. Decomposition Reactions of Radicals. *Q. Rev. Chem. Soc.* **1968**, *22* (4), 549–577.
- (85) Horváth, O. Photochemistry of Copper (I) Complexes. *Coord. Chem. Rev.* **1994**, *135/136*, 303–324.
- (86) Armaroli, N.; Gianluca, A.; Francois, C. Photochemistry and Photophysics of Coordination Compounds : Copper. *Top. Curr. Chem.* **2007**, *280*, 69–115.
- (87) Ferraudi, G. Photochemistry of Macrocyclic copper(II) Complexes. Photoinduced Redox Reactions of $\text{Cu}[\text{13-AtH}]_2^+$. *Inorg. Chem.* **1978**, *17* (7), 1741–1747.
- (88) Grodzicki, A.; Lakomska, I.; Piszczek, P.; Szymanska, I.; Szlyk, E. Copper(I), silver(I) and gold(I) Carboxylate Complexes as Precursors in Chemical Vapor Deposition of Thin Metallic Films. *Coord. Chem. Rev.* **2005**, *249* (21-22), 2232–2258.
- (89) Jakob, A.; Shen, Y.; Waechtler, T.; Schultz, S. E.; Gessner, T.; Riedel, R.; Fasel, C.; Lang, H. Copper(I) Carboxylates of Type $[(n\text{Bu}_3\text{P})_m\text{CuO}_2\text{CR}]$ ($m = 1,2,3$) - Synthesis, Properties, and Their Use as CVD Precursors. *Zeitschrift fuer Anorg. und Allg. Chemie* **2008**, *634* (12-13), 2226–2234.
- (90) Harmand, L.; Cadet, S.; Kauffmann, B.; Scarpantonio, L.; Batat, P.; Jonusauskas, G.; McClenaghan, N. D.; Lastecoueres, D.; Vincent, J.-M. Copper Catalyst Activation Driven by Photoinduced Electron Transfer: A Prototype Photolatent Click Catalyst. *Angew. Chemie, Int. Ed.* **2012**, *51* (29), 7137–7141, S7137/1–S7137/23.
- (91) Harmand, L.; Lambert, R.; Scarpantonio, L.; McClenaghan, N. D.; Lastecoueres, D.; Vincent, J.-M. A Photoreducible Copper(II)-Tren Complex of Practical Value: Generation of a Highly Reactive Click Catalyst. *Chem. - A Eur. J.* **2013**, *19* (48), 16231–16239.
- (92) Armaroli, N. Photoactive Mono and Polynuclear Cu(I)- Phenanthrolines . A Viable Alternative to Ru(II)- Polypyridines? *Chem. Soc. Rev.* **2001**, *30* (2), 113–124.

- (93) Zgierski, M. Z. Cu(I)-2, 9-Dimethyl-1, 10-Phenanthroline : Density Functional Study of the Structure, Vibrational Force-Field , and Excited Electronic States. *J. Chem. Phys.* **2003**, *118* (9), 4045–4051.
- (94) Ichinaga, A. K.; Kirchhoff, J. R.; Mcmillin, D. R.; Dietrich-buchecker, C.; Marnot, P. A.; Sauvage, J. Charge Transfer Absorption and Emission of Cu(NN)²⁺ Systems. *Inorg. Chem.* **1987**, *26* (3), 4290–4292.
- (95) Sugasaka, K.; Fujii, A. A Spectrophotometric Study of copper(I) Chloro-Complexes in Aqueous 5M Sodium(chloride, Perchlorate) Solutions. *Bull. Chem. Soc. Jpn.* **1976**, *49* (1), 82–86.
- (96) Davis, D. D.; Stevenson, K. L.; Davis, C. R. Photooxidation of Dichloro- and trichlorocuprate(I) Ions in Acid Solution. *J. Am. Chem. Soc.* **1978**, *100* (17), 5344–5349.
- (97) Davis, D. D.; King, G. K.; Stevenson, K. L.; Birnbaum, E. R.; Hageman, J. H. Photoredox Reactions of Metal Ions for Photochemical Solar Energy Conversion. *J. Solid State Chem.* **1977**, *22* (1), 63–70.
- (98) Stevenson, K. L.; Davis, D. D. The copper(I)-Catalyzed Photooxidation of titanium(III) Salts. *Inorg. Nucl. Chem. Lett.* **1976**, *12* (12), 905–909.
- (99) Horvath, O.; Papp, S. Photooxidation of copper(I) Chloro Complexes: Individual Quantum Yields of Copper Chloride Ions [CuCl₂]- and [CuCl₃]²⁻. *J. Photochem.* **1985**, *30* (1), 47–61.
- (100) Kochi, J. K. Photolysis of Metal Compounds: Cupric Chloride in Organic Media. *J. Am. Chem. Soc.* **1962**, *84*, 2121–2127.
- (101) Cervone, E.; Diomedi, F. Cyclic Chlorination Reactions Induced by Visible Light with chlorocopper(II) Complexes as Mediators. *J. Photochem.* **1981**, *15* (3), 203–212.
- (102) Jenkins, C. L.; Kochi, J. K. Ligand Transfer of Halides (Cl, Br, I) and Pseudohalides (SCN, N₃, CN) from Copper (II) to Alkyl Radicals. *J. Org. Chem.* **1971**, *36* (21), 3095–3102.
- (103) Horvath, O. Intermediates in Photoinduced Redox Reactions of chlorocuprate(I) Complexes. *J. Photochem. Photobiol. A Chem.* **1988**, *44* (3), 259–265.
- (104) Horvath, O.; Papp, S. Investigation of a Long-Lived Intermediate in the Photooxidation of chlorocuprate(I) Complexes. *J. Photochem.* **1985**, *31* (2-3), 211–222.
- (105) Chang, Q.; Chen, J.; Liu, W.; Ye, Q.; Chen, X.; Yu, Y.; Chen, L.; Hu, C. Study on the Coordinate Mode of Acetylacetonate in Ir(acac)₃ and Ir(acac)₃(H₂O). *Guijinshu* **2011**, *32* (3), 64–68.
- (106) Khranenko, S. P.; Plusnin, P. E.; Sheludyakova, L. A.; Gerasimova, Y. V.; Korolkov, I. V.; Korenev, S. V. A Study of Complexation between Crystalline Trans-[Pd(H₂O)₂(NO₃)₂] and Acetylacetone. *Russ. J. Coord. Chem.* **2009**, *35* (9), 681–686.
- (107) Semenov, V. V.; Zolotareva, N. V.; Klapshina, L. G.; Kurskii, Y. A.; Lopatin, M. A.; Domrachev, G. A. Synthesis of C-Functionalized Acetylacetone and Its Europium Complex. Preparation and Study of Luminescence of Europium-Containing Sol-Gel Films. *Russ. J. Gen. Chem.* **2009**, *79* (9), 1802–1810.
- (108) Zhang, Q.-L.; Zhang, Y.-Q.; Zhu, B.-X. Synthesis and Crystal Structure of Co(II) and Zn(II) Complexes with One-Dimensional Chain Structure. *Wuji Huaxue Xuebao* **2011**, *27* (5), 923–927.
- (109) Le, V. H.; Nguyen, H. K.; Nguyen, V. X.; Nguyen, M. T. Study of the Formation of Complex Catalysts of Co(II) with Acetylacetone (Acac) in the System: H₂O-Co₂⁺-Acac. *Tap Chi Hoa Hoc* **2011**, *49* (3), 321–325.
- (110) Yadav, R. S. Studies on Schiff Base Complexes of cobalt(II) and cadmium(II) Derived from Histidine with Acetylacetone. *Asian J. Chem.* **2010**, *22* (4), 2849–2852.

- (111) Bailey, N. A.; Fenton, D. E.; Franklin, M. V; Hall, M. Ternary Complexes of copper(II) with Mixed Acetylacetonate and Nitrogen-Containing Ligands. *J. Chem. Soc. Dalton Trans. Inorg. Chem.* **1980**, No. 6, 984–990.
- (112) Marciniak, B.; Chow, Y. L. The Interaction of Triplet Excited State Ketones with copper(II) Complexes: Effects of β -Diketonate Ligands. *J. Photochem. Photobiol. A Chem.* **1987**, *41* (1), 31–36.
- (113) Omarsson, B.; Engmann, S.; Ingolfsson, O. Dissociative Electron Attachment to the Complexation Ligands Hexafluoroacetylacetone, Trifluoroacetylacetone and Acetylacetone; a Comparative Experimental and Theoretical Study. *RSC Adv.* **2014**, *4* (63), 33222–33235.
- (114) Delchev, V. B.; Mikosch, H.; St. Nikolov, G. The Keto-Enol Equilibrium of Pentane-2,4-Dione Studied by Ab Initio Methods. *Monatshefte fuer Chemie* **2001**, *132* (3), 339–348.
- (115) Koudriavtsev, A. B.; Linert, W. Keto-Enol Equilibrium from NMR Data: A Closer Look at the Laboratory Experiment. *J. Chem. Educ.* **2009**, *86* (10), 1234–1237.
- (116) Gafney, H. D.; Lintvedt, R. L. Photochemical Reactions of Copper(II) 1,3 Diketonate Complexes. *J. Am. Chem. Soc.* **1971**, *93* (7), 1623–1628.
- (117) Lintvedt, R. L.; Russell, H. D.; Holtzclaw, H. F. J. Polarographic Reduction of Copper Chelates of 1,3-Diketones. IV. Chelate Stability and Electron-Transfer Mechanism. *Inorg. Chem.* **1966**, *5* (9), 1603–1607.
- (118) Giuffrida, S.; Condorelli, G. G.; Costanzo, L. L.; Fragala, I. L.; Ventimiglia, G.; Vecchio, G. Photochemical Mechanism of the Formation of Nanometer-Sized Copper by UV Irradiation of Ethanol bis(2,4-pentandionato)copper(II) Solutions. *Chem. Mater.* **2004**, *16* (ii), 1260–1266.
- (119) Blair, S.; Goolsby, B.; Brodbelt, J. Solvent Displacement in Transition Metal Complexes. *Int. J. Mass Spectrom.* **1999**, *185/186/187*, 49–59.
- (120) Denison, G. M.; Evans, A. O.; Bessel, C. A.; Skaf, D. W.; Murray, R. W.; DeSimone, J. M. Electrochemical Behavior of Bis(β -Diketonate)copper Complexes. *J. Electrochem. Soc.* **2005**, *152* (11), B435–B440.
- (121) Aggett, J.; Billingham, M. W. Solvent Extraction of Pyridine Complexes of copper(II). *J. Inorg. Nucl. Chem.* **1969**, *31* (2), 513–525.
- (122) Tsuchida, E.; Kaneko, M.; Nishide, H. Role of Oxygen in the Oxidative Polymerization of 2,6-Xylenol Catalyzed by Copper-Amine Complexes. *Makromol. Chemie* **1972**, *151*, 235–244.
- (123) Balogh-Hergovich, E.; Speier, G. Oxygenation of Enamines Catalyzed by a copper(I)-Pyridine Complex. *React. Kinet. Catal. Lett.* **1975**, *3* (2), 139–141.
- (124) Yukimasa, H.; Sawai, H.; Takizawa, T. Oxidative Cleavage of Indoles Using Copper-Pyridine Complex. *Chem. Pharm. Bull. (Tokyo)*. **1979**, *27* (2), 551–553.
- (125) Yang, Y.-S.; Hsu, W.-Y.; Lee, H.-F.; Huang, Y.-C.; Yeh, C.-S.; Hu, C.-H. Experimental and Theoretical Studies of Metal Cation-Pyridine Complexes Containing Cu and Ag. *J. Phys. Chem. A* **1999**, *103* (51), 11287–11292.
- (126) Rodgers, M. T.; Stanley, J. R.; Amunugama, R. Periodic Trends in the Binding of Metal Ions to Pyridine Studied by Threshold Collision-Induced Dissociation and Density Functional Theory. *J. Am. Chem. Soc.* **2000**, *122* (44), 10969–10978.
- (127) Miyawaki, J.; Sugawara, K. ZEKE Spectroscopy of the Copper-Pyridine Complex. *Chem. Phys. Lett.* **2004**, *386* (1-3), 196–199.

- (128) Miyawaki, J.; Sugawara, K. ZEKE Photoelectron Spectroscopy of the Silver- and Copper-Ammonia Complexes. *J. Chem. Phys.* **2003**, *119* (13), 6539–6545.
- (129) Walter, D.; Armentrout, P. B. Sequential Bond Dissociation Energies of $M^+(NH_3)_x$ ($x = 1-4$) for $M = Ti-Cu$. *J. Am. Chem. Soc.* **1998**, *120* (13), 3176–3187.
- (130) Puskar, L.; Barran, P. E.; Wright, R. R.; Kirkwood, D. A.; Stace, A. J. The Ultraviolet Photofragmentation of Doubly Charged Transition Metal Complexes in the Gas Phase: Initial Results for $[Cu.(pyridine)_n]^{2+}$ and $[Ag.(pyridine)_n]^{2+}$ Ions. *J. Chem. Phys.* **2000**, *112* (18), 7751–7754.
- (131) Puskar, L.; Stace, A. J. Gas Phase Ligand Field Photofragmentation Spectroscopy. *J. Chem. Phys.* **2001**, *114* (15), 6499–6501.
- (132) Puskar, L.; Cox, H.; Goren, A.; Aitken, G. D. C.; Stace, A. J. Ligand Field Spectroscopy of Cu(II) and Ag(II) Complexes in the Gas Phase: Theory and Experiment. *Faraday Discuss.* **2003**, *124*, 259–273.
- (133) Walker, N. R.; Firth, S.; Stace, A. J. Stable Cu(II) Coordination Complexes in the Gas Phase. *Chem. Phys. Lett.* **1998**, *292* (1,2), 125–132.
- (134) Walker, N. R.; Wright, R. R.; Stace, A. J. Stable Ag(II) Coordination Complexes in the Gas Phase. *J. Am. Chem. Soc.* **1999**, *121* (20), 4837–4844.
- (135) Walker, N. R.; Wright, R. R.; Barran, P. E.; Stace, A. J. Stable Gold(II) Complexes in the Gas Phase. *Organometallics* **1999**, *18* (18), 3569–3571.
- (136) Walker, N. R.; Wright, R. R.; Barran, P. E.; Murrell, J. N.; Stace, A. J. Comparisons in the Behavior of Stable Copper(II), Silver(II), and Gold(II) Complexes in the Gas Phase: Are There Implications for Condensed-Phase Chemistry?. *J. Am. Chem. Soc.* **2001**, *123* (18), 4223–4227.
- (137) Wu, G.; Guan, J.; Aitken, G. D. C.; Cox, H.; Stace, A. J. Infrared Multiphoton Spectra from Metal Dication Complexes in the Gas Phase. *J. Chem. Phys.* **2006**, *124* (20), 201103/1–201103/4.
- (138) Revesz, A.; Milko, P.; Zabka, J.; Schroeder, D.; Roithova, J. Reduction from copper(II) to copper(I) upon Collisional Activation of $(pyridine)_2CuCl^+$. *J. Mass Spectrom.* **2010**, *45* (11), 1246–1252.
- (139) Wei, H.-H.; Tsai, C.-W. The Polarographic Studies of Substituent Effects in Pyridine Complexes of Transition Metals. *J. Chinese Chem. Soc. (Taipei, Taiwan)* **1975**, *22* (4), 285–290.
- (140) Russo, U.; Vidali, M.; Zarli, B.; Purrello, R.; Maccarrone, G. Synthesis and Characterization of Binuclear Complexes and Their Catalytic Activity on the Oxidation of Catechol. *Inorganica Chim. Acta* **1986**, *120* (2), L11–L13.
- (141) Wendt, F.; Naether, C.; Tuzek, F. Tyrosinase and Catechol Oxidase Activity of copper(I) Complexes Supported by Imidazole-Based Ligands: Structure-Reactivity Correlations. *JBIC, J. Biol. Inorg. Chem.* **2016**, *21* (5-6), 777–792.
- (142) Castro, K. A. D. F.; Rodrigues, J. M. M.; Mendes, R. F.; Neves, M. da G. P. M. S.; Simoes, M. M. Q.; Cavaleiro, J. A. S.; Almeida Paz, F. A.; Tome, J. P. C.; Nakagaki, S. New Copper Porphyrins as Functional Models of Catechol Oxidase. *J. Catal.* **2016**, *344*, 303–312.
- (143) Caglar, S.; Aydemir, I. E.; Adiguzel, E.; Caglar, B.; Demir, S.; Buyukgungor, O. Four copper(II) Diclofenac Complexes with Pyridine Derivatives: Synthesis, Crystal Structures, Spectroscopic Properties, Thermal Analysis and Catechol Oxidase Activities. *Inorganica Chim. Acta* **2013**, *408*, 131–138.
- (144) Csonka, R.; Kaizer, J.; Giorgi, M.; Réglie, M.; Hajba, L.; Mink, J.; Speier, G. Oxidative CH and CC Bond Cleavage by a (2,2'-Bipyridine) Copper (I) Chloride Complex. *Inorg. Chem.* **2008**, *47* (14), 6121–6123.

- (145) Fujita, S. *Organic Chemistry of Photography*; Springer, 2004.
- (146) Tsuji, J.; Takayanagi, H. Oxidative Cleavage Reactions of Catechol and Phenol to Monoester of Cis,cis-Muconic Acid with the Oxidizing Systems of Oxygen/cuprous Chloride, Potassium Hydroxide/cupric Chloride, and Potassium Superoxide/cupric Chloride in a Mixture of Pyridine and Alcohol. *Tetrahedron* **1978**, *34* (6), 641–644.
- (147) Tsuji, J.; Takayanagi, H.; Sakai, I. Organic Synthesis by Means of Metal Complexes. XIV. Oxidative Cleavage of Catechol with Labeled Oxygen Activated by Cuprous Chloride. *Tetrahedron Lett.* **1975**, No. 14, 1245–1246.
- (148) Rogic, M. M.; Demmin, T. R.; Hammond, W. B. Cleavage of Carbon-Carbon Bonds. Copper(II)-Induced Oxygenolysis of O-Quinones, Catechols, and Phenols. *J. Am. Chem. Soc.* **1976**, *98* (23), 7441–7443.
- (149) Brown, D. G.; Beckmann, L.; Hill, C. Oxygen Dependent Ring Cleavage in a Copper Coordinated Catechol. *Tetrahedron Lett.* **1977**, No. 16, 1363–1364.
- (150) Abakumov, G. A.; Cherkasov, V. K. Free Radical-O-Semiquinone Complexes of Transition Metals. Structural Dynamics in Solution. *Met. Khimiya* **1990**, *3* (4), 838–852.
- (151) Abakumov, G. A.; Garnov, V. A.; Nevodchikov, V. I.; Cherkasov, V. K. Synthesis of Redox-Isomeric Diazabutadiene Copper Complexes with O-Benzoquinone Derivatives. *Dokl. Akad. Nauk SSSR* **1989**, *304* (1), 107–111 [Chem.].
- (152) Pierpont, C. G.; Lange, C. W. *The Chemistry of Transition Metal Complexes Containing Catechol and Semiquinone Ligands*; 1994; Vol. 4.
- (153) Larson, R. C.; Iwamoto, R. T. Solvent Effects on the Polarographic Reduction of Metal Ions. II. Nitrile Solvents. *J. Am. Chem. Soc.* **1960**, *82*, 3526–3527.
- (154) Taube, H. Bridging and Nonbridging Ligand Effects in Redox Reactions of Metal Ions. *Can. J. Chem.* **1959**, *37*, 129–137.
- (155) Condikey, G. F.; Martell, A. E. Mixed Ligand Chelates of Copper (II). *J. Inorg. Nucl. Chem.* **1969**, *31* (1969), 2455–2466.
- (156) L'Heureux, G. A.; Martell, A. E. Mixed Ligand Chelates of Copper(II). *J. Amer. Chem. Soc.* **1967**, *89* (12), 2859–2865.
- (157) Blades, A. T.; Jayaweera, P.; Ikononou, M. G.; Kebarle, P. Ion-Molecule Clusters Involving Doubly Charged Metal Ions (M²⁺). *Int. J. Mass Spectrosc. Ion Process.* **1990**, *102*, 251–267.
- (158) Titinchi, S. J. J.; Von Willingh, G.; Abbo, H. S.; Prasad, R. Tri- and Tetradentate Copper Complexes: A Comparative Study on Homogeneous and Heterogeneous Catalysis over Oxidation Reactions. *Catal. Sci. Technol.* **2015**, *5* (1), 325–338.
- (159) Rayner, D. G.; Mulley, J. S.; Bennett, R. A. Copper Deposition on TiO₂ from copper(II) hexafluoroacetylacetonate. *J. Vac. Sci. Technol. A Vacuum, Surfaces, Film.* **2013**, *31* (1), 01A121/1–01A121/5.
- (160) Davis, B.; Slaven, W. Characterization of a Novel Low Oxidation State Transition-Metal Peroxide from the Reaction of Copper (I) Chloride with Oxygen in Pyridine. *J. Am. Chem. Soc. Chem. Commun.* **1975**, No. 606, 606–607.
- (161) Bowmaker, G. A.; Di Nicola, C.; Pettinari, C.; Skelton, B. W.; Somers, N.; White, A. H. Mechanochemical Synthesis in Copper(II) Halide/pyridine Systems: Crystal X-Ray Diffraction and IR Spectroscopic Studies. *Dalt. Trans.* **2011**, No. 40, 5102–5115.
- (162) Gupta, R. K.; Yadav, M.; Pandey, R.; Pandey, D. S. Synthesis and Characterization of Some Heteroleptic Copper (II) Complexes Based on Meso-Substituted Dipyrins. *J. Chem. Sci.* **2011**, *123* (6), 819–826.

- (163) Sigel, H.; Huber, P. R.; Griesser, R.; Prijs, B. Ternary Complexes in Solution. XV. Mixed-Ligand copper(II) Complexes with 2,2'-Bipyridyl or 1,10-Phenanthroline and Pyrocatecholate or Derivatives Thereof. *Inorg. Chem.* **1973**, *12* (5), 1198–1200.
- (164) Gergely, A.; Kiss, T. Complexes of 3,4-Dihydroxyphenyl Derivatives. I. Copper(II) Complexes of DL-3,4-Dihydroxyphenylalanine. *Inorganica Chim. Acta* **1976**, *16*, 51–59.
- (165) Huber, P. R.; Griesser, R.; Prijs, B.; Sigel, H. Ternary Complexes in Solution. *Eur. J. Biochem.* **1969**, *10*, 238–242.
- (166) Speier, G.; Tisza, S.; Tyeklar, Z.; Lange, C. W.; Pierpont, C. G. Coligand-Dependent Shifts in Charge Distribution for Copper Complexes Containing 3,5-Di-Tert-Butylcatecholate and 3,5-Di-Tert-Butylsemiquinonate Ligands. *Inorg. Chem.* **1994**, *33* (9), 2041–2045.
- (167) Brown, D. G.; Reinprecht, J. T.; Vogel, G. C. Synthesis and Characterization of copper(II) Catecholato Complexes. *Inorg. Nucl. Chem. Lett.* **1976**, *12* (5), 399–404.
- (168) Gottwald, W. *UV/VIS-Spektroskopie für Anwender*; Wiley - VCH: Weinheim, 1998.
- (169) Groom, C. R.; Bruno, I. J.; Lightfoot, M. P.; Ward, S. C. The Cambridge Structural Database. *Acta Crystallogr. Sect. B* **2016**, No. B72, 171–179.
- (170) Macrae, C. F.; Bruno, I. J.; Chisholm, J. A.; Edgington, P. R.; McCabe, P.; Pidcock, E.; Rodriguez-monge, L.; Taylor, R.; Streek, J. Van De; Wood, P. A. Mercury CSD 2 .0 - New Features for the Visualization and Investigation of Crystal Structures. *J. Appl. Crystallogr.* **2008**, No. 41, 466–470.
- (171) Schmidt, M. W.; Baldrige, K. K.; Boatz, J. A.; Elbert, S. T.; Gordon, M. S.; Jensen, J. H.; Koseki, S. K.; Matsunaga, N. M.; Nguyen, K. A.; Su, S. J.; et al. General Atomic and Molecular Electronic Structure System. *J. Comput. Chem.* **1993**, No. 14, 1347–1363.
- (172) Gordon, M. S.; Schmidt, M. W. Advances in Electronic Structure Theory: GAMESS a Decade Later. In *Theory and Applications of Computational Chemistry: the first forty years*; Dykstra, C. E., Frenking, G., Kim, K. S., Scuseria, G. E., Eds.; Elsevier: Amsterdam, 2005; pp 1167–1189.
- (173) Gaussian09; RevisionA0.2; Frisch, M. J.; Trucks, G. W.; Schlegel, H. B.; Scuseria, G. E.; Robb, M. A.; Cheeseman, J. R.; Scalmani, G.; Barone, V.; et al. Gaussian09. 2016.
- (174) Kendall, R. A.; Dunning, T. H.; Harrison, R. J. Electron Affinities of the First-Row Atoms Revised. Systematic Basis Sets and Wave Functions. *J. Chem. Phys.* **1992**, *96* (9), 6796–6806.
- (175) Lu, T.; Chen, F. Multiwfn : A Multifunctional Wavefunction Analyzer. *J. Comput. Chem.* **2012**, No. 33, 580–592.
- (176) Bode, B. M.; Gordon, M. S. MacMolPlt : A Graphical User Interface for GAMESS. *J. Mol. Graph. Model.* **1998**, *3263* (99), 133–138.
- (177) Hanwell, M. D.; Curtis, D. E.; Lonie, D. C.; Vandermeersch, T.; Zurek, E.; Hutchison, G. R. Avogadro : An Advanced Semantic Chemical Editor , Visualization , and Analysis Platform. *J. Cheminform.* **2012**, *4* (1), 1–17.
- (178) Halbritter, W. *Bericht TB/L-M 115/00*; 2000.
- (179) Kavarnos, G. J. *Fundamentals of Photoinduced Electron Transfer*; VCH Publishers, 1993.
- (180) Najbar, J.; Dorfman, F. L. C.; Fayer, M. D. Solvent Relaxation Effects on the Kinetics of Photoinduced Electron Transfer Reactions. *J. Chem. Phys.* **1991**, *94* (2), 1081–1092.
- (181) Haynes, W. M. *CRC Handbook of Chemistry and Physics, 94th Edition.*; CRC Press, 2013.
- (182) Turro, N. J. *Modern Molecular Photochemistry*; Benjamin/Cummings Pub. Co.: Menlo Park, Calif., 1978.

- (183) Baker, R. H.; Adkins, H. Oxidation Potentials of Ketones and an Aldehyde. *J. Am. Chem. Soc.* **1940**, *62*, 3305–3314.
- (184) Golchoubian, H. Redetermination of Crystal Structure of The Structure of bis(2, 4-Pentanedionato) Copper (II). *Asian J. Chem.* **2008**, *20* (8), 5834–5838.
- (185) Hamid, M.; Mazhar, M.; Zeller, M.; Hunter, A. D. Copper (II) Diacetylacetonate (remeasurement). *Priv. Commun. to Cambridge Crystallogr. Data Cent.* **2005**, *CCDC 28102*.
- (186) Gromilov, S. A.; Baidina, I. A.; Stabnikov, P. A. Crystal Structure of copper(II) Bis Hexafluoroacetylacetonate. *J. Struct. Chem.* **2004**, *45* (3), 476–481.
- (187) Nakanishi, H.; Morita, H.; Nagakura, S. Electronic Structures and Spectra of the Keto and Enol Forms of Acetylacetonate. *Bull. Chem. Soc. Jpn.* **1977**, *50* (9), 2255–2261.
- (188) Fackler Jr., J. P.; Cotton, F. A. Electronic Spectra of β -Diketone Complexes. IV. γ -Substituted Acetylacetonates of copper(II). *Inorg. Chem.* **1963**, *2*, 102–106.
- (189) Fackler Jr., J. P.; Cotton, F. A.; Barnum, D. W. Electronic Spectra of β -Diketone Complexes. III. α -Substituted β -Diketone Complexes of copper(II). *Inorg. Chem.* **1963**, *2*, 97–101.
- (190) Maverick, A. W.; Fronczek, F. R.; Maverick, E. F.; Billodeaux, D. R.; Cygan, Z. T.; Isovitsch, R. A. Structures of Anhydrous and Hydrated Copper(II) Hexafluoroacetylacetonate. *Inorg. Chem.* **2002**, *41* (24), 6488–6492.
- (191) Japar, S.; Ramsay, D. A. Triplet-Singlet Absorption in Pyridine. *J. Chem. Phys.* **1973**, *58* (12), 5832–5833.
- (192) Chachisvilis, M.; Zewail, A. H. Femtosecond Dynamics of Pyridine in the Condensed Phase: Valence Isomerization by Conical Intersections. *J. Phys. Chem. A* **1999**, *103* (37), 7408–7418.
- (193) Terazima, M.; Azumi, T. The Quantum Yield of Triplet Formation and Triplet Lifetime of Pyridine in the Liquid Phase by the Two-Photon-Excited Time-Resolved Thermal Lens Method. *Chem. Phys. Lett.* **1988**, *153* (1), 27–32.
- (194) Weisman, R. B.; Holt, P. L.; Selco, J. I. Dynamical Spectroscopy of Triplet State Pyridine. *J. Chem. Phys.* **1982**, *77*, 1600–1601.
- (195) Srivastava, K. P.; Srivastava, S. K.; Singh, V. K.; Sinha, G. Quantum Chemical Studies on Molecular Structures of Copper-Pyridine Complexes. *Chem. Sci. Trans.* **2013**, *2* (4), 1379–1385.
- (196) Bridge, M. E.; Connolly, M.; Lloyd, D. R.; Somers, J.; Jakob, P.; Menzel, D. Electron Spectroscopic Studies of Pyridine on Metal Surfaces. *Spectrochim. Acta - Part A Mol. Biomol. Spectrosc.* **1987**, *43* (12), 1473–1478.
- (197) Borsub, N.; Chang, S.-C.; Kutal, C. Ligand Control of the Mechanism of Photosensitization by Copper(I) Compounds. *Inorg. Chem.* **1982**, *21*, 538–543.
- (198) Wu, D. Y.; Hayashi, M.; Shiu, Y. J.; Liang, K. K.; Chang, C. H.; Yeh, Y. L.; Lin, S. H. A Quantum Chemical Study of Bonding Interaction, Vibrational Frequencies, Force Constants and Vibrational Coupling of Pyridine - M_n ($M=Cu, Ag, Au$; $n = 2 - 4$). *J. Phys. Chem. A* **2003**, *107*, 9658–9667.
- (199) Gill, N. S.; Nyholm, R. S.; Barclay, G. A.; Christie, T. I.; Pauling, P. J. Structure of Bis Pyridine Metal Dihalide Complexes. *J. Inorg. Nucl. Chem.* **1961**, *18*, 88–97.
- (200) Benedix, R.; Vogler, A. Electronic Structure and Spectroscopic Properties of Copper Catecholate Complexes with Interligand Charge-Transfer Behavior. *Inorganica Chim. Acta* **1993**, *204* (2), 189–193.

- (201) Balogh-Hergovich, E.; Speier, G. The Formation of Dinuclear Catecholato copper(II) Complexes from Strongly Oxidizing O-Quinones and copper(I) Halides. *Inorganica Chim. Acta* **1985**, *108* (1), 59–62.
- (202) Nast, R.; Mohr, R.; Schultze, C. Zur Kenntnis von kupfer(I)-Acetylacetonat. *Zeitschrift für Anorg. und Allg. Chemie* **1963**, *307* (15), 2127–2131.
- (203) Roeges, N. P. G. *A Guide to the Complete Spectra of Infrared Spectra of Organic Structures*; Wiley, 1994.
- (204) Nakamoto, K. *Infrared and Raman Spectra of Inorganic and Coordination Compounds*, 4th ed.; Wiley, 1986.
- (205) Movahedi, E.; Golchoubian, H. Substituent and Solvent Effects in the Spectra of New Mixed-Chelate copper(II) Complexes Containing N,N'-Disubstituted Ethylenediimine and Acetylacetonate Ligands. *J. Mol. Struct.* **2006**, *787* (1-3), 167–171.
- (206) Howard, D. L.; Kjaergaard, H. G.; Huang, J.; Meuwly, M. Infrared and Near-Infrared Spectroscopy of Acetylacetone and Hexafluoroacetylacetone. *J. Phys. Chem. A* **2015**, *119* (29), 7980–7990.
- (207) Ogoshi, H.; Nakamoto, K. Normal-Coordinate Analyses of Hydrogen-Bonded Compounds. V. The Enol Forms of Acetylacetone and Hexafluoroacetylacetone. *J. Chem. Phys.* **1966**, *45* (8), 3113–3120.
- (208) Liptay, G.; Burger, K.; Mocsari-Fulop, E.; Porubszky, I. Thermal Analysis of Metal Complexes. III. Thermal Decomposition of Pyridine Halide (pseudohalide) Mixed Complexes and of Their Decomposition Products. *J. Therm. Anal.* **1970**, *2* (1), 25–36.
- (209) Gill, N. S.; Nuttall, R. H.; Scaife, D. E.; Sharp, D. W. A. Infrared Spectra of Pyridine Complexes and Pyridinium Salts. *J. Inorg. Nucl. Chem.* **1961**, *18*, 79–87.
- (210) Katta, V.; Chowdry, S. K.; Chait, B. T. Electrospray Ionization: A New Tool for the Analysis of Ionic Transition Metal Complexes. *J. Am. Chem. Soc.* **1990**, *112* (13), 5348–5349.
- (211) Wilson, S. R.; Wu, Y. A Study of Nickel Catalyzed Coupling Reactions by Electrospray Ionization Mass Spectrometry. *Organometallics* **1993**, *12*, 1478–1480.
- (212) Gatlin, C. L.; Turecek, F.; Vaisar, T. Determination of Soluble Cu(I) and Cu(II) Species in Jet Fuel by Electrospray Ionization Mass Spectrometry. *Anal. Chem.* **1994**, *66*, 3950–3958.
- (213) Gatlin, C. L.; Rao, R. D.; Turecek, F.; Tomás, V. Carboxylate and Amine Terminus Directed Fragmentations in Gaseous Dipeptide Complexes with Copper (II) and Diimine Ligands Formed by Electrospray. *Anal. Chem.* **1996**, *68* (2), 263–270.
- (214) Buchanan, R. M.; Wilson-Blumenberg, C.; Trapp, C.; Larsen, S. K.; Greene, D. L.; Pierpont, C. G. Counter Ligand Dependence of Charge Distribution in Copper-Quinone Complexes. Structural and Magnetic Properties of (3,5-Di-Tert-butylcatecholato)(bipyridine) copper(II). *Inorg. Chem.* **1986**, *25* (17), 3070–3076.
- (215) Dapprich, S.; Frenking, G. Investigation of Donor- Acceptor Interactions: A Charge Decomposition Analysis Using Fragment Molecular Orbitals. *J. Phys. Chem.* **1995**, No. 99, 9352–9362.
- (216) Lu, T. *Multiwfn a Multifunctional Wavefunction Analyzer, Software Manual*; 2015.
- (217) Bagus, P. S.; Hermann, K.; Bauschlicher Jr., C. W. On the Nature of the Bonding of Lone Pair Ligands to a Transition Metal. *J. Chem. Phys.* **1984**, *81* (4), 1966–1974.
- (218) Galiano, L.; Alcamí, M.; Mó, O.; Yáñez, M. Gas-Phase Chemistry of Ethynylamine, -Phosphine and -Arsine. Structure and Stability of Their Cu⁺ and Ni⁺ Complexes. **2003**, 72–78.

- (219) M6, O.; Y6ñez, M.; Gal, J.-F.; Decouzon, M.; Maria, P.; Guillemin, J. Gas-Phase Basicity and Acidity Trends in α,β -Unsaturated Amines, Phosphines and Arsines. *J. Am. Chem. Soc.* **1999**, *121*, 4653–4663.
- (220) Guillemin, J.; Decouzon, M.; Maria, P.; Gal, J.-F.; M6, O.; Y6ñez, M. Gas-Phase Basicities and Acidities of Ethyl-, Vinyl-, and Ethynylarsine. An Experimental and Theoretical Study. *J. Phys. Chem. A* **1997**, *101*, 9525–9530.
- (221) Rodriguez, J. A. The Bonding of Acetate, Methoxy, Thiomethoxy and Pyridine to Cu Surfaces: A Molecular Orbital Study. *Surf. Sci.* **1992**, *273*, 385–404.
- (222) Huang, H. H.; Yan, F. Q.; Kek, Y. M.; Chew, C. H.; Xu, G. Q.; Ji, W.; Oh, P. S.; Tang, S. H. Synthesis, Characterization, and Nonlinear Optical Properties of Copper Nanoparticles. *Langmuir* **1997**, *13* (18), 172–175.
- (223) Pestryakov, a. N.; Petranovskii, V. P.; Kryazhov, A.; Ozhereliev, O.; Pf6nder, N.; Knop-Gericke, A. Study of Copper Nanoparticles Formation on Supports of Different Nature by UV–Vis Diffuse Reflectance Spectroscopy. *Chem. Phys. Lett.* **2004**, *385* (3-4), 173–176.
- (224) Al-Mamun, A.; Kusumoto, Y.; Muruganandham, M. Simple New Synthesis of Copper Nanoparticles in Water/acetonitrile Mixed Solvent and Their Characterization. *Mater. Lett.* **2009**, *63* (23), 2007–2009.
- (225) Joshi, S. S.; Patil, S. F.; Iyer, V.; Mahumuni, S. Radiation Induced Synthesis and Characterization of Copper Nanoparticles. *Nanostructured Mater.* **1999**, *10* (7), 1135–1144.
- (226) Murray, J. S.; Politzer, P. Correlations between the Solvent Hydrogen-Bond-Donating Parameter α and the Calculated Molecular Surface Electrostatic Potential. *J. Org. Chem.* **1991**, *56* (23), 6715–6717.
- (227) Kamlet, M. J.; Abboud, J. L. M.; Abraham, M. H.; Taft, R. W. Linear Solvation Energy Relationships. 23. A Comprehensive Collection of the Solvatochromic Parameters, π^* , α , and β , and Some Methods for Simplifying the Generalized Solvatochromic Equation. *J. Org. Chem.* **1983**, *48* (17), 2877–2887.
- (228) Palmer, B. J. Photochemistry of Inorganic and Organometallic Complexes in Various Media, Simon Fraser University, 1992.
- (229) Balzani, V.; Bolletta, F.; Moggi, L. Energy and Electron Transfer in the Field of Transition Metal Complexes. *Spectrosc. Lett.* **1978**, No. November.
- (230) Borkman, R. F.; Kearns, D. R. Electronic-Relaxation Processes in Acetone. *J. Chem. Phys.* **1966**, *44* (3), 945–949.
- (231) Lind, S.; Trost, J.; Zigan, L.; Leipertz, A.; Will, S. Application of the Tracer Combination TEA/acetone for Multi-Parameter Laser-Induced Fluorescence Measurements in IC Engines with Exhaust Gas Recirculation. *Proc. Combust. Inst.* **2015**, *35* (3), 3783–3791.
- (232) Bayrakceken, F. Triplet-Triplet Optical Energy Transfer from Benzophenone to Naphthalene in the Vapor Phase. *Spectrochim. Acta, Part A Mol. Biomol. Spectrosc.* **2008**, *71A* (2), 603–608.
- (233) Koch, J. D.; Hanson, R. K.; Koban, W.; Schulz, C. Rayleigh-Calibrated Fluorescence Quantum Yield Measurements of Acetone and 3-Pentanone. *Appl. Opt.* **2004**, *43* (31), 5901–5910.
- (234) Hecklen, J. The Fluorescence and Phosphorescence of Biacetyl Vapor and Acetone Vapor. *J. Am. Chem. Soc.* **1959**, *81*, 3863–3866.
- (235) Adkins, H.; Eloffson, R. M.; Rossow, A. G.; Robinson, C. C. Oxidation Potentials of Aldehydes and Ketones. *J. Am. Chem. Soc.* **1949**, *71*, 3622–3629.

- (236) Buxton, G. V.; Sellers, R. M. Compilation of Rate Constants for the Reactions of Metal Ions in Unusual Valency States. *Natl. Stand. Ref. Data Ser. (United States, Natl. Bur. Stand.* **1978**, *62*, 80 pp.
- (237) Walling, C.; El-Taliawi, G. M.; Johnson, R. A. Fenton's Reagent. IV. Structure and Reactivity Relations in the Reactions of Hydroxyl Radicals and the Redox Reactions of Radicals. *J. Am. Chem. Soc.* **1974**, *96* (1), 133–139.
- (238) Gade, L. H. *Koordinationschemie*; 1998.
- (239) Hammond, G. S.; Leermakers, P. A. Mechanisms of Photoreactions in Solution. X. Relative Efficiencies of Various Quenchers in the Photoreduction of Benzophenone. *J. Phys. Chem.* **1962**, *66*, 1148–1150.
- (240) Linschitz, H.; Pekkarinen, L. The Quenching of Triplet States of Anthracene and Porphyrins by Heavy Metal Ions. *J. Am. Chem. Soc.* **1960**, *82*, 2411–2416.
- (241) Hammond, G. S.; Foss, R. P. Mechanisms of Photoreactions in Solution. XX. Quenching of Excited States of Benzophenone by Metal Chelates. *J. Phys. Chem.* **1964**, *68* (12), 3739–3746.
- (242) Das, P. K. Electron Transfer Reactions from Aromatic Carbonyl Triplets to Paraquat Dication. *Tetrahedron Lett.* **1981**, *22* (14), 1307–1310.
- (243) Adams, G. E.; Baxendale, J. H.; Boag, J. W. Electron Attachment in Irradiated Solutions. *Proc. R. Soc. London, Ser. A Math. Phys. Eng. Sci.* **1964**, *277* (1371), 549–561.
- (244) Trentelman, K. A.; Kable, S. H.; Moss, D. B.; Houston, P. L. Photodissociation Dynamics of Acetone at 193 Nm: Photofragment Internal and Translational Energy Distributions. *J. Chem. Phys.* **1989**, *91* (12), 7498–7513.
- (245) Takatori, Y.; Kajii, Y.; Shibuya, K.; Obi, K. Dissociation of Highly Excited Triplet Benzophenone into Phenyl Radicals and Carbon Monoxide: Determination of the Reaction Quantum Yield and the Heat of Reaction by Time-Resolved Thermal Lensing Technique. *Chem. Phys.* **1994**, *180* (1), 99–107.
- (246) Matsushita, Y.; Kajii, Y.; Obi, K. Photochemical Reaction of Excited Benzophenone in the Gas Phase. *J. Phys. Chem.* **1992**, *96* (11), 4455–4458.
- (247) Beckett, A.; Porter, G. Primary Photochemical Processes in Aromatic Molecules. X. Photochemistry of Substituted Benzophenones. *Trans. Faraday Soc.* **1963**, *59* (489), 2051–2057.
- (248) Wang, S.; Singh, P. S.; Evans, D. H. Concerted Proton-Electron Transfer: Effect of Hydroxylic Additives on the Reduction of Benzophenone, 4-Cyanobenzophenone, and 4,4'-Dicyanobenzophenone. *J. Phys. Chem. C* **2009**, *113* (38), 16686–16693.
- (249) Tachikawa, H.; Kawabata, H. Direct Ab Initio MD Study on the Hydrogen Abstraction Reaction of Triplet State Acetone from Methanol Molecule. *Theor. Chem. Acc.* **2011**, *128* (2), 207–213.
- (250) Neta, P.; Grodkowski, J. Rate Constants for Reactions of Phenoxyl Radicals in Solution. *J. Phys. Chem. Ref. Data* **2005**, *34* (1), 109–199.
- (251) Nau, W. M.; Cozens, F. L.; Scaiano, J. C. Reactivity and Efficiency of Singlet- and Triplet-Excited States in Intermolecular Hydrogen Abstraction Reactions. *J. Am. Chem. Soc.* **1996**, *118* (9), 2275–2282.
- (252) Du, Y.; Ma, C.; Kwok, W. M.; Xue, J.; Phillips, D. L. Time-Resolved Resonance Raman Identification and Structural Characterization of a Light Absorbing Transient Intermediate in the Photoinduced Reaction of Benzophenone in 2-Propanol. *J. Org. Chem.* **2007**, *72* (19), 7148–7156.

- (253) Lilie, J.; Beck, G.; Henglein, A. Pulse Radiolysis and Polarography. Halfwave Potentials for the Oxidation and Reduction of Short-Lived Organic Radicals at the Mercury Electrode. *Berichte der Bunsen-Gesellschaft* **1971**, *75* (5), 458–465.
- (254) Nau, W. M.; Scaiano, J. C. Oxygen Quenching of Excited Aliphatic Ketones and Diketones. *J. Phys. Chem.* **1996**, *100* (27), 11360–11367.
- (255) Butler, J.; Jayson, G. G.; Swallow, A. J. Oxidation of Ferrous Ions by an Aliphatic Dioxygen Radical. *J. Chem. Soc. Faraday Trans. 1 Phys. Chem. Condens. Phases* **1974**, *70* (7), 1394–1401.
- (256) Ruscic, B.; Berkowitz, J. Photoionization Mass Spectrometric Studies of the Isomeric Transient Species Hydroxymethyl-D₂ and Methoxy-D₃ (CD₂OH and CD₃O). *J. Chem. Phys.* **1991**, *95* (6), 4033–4039.
- (257) Ramond, T. M.; Davico, G. E.; Schwartz, R. L.; Lineberger, W. C. Vibronic Structure of Alkoxy Radicals via Photoelectron Spectroscopy. *J. Chem. Phys.* **2000**, *112* (3), 1158–1169.
- (258) Jagannadham, V.; Sanjeev, R. The Marvelous Marcus Equation. *Bulg. Chem. Commun.* **2011**, *43* (3), 383–394.
- (259) Porter, G.; Suppan, P. Reactivity of Excited States of Aromatic Ketones. *Pure Appl. Chem.* **1964**, *9* (4), 499–505.
- (260) Taube, H.; Gould, E. S. Organic Molecules as Bridging Groups in Electron-Transfer Reactions. *Acc. Chem. Res.* **1969**, *2* (11), 321–329.
- (261) Gould, E. S.; Taube, H. Isomeric Pyridinecarboxylates as Bridging Groups in Oxidation-Reduction Reactions. Electron Transfer through Nitrogen. *J. Am. Chem. Soc.* **1963**, *85* (22), 3706–3707.
- (262) Than, S.; Maeda, H.; Irie, M.; Itoh, S.; Kikukawa, K.; Mishima, M. Structural Effect on the Stability of (Pyridine)₂Cu⁺ Complexes in the Gas Phase: Nature of the Bond between Copper(I) Ion and Neutral Molecules. *J. Phys. Chem. A* **2007**, *111* (27), 5988–5994.
- (263) Nysh, G. V.; Trushina, L. F.; Savel'ev, G. G. Increase in the Sensitivity of Photosensitive Copper Oxalate Films. *Zhurnal Nauchnoi i Prikl. Fotogr. i Kinematogr.* **1976**, *21* (6), 440–442.